THE CATHOLIC UNIVERSITY OF AMERICA

A New Framework for Airborne Minefield Detection using Markov Marked Point Processes

A DISSERTATION

Submitted to the faculty of the

Department of Electrical Engineering and Computer Science

School of Engineering

Of The Catholic University of America

In Partial Fulfillment of the Requirements

For the Degree

Doctor of Philosophy

By

Anh Hoang Trang

Washington, D.C.

2011

A New Framework for Airborne Minefield Detection using Markov Marked Point Processes

Anh Hoang Trang, Ph.D.

Director: Phillip A. Regalia, Ph.D.

Detecting both patterned and unpatterned minefields from an airborne platform is particularly challenging because of low signal contrast, high variability of mine signatures, relatively high density of man-made and natural clutter objects, and variability of minefield layouts. This dissertation is an investigation into how shape/spectral similarity of the mine signature and the minefield-like spatial distribution can be exploited simultaneously to improve the performance for patterned and unpatterned minefield detection in highly cluttered environments. The minefield decision is based on the detected targets obtained by an anomaly detector, such as the RX algorithm, in the image of a given field segment. Spectral, shape or texture features at the target locations are used to model the likelihood of the targets being potential mines. The spatial characteristic of the minefield structure is captured by the expected distribution of nearest neighbor distances of the detected mine locations. The clutter targets in the minefield are assumed to constitute a Poisson point process. The overall minefield detection problem is formulated as a Markov marked point process (MMPP) that is based on local attributes and relative spatial distribution of the target signatures. Minefield decision is formulated under binary hypothesis testing using maximum log-likelihood ratio. A quadratic heuristic search algorithm is developed to identify a set of detections that maximizes the minefield log-likelihood ratio. Furthermore, a procedure based on expectation maximization is developed for estimating unknown parameters like mine-level probability of detection and mine-to-mine separation. The

minefield detection performance under this MMPP formulation is compared to baseline algorithm using simulated data. Results based on thousands of minefield and background segments show that the minefield performance based on MMPP formulation is much better than the performance of the baseline for both patterned and unpatterned minefields. An analytical solution for a detection problem is also derived. The minefield performance of analytical and simulated-based solutions based on the minefield likelihood values for three different clutter rates are compared.

This dissertation by Anh Trang fulfills the dissertation requirement for the doctoral degree in electrical engineering approved by Dr. Phillip A. Regalia, Ph.D., as the Director, and by Nader Namazi, Ph.D., and Mohammed Arozullah, Ph.D., as Readers.

Phillip A. Regalia, Ph.D., Director

Nader Namazi, Ph.D., Reader

Mohammed Arozullah, Ph.D., Reader

DEDICATION

My appreciation and love goes to my wife, Tuyet Tran. Her unselfish gift of time and support has allowed me to continue my education and academic pursuits since 1983.

Table of Contents

List of Figures

List of Tables

ACKNOWLEDGEMENTS

My graduate training academic advisors, Dr. Phillip Regalia, Dr. Nade Namazi, and Dr. Mohammed Arozullah, have provided valuable comments and guidance during the development of the minefield detection algorithm for the U.S. Army Airborne Countermine programs.

My supervisor, Mr. Tom Smith, has provided an opportunity for me to be in school and has been patient with me during the years in school. Dr. Sanjeev Agarwal of Night Vision and Electronic Sensors Directorate (NVESD) has provided guidance, discussions, and technical support, and he has always made his time available for me. Dr. Tom Broach of NVESD, Dr. Larry Lynch and Mr. Bart Durst of ERDC, and Mr. Richard Ess of PM – Countermine & EOD have continuously supported the minefield algorithm development from the beginning.

Chapter 1 Introduction

The problem of detecting spatial distribution of similar targets in the presence of substantial clutter is considered. One example is the detection of patterned and unpatterned minefields along a specified path using airborne imaging systems. The proliferation of land mines worldwide has created an urgent requirement for minefield detection, particularly from an airborne platform to maximize standoff distances and search speeds. In the last decade, there has been a significant and concerted interest in airborne minefield detection and reconnaissance systems in the United States as well as in other countries around the world. The main objective of these airborne programs is to reliably locate both patterned and unpatterned minefields from a lightweight airborne platform around the clock, and in all environmental conditions and different backgrounds [1].

Mine detection performance has improved these past few years by using high-resolution sensors and multi-spectral bands from a single-sensor or multiple-sensor platform. However, detecting both patterned and unpatterned minefields has remained problematic. The problem is particularly challenging because of low signal contrast, high variability of mine signatures, the relatively high density of man-made and natural clutter objects, and the variability of minefield layouts and patterns. Ware et al. provide a list of challenges inherent in the detection of minefields [2].

A typical minefield detection approach is based on a sequential process employing anomaly detection followed by false alarm mitigation and minefield detection. The potential targets located by the anomaly detector [3] include mines, in addition to natural and man-

made objects that stand out from the background. The false alarm mitigation (FM) seeks to reduce false alarms by selecting/rejecting targets based on some pre-specified criteria or by using elaborate shape and color features [4]. Significant work has been done on anomaly detection, feature selection, and FM to improve detections of individual mines [5, 6]. However, since target features change with time, vary under different environmental conditions, and are affected by background characteristics, the false alarms rate is often high with the utilization of FM. Minefield detection statistics are evaluated separately using algorithms for either patterned minefield detection [1, 7, 8] or unpatterned minefield detection [9] based on detected target locations. Most of the minefield detection algorithms perform well if the false alarm rate is low, such that the number of detected mines is equal to or greater than the number of false alarms in the interrogated segment. However, their performance is reduced significantly when the false alarm rate is relatively high. Moreover, since the current (typical) approach is based on sequential processing, it is not capable of exploiting the interdependencies of mine signatures and the spatial layouts of mines in the minefield.

The proposed research is motivated by some of the previously successful patterned minefield detection approaches discussed and by observed patterned and unpatterned minefield lay-out structures. Patterned minefields contain patterns of hand-laid mines, while unpatterned mines are often distributed by artillery shells, vehicles, or airplanes. The relative spatial distribution of mines in patterned or unpatterned configurations can be predicted or estimated because these minefields are built for mine recovering or effectiveness. On the other hand, the relative spatial distribution of clutter targets often

varies from place to place. Therefore, clutter target and mine spatial distributions are expected to be from two distinguishable processes.

Another interest concerns mine signatures changing with time and different environments, but the features of most similar mines are often similar in a local area at a particular time and they are often distinguished from clutter target features. A few "reliable" features of mine signatures and clutter target features were presented in the past [4]. McFee et al. [23] discussed the selection of 15 features out of 26 features for mines extracted from each region and a cluster analysis of the feature vectors from mines and background materials carried out using a pattern recognition program. These features consist of a measure of the area, intensity mean, intensity variance, maximum intensity, minimum intensity, perimeter, size, compactness, center of gravity, 0^{th} to 3^{rd} central moments, and a height/width ratio. Analysis of the feature vectors generated by the local region feature vector shows mine classes separated from the non-mine classes. These features are worthy of further investigation.

Schumacher and Zhang [27] used discrete wavelet transform (DWT) for feature extraction before using four neural networks (NN) for classification. The classification is performed separately at all three resolution levels, with the four DWT coefficient sub-matrices used as inputs into the four separate neural networks at each level. Each neural network is trained separately using the locally-connected network with weight sharing. Four voting network systems are used to classify four types of textured images outputted from the NN. The best result was 99.5% correct classification. Translation invariance can be the problem with this method.

Ling and Cavalcanti [28] developed a novel and efficient approach for feature extraction for pattern classification using neural networks. The method searches for the minimum amount of features necessary for solving a given pattern classification problem, which is based on the structure of an adequately trained multilayer perceptrons (MLP) neural network. When the feature vector is highly informative, a feed-forward MLP trained by a back-propagation algorithm minimizes the classification error probability that can determine the optimal decision hyper-plane for classification. However, such neural network based training often suffers from over training and results in a lack of generalization.

Clark et al. [6] used a supervised-learning scheme with a probabilistic neural network classifier, which was trained to classify image regions as belonging to one of two classes: “mine” or “background”. With this approach, the authors use the pre-processing algorithm, pixel classification, region formation algorithms, and post processing algorithms; this is a common mine detection approach. The supervised learning scheme does not seem to be robust since mine signatures are always changing. This observation has agreed with the authors’ conclusion that size constraints applied to this image produced a degradation in the results.

Breen et al. [29] presented a scalable system capable of examining images and accurately classifying the image based on its visual content. The approach uses neural networks together with domain-dependant ontologies. The supervised network takes an image as input and gives it a classification as output. The ontology then processes the classified output, revealing relationships among objects that can be used to provide semantic meaning to the entire image. The training is based on color and shape of each object. This

work uses spectral features as well as interrelationships. Agarwal et al [1] exploited the critical criteria of "similar" objects. They employed an unsupervised self-organizing algorithm to cluster similar targets based on shape profile. Then they applied the spatial constraints between mines to detect patterned minefields. Their limited results show that minefield detection performance improves when target signatures are well defined, the number of targets is large in a search area, and targets are laid out in a pattern.

This research investigates the shape/spectral similarity of mine signatures and the minefield-like spatial distribution exploited simultaneously to improve the performance for patterned and unpatterned minefield detection. The detection in the segment is formulated as a Markov marked point process (MMPP), based on local attributes and relative spatial distribution of the target signatures, and the minefield decision is based on the log-likelihood ratio test of a binary hypothesis problem. Hough transform is used to speed up the processing speed for patterned minefield detection, while the developed quadratic heuristic search algorithm is used to identify a set of detections that maximizes the minefield likelihood for general minefield detection. Often the parameters in the log likelihood function are unknown and must be estimated. The iterative expectation maximization (EM) algorithm is used to estimate these unknown parameters wherever possible.

The minefield performance of three algorithms based on two thresholding methods and high clutter rates is evaluated and compared. These algorithms are the baseline algorithm with false alarm mitigation (SPP-FM) where only detection locations are accounted for, the marked point process (MPP) algorithm where the detection locations included the spectral attribute such as the target size, and the developed algorithm based on

MMPP model where both spectral feature and spatial distribution are used simultaneously. Also, the minefield performance of the MMPP algorithm with known parameters and the MMPP algorithm with the parameter estimation (MMPP-EM) is evaluated and compared.

Most current patterned minefield detection algorithms do not take advantage of the detection of more than one mine row. In this research, an algorithm to automatically detect a number of rows in each segment is developed. The MMPP algorithm is assessed on equally generated minefield segments of 1-row, 2-rows, and 3-rows at two high clutter rates of 0.006 and 0.008 clutter target per m^2.

Exploiting spatial distribution of unpatterned mines is not trivial. The spatial structures of unpatterned minefields are not often as pronounced as the spatial structures of patterned minefields. In this research, the performance of unpatterned minefields where potential mines are assumed to be randomly and regularly distributed, and where clutter targets are assumed to be randomly distributed is evaluated. The results that are obtained at the high clutter rate of 0.008 clutter target per m^2 and the mine density of 0.0024 mine per m^2 for two spatially distributed cases are shown. In both cases, the comparative results among the baseline algorithm (SPP-FM), the algorithm based only on target feature (MPP), and the algorithm based on both target feature and target spatial distribution (MMPP) are provided.

As the results are based on the simulated data, it is not clear whether the MMPP detection algorithm has fully achieved its best performance. To validate its performance, an analytical solution for the minefield detection problem is developed, and its performance is compared with the performance of the simulated solution. The analytical solution for the

complete minefield detection problem is intractable due to a large number of detections and the variation of the number of detected mines in the minefield process. Therefore, an analytical solution for a simplified detection problem is derived, and its minefield performance is compared with the minefield performance obtained from the simulation in the same MMPP framework for three different clutter rates of 0.01, 0.02, and 0.03.

Chapter 2 Literature Review

The proliferation of landmines worldwide has created an urgent requirement for minefield detection, particularly from an airborne platform, to quickly locate the minefields at a safe standoff distance. The United States and other countries have initiated airborne countermine programs using multi-spectral sensors and advanced minefield detection algorithms to improve detection performance, ultimately increasing the speed of advance. Previous airborne countermine programs, which were instituted to meet this need, included the Remote Minefield Detection System, Coastal Battlefield Reconnaissance and Analysis, and Lightweight Airborne Multispectral Minefield Detection. The main objective of these airborne programs is to reliably locate minefields from a lightweight airborne platform, around the clock, and in all environmental conditions and different backgrounds [1].

Most minefields can be classified as either patterned, unpatterned, or tactical minefields [12]. The patterned minefields are often placed in linear, almost linear, or zigzag patterns. These are often arranged according to a predefined doctrine that takes consideration of the terrain and strategic requirements. Mines for unpatterned minefields can be surface laid or distributed by artillery shells, vehicles, or airplanes in predefined-spatial doctrines. A tactical or nuisance minefield is probably the most difficult to detect since it employs very few mines and does not confirm to any pattern of mines or distribution characteristics. This effort, however, will not be capable of solving nuisance minefield scenarios/problems.

A typical minefield detection approach based on sequential processing is shown in Figure 2-1. The mine detection module uses the "RX" algorithm originally from the Generalized Maximum Likelihood Ratio Test by Reed and Yu [3], and later implemented in modified forms by Holmes et al [13] and Agarwal et al [1]. It is primarily a local anomaly detector. The potential targets located by the RX algorithm inevitably consist of natural and man-made anomalies that contrast themselves from the background. An intermediate step seeks to reduce these false alarms by selecting or rejecting targets based on some pre-specified criteria, such as the upper and lower limits of the RX values, size of targets, etc. Sophisticated false alarm mitigation procedures use more elaborate features to select mine-like objects or reject non-mine-like objects [4].

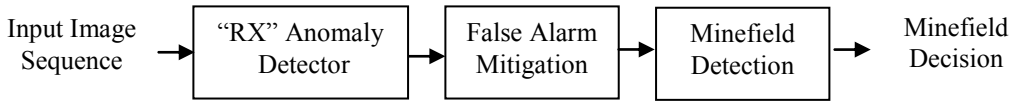

Figure 2-1 A flow diagram for a typical sequential minefield detection scheme

2.1 Mine Detection

Since a typical platform employs multi-spectral sensors, the "RX" anomaly detector seems to be a good algorithm to process the multi-spectral signals and has performed reasonably well when the specific characteristic of the search area is not known *a priori*. There are other mine detection approaches that have been used to process airborne data but none of them performed better than the RX in all areas. Liao [14] developed the Estimator and Correlator (EC) or Wiener algorithm to detect mines. His technique is built on the prior knowledge of the target signatures. These signatures are allowed to be distorted by the viewing geometry, illumination conditions, environmental factors, and the assumption of

known clutter spatial covariance matrix not necessarily white. Also, he uses a filter bank approach to include multiple mine signatures and relies on data fusion to make a final mine detection decision. The comparative analysis among these algorithms shows the EC works better than the RX for surface mines. On the other hand, the EC performs worse than the RX for buried mines since the EC is sensitive to the target signatures and signatures of buried mines are not consistent.

A highly sophisticated mine detection technique was introduced recently by Batman and Goutsias [5]. They apply an unsupervised iterative scheme for landmine detection in heavily cluttered scenes. The main claims by the authors include the improvement in mine detection performance, robustness with respect to clutter heterogeneities, a completely unsupervised operation, and computational efficiency. One drawback of this method includes the assumption of *a priori* knowledge of the mine signatures; however, actual mine signatures often vary. Thus, the method will not always be robust. Additionally, since this method relies on hand-picked band parameters and the parameters associate with histogram stretching and thresholding to optimize the detection and false alarm performance, the method cannot be implemented in real time for the same performance.

2.2 False Alarm Mitigation

General anomaly detectors can be tuned to obtain a higher probability of detection, but inversely detect a large number of false alarms. Miao et al. [15] reviewed the literature and reported that a number of automatic target detection and recognition schemes had been partially successful, but had obtained high false alarm rates. Contributing factors include the

diverse sizes and compositions of targets, variation of soil properties with location and moisture conditions, non-reliability of the target signature, competing clutter objects having similar responses as the actual targets, and partially obscured targets.

Several existing false alarm mitigation (FM) techniques were built on the prior knowledge of mine and clutter target signatures at particular times and environments. The main goal of these techniques is to retain mine signatures while suppressing clutter targets or false alarms. Mine signatures change with times and environments [4, 16]. Figures 2.2-1 through 2.2-4 show several examples of different mine types, sizes, (LM: large metal mine, SM: small metal mine, LP: large plastic mine, and MP: medium plastic mine) and false alarms collected during the daytime and nighttime. These signatures are detected by the RX detector. Daytime and nighttime signatures [17] of the same mines are completely different, while some clutter target and mine signatures are somewhat similar, thus introducing a challenge.

Hence the ability to decide on the best FM technique for a given set of imaging conditions is critical. Menon et al. [4] developed three different false alarm mitigation techniques utilizing different characteristics of mine signatures. In some instances, mine signatures were observed to be circular so the researchers developed a technique to compute their circularity, circularity being a measure of the compactness of the signature. In other instances, as observed during the daytime, mine signatures are bi-polar (i.e., a bright highlight due to reflection from the mine target and a dark shadow due to the sun), so they developed reflection symmetry technique based on this phenomenon. The technique

measures the reflection symmetry about the sun angle through the centroid of a target signature.

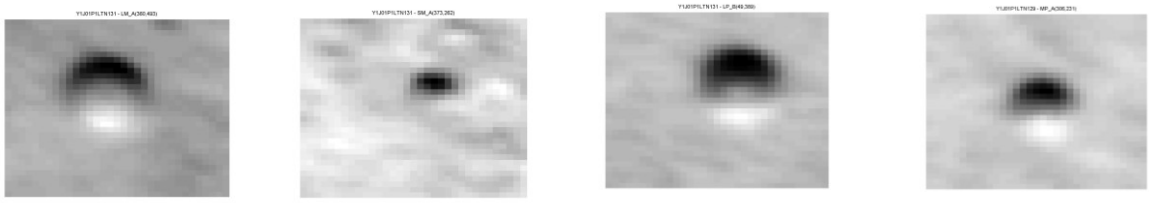

LM SM LP MP

Figure 2.2-1 Mine signatures during daytime

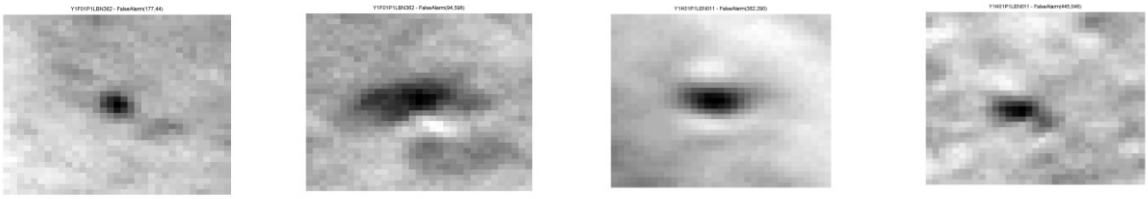

Figure 2.2-2 Clutter target signatures during daytime

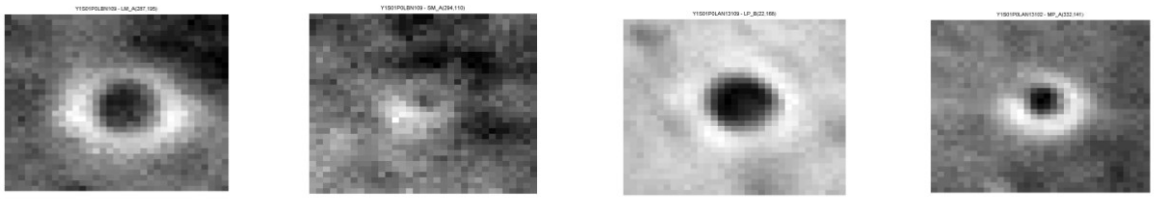

LM SM LP MP

Figure 2.2-3 Mine signatures during nighttime

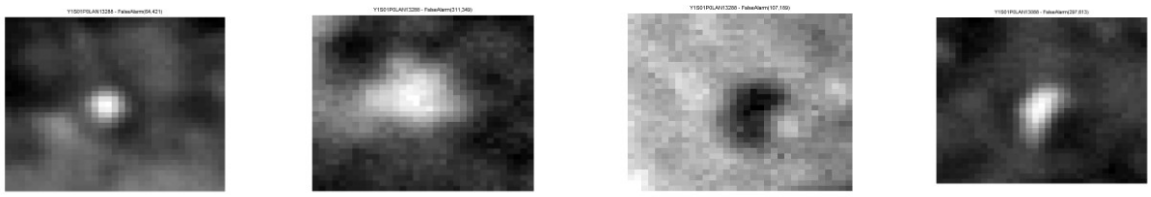

Figure 2.2-4 Clutter target signatures during nighttime

Another technique was developed to compute the gray scale moments that exploit the gray-value profile of mine signatures [4]. This technique uses 11-dimensional feature vectors in the 4^{th} order of two dimensional gray scale moments for each mine signature. The results based on MWIR indicate that circularity and gray-scale moments reduce false alarms by a factor of 6-12 for nighttime large mine signatures, while the reflection symmetry reduces a factor of 2-3 for daytime large mine signatures when the detection performance is already good. The results suggest that FM, which utilizes known prior information, does not work well consistently**.**

2.3 Minefield Detection

The minefield detection algorithms count the number of detections after the false alarm mitigation to determine the presence or absence of a minefield in an interrogation area. The sequential minefield approach implies that mines which are missed at any of the previous stages cannot contribute to the detection of minefields, while false alarms remaining after the false alarm mitigation stage erroneously influence the minefield detection statistics.

In patterned minefields, mines are large in size but are often buried or occluded, and are not necessarily lined up linearly due to the registration error and variability in mine placement. There are many patterned minefield configurations; however, linear patterns with one or more rows of mines at relatively regular intervals are more common [12]. Many different patterned minefield detection technologies have been investigated in the past 20 years. Lake et al. [18] used Hough transform along with a modified Euclidian algorithm to explicitly take advantage of collinearity and equal-spacing of patterned minefields. Walsh and Raftery [8] developed a sequential placement model that includes the information of distances between sequential mines, the mean distance between rows, and the direction of the rows. They constructed a Bayesian estimation via the Markov chain Monte Carlo algorithm to assign posterior probabilities for each point being a mine. Robins and Robinson [19] developed an algorithm for mine detection that can tolerate inaccuracies due to mine placement, drift due to soil shifting, and imprecision inherent in the imaging technology. However, the algorithm relies on computational geometric and combinatorial techniques, and runs in $O(n^{5/2})$ time. Later, Robins et al [20] extended their previous work to noisy images to overcome imprecision that might be inherent in the measurement process. However, the computational cost of the algorithm was even higher. Baertlein and Liao [7] developed wavelet-based higher order neural networks for mine detection. The performance result of the 2nd order High Order Neural Network for straight line minefields is lower than the Hough transform but its performance is superior for curved minefields. Bargel et al. [21] developed a hierarchical approach based on collection of mine clusters (or patterns) such as mines, mine-pairs, mine-groups and mine-formations to detect patterned minefields.

In the case of unpatterned minefields, mines are small in size and their signatures are often weak. The threshold for unpatterned mine detection is often adjusted low so that these mines can be detected by the detection algorithm. At the same time, the signatures of clutter objects such as rocks, piles of dirt, shrubs, and small plants can easily slip through the detection algorithm to create a large number of false alarms. The high false alarm rate has been a challenge in minefield detection. Earp, Elkins, and Conrath [9] developed an unpatterned minefield detection algorithm based on log likelihood assuming Poisson distribution for both mines and clutter targets. This algorithm takes the log sum of the confidences of all minelike objects to produce a minefield confidence statistic. Byers and Raftery [22] have used K^{th} nearest neighbor distances (NND) of points in the process to classify the detection as a cluttered background or otherwise. The observed K^{th} NND was modeled as a mixture distribution. This method has been applied to minefield detection and to outlining seismic faults with some successes. McFee, Russell, and Ito [23] have developed an approach in which at the top level, spatial relationships between "mine-like" regions are determined and are used by knowledge-based methods to classify the imaged area as being a minefield with a specified likelihood. However, the spatial relationships between mines were not employed. Ware et al. [2] discussed the detection of unpatterned minefields. In general, an unpatterned minefield algorithm is designed to look for density of points, thus a low number of false alarms are in evidence. In cases where a general shape of the minefield is known, the minefield detection algorithm may use the template matching technique.

Regalia [24, 25] has recently developed an algorithm based on belief propagation (BP) for patterned and unpatterned minefield detection. The use of a BP algorithm is for computational reduction compared to an exhaustive search by virtue of factoring a likelihood function into simpler "compatibility" functions, which are supposed to capture the local interactions between variables. His latest work pursues factor graph construction in a more robust manner that renders the detection algorithm insensitive to rotation, translation or reflection of the field pattern, and likewise insensitive to node reordering. Also, his approach allows for variable degree factor graphs through a user-set parameter, and incorporates parameter estimation steps to adapt to ground terrain. Figures 2.3-1 and 2.3-2 show the detection performance on simulated patterned minefields using BP algorithm. Convergence occurred within four and five iterations of the BP algorithm for Figures 2.3-1 and 2.3-2, respectively. Although the results show promise, more work of the compatibility functions needs to be conducted. Also, detection of unpatterned mines should be evaluated in future efforts.

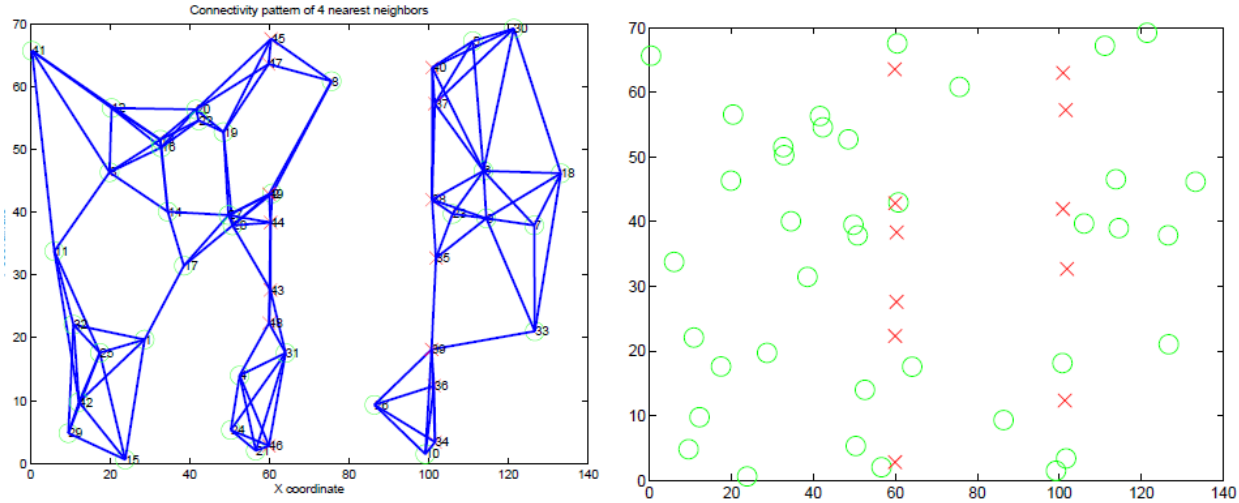

Figure 2.3-1(Left) ground truth and graph connectivity using d = 4 nearest neighbors; (Right) converged belief values, identifying eleven of thirteen mines, with no false positives. Red crosses are mines and green circles are clutter targets

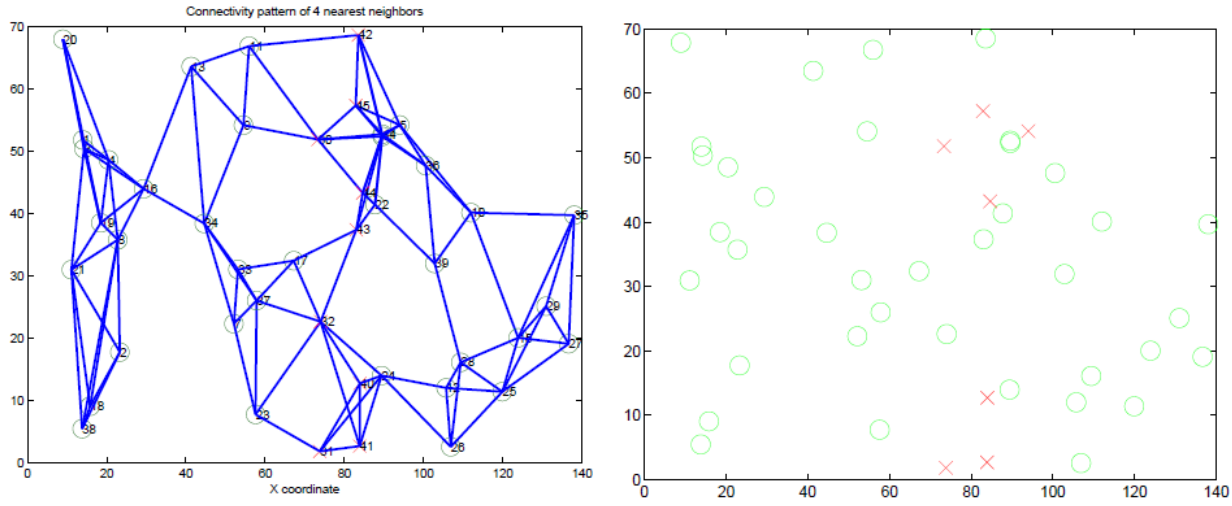

Figure 2.3-2 (Left) ground truth and graph connectivity using d = 4 nearest neighbors; (Right) converged belief values, identifying six of eight mines, with one false positive. Red crosses are mines and green circles are clutter targets

Chapter 3 Minefield Detection Problem

The majority of these algorithms implicitly assumes a spatial random layout for mines as well as clutter targets not always applicable with unpatterned minefields, which often follow some sort of patterns. Furthermore, most current approaches for both patterned and unpatterned minefields follow a sequential detection process wherein target attributes are used after target detection followed by the spatial relationship of detected targets to classify the interrogated area on whether it is a minefield or a background. The sequential process has some limitations: 1) the approach may be based on "hard" clustering (i.e., a predetermined threshold is chosen) so mine signatures below the chosen threshold will be lost; 2) the predefined mine features may be biased and may not provide a reliable representation of the overall characteristics of the signature of the targets; 3) there is no natural way to incorporate different spatial distributions of the mine targets in the field.

Clearly, the current sequential processing scheme has not delivered desired results under varying environment conditions that are typical of the airborne minefield detection problem. There is a need for a new minefield detection scheme that thoroughly addresses the problems in minefield detection that are only partially solved by previous methods.

The aim of this research will be to advance the state of the art in detection of both patterned and unpatterned minefield in highly cluttered environments. The proposed method seeks to combine the false alarm (FM) rejection module and the minefield detection module of the current architecture by employing Markov Marked Point Process formulation. The

approach simultaneously exploits the feature characteristics of the target signature and spatial distribution of the targets in the interrogation region. The method is based on the premise that most minefields can be characterized by some types of distinctive spatial distributions of "similar" looking mine targets. The minefield detection problem is formulated as a Markov Marked Point Process (MMPP) [Figure 3-1] where the set of possible mine targets is divided into a possibly overlapping mixture of targets. The likelihood of the minefield depends simultaneously on feature characteristics of the target and their spatial distribution.

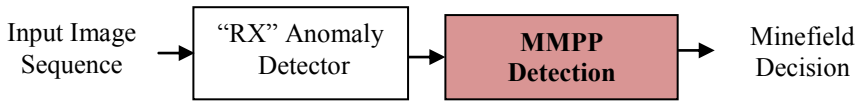

Figure 3-1 MMPP minefield detection architecture

3.1 Mine Detection and Target Selection

The minefield decision is based on the detected targets in the area of segment A. A set of selected targets is obtained using an anomaly detector (AD), like the RX algorithm. In this development, two types of target selections are considered: Constant False Alarm Rate (CFAR) and Constant Target Rate (CTR). In the case of CFAR target selection, the threshold for the AD value is selected so that the average number of false alarms in any segment is constant. In the case when the anomaly detector does not satisfy the CFAR property, or CFAR thresholding using adaptive threshold selection [30] is not reliable, CTR thresholding is often used. When discussing CTR, a fixed number of targets (false alarms and mines) with the highest anomaly statistics are selected in each segment. For this case,

the threshold for the AD value will change from segment to segment. Minefield detection algorithms will be developed under both types of selection strategies and their performance will be compared.

3.2 Minefield Detection as Binary Hypothesis

Once a set of targets is selected for a given segment using CFAR or CTR thresholding, the minefield decision is based on these detected targets. Let the set of detected targets be called an observation *X* and the number of detections in the segment (cardinality of *X*) be *n.* The segment is said to be a minefield segment (from a minefield process) if the observation *X* includes mines, and is called a background segment (from a background only process) if all the detected targets in the observation *X* are non-mines or clutter targets. Let $x_i \equiv \{l_i, a_i\}$ be an individual detection. Each detection consists of the geo-locations and local attribute(s), such as target size or other sets of attributes (e.g., target shape, polarity, etc). This detection represents a clutter target in the case of a background process, and either a clutter target or a mine in the case of a minefield process.

The minefield decision problem is to determine whether observation X belongs to the minefield process or the background process. This problem is posed under hypothesis testing framework, where H_0 and H_1 are the background only and the minefield hypothesis, respectively. Observation X with *n* detected targets under two hypotheses is given by

$$\textbf{Background}: \; H_0 : X = \left\{ x_i \middle| x_i \in \text{clutter target}, \, i = 1, 2, ..., n \right\} \tag{3.2-1}$$

$$\textbf{Minefield}: \quad H_1 : X = \left\{ x_i \middle| x_i \in \text{mine or clutter target}, \; i = 1, 2, ..., n \right\} \tag{3.2-2}$$

To simplify the notation, the assignment of the detection as a mine or a false alarm is captured by a classification function Z that is defined such that

$$Z = \{z_i, i = 1, 2, ..., n\} \tag{3.2-3}$$

where $$z_i = \begin{cases} 1 & \text{if the detection } x_i \text{ is a mine} \\ 0 & \text{if the detection } x_i \text{ is a clutter target} \end{cases}$$

It is important to note that the classification function Z is not known *a priori* and should be estimated from the data. Without loss of generality, assume that the detections are ordered such that the first n_m ($n_m \le n$) detections are mines and the remainders are clutter targets. With this assumption, Z is defined as

$$Z = \{z_i, i = 1, 2, ..., n\}, \quad z_i = \begin{cases} 1 & i = 1, ..., n_m \\ 0 & i = n_m + 1, ..., n \end{cases}$$

Under the null hypothesis (H_0), Z is a zero vector, while it is a non-zero vector under a non-null (H_1) hypothesis. Thus the null and non-null hypotheses in Equations (3.2-1) and (3.2-2) can be re-written as

Background: $H_0 : Z = \mathbf{0}$ (3.2-4)

Minefield: $H_1 : Z \neq \mathbf{0}$ (3.2-5)

3.3 Detection Attributes

From the previous section, each detection, x_i is identified by its location l_i and mark(s) or attributes a_i. For the current development, it is assumed that for any detection, mark a_i is independent of other detections, and it depends only on the identity of the

detection, as a mine ($z_i = 1$) or a clutter target ($z_i = 0$). Thus, the probability distributions for mark a_i in the case of mines and clutter targets can be given by

$$p(a_i | z_i = 1) = g_m(a_i) \tag{3.3-1}$$

$$p(a_i | z_i = 0) = g_c(a_i) \tag{3.3-2}$$

The distributions $g_m(a_i)$ and $g_c(a_i)$ describe mineness and non-mineness measures of the detections based on attributes of the target signature. They are known either in parametric (such as Gaussian with some mean and variance) or some non-parametric forms, such as a neural network output, Bayesian network estimate, or kernel density estimation.

3.4 Spatial Distributions

This research is motivated by some of the previously successful patterned minefield detection approaches and observed patterned and unpatterned minefield laid-out structures. The relative spatial distribution of mines in patterned or unpatterned configurations can be predicted or estimated because these minefields are built for mine recovering or effectiveness. On the other hand, the relative spatial distribution of clutter targets often varies between locations. Therefore, clutter and mine spatial distributions are expected to be from two distinguishable processes. Even though there are conditions under which clutter targets may follow a distinguishable spatial distribution, for the current discussion it is assumed that they are homogeneously Poisson distributed. The distribution of nearest neighbor distances k_i for clutter targets denoted as $f_c(k_i)$ with the clutter rate λ_c in this case is given by [33]

$$f_c\left(k_i\right)=2\lambda_c\pi k_i e^{-\lambda_c\pi k_i^2} \tag{3.4-1}$$

Furthermore, in the non-minefield case a clutter target can be identified as a mine. Clutter targets that are identified as mines by the minefield detection processes are actually false alarms. In this case, the probability distribution for a random clutter detections identified as mines to occur at distance k_i is considered and developed. The probability of the clutter targets identified as mines at distance k_i is given by

$$f_r\left(k_i\right)=\frac{4\pi k_i}{A}\left(1-\frac{\pi k_i^2}{A}\right),\quad \pi k_i^2 < A \tag{3.4-2}$$

The distributions of nearest neighbor distances for patterned mines and unpatterned mines $f_m\left(k_i\right)$ will be discussed in the following sections.

3.4.1 Spatial Distribution of Detections for Patterned Minefields

The clutter targets detected by the anomaly detection process are assumed to follow a spatially identical independent point process with intensity λ_c. To simplify the analysis, assume that the patterned minefield contains only one row of mines with *M* mines in the given minefield segment. The mines are located at an approximately regular interval *s* in the row with a probability of mine detection *p*. The number of detected mines n_m is distributed binomially, given by

$$f(\left|\{z_i=1\}\right|=n_m)=\binom{M}{n_m}p^{n_m}\left(1-p\right)^{M-n_m} \tag{3.4.1-1}$$

The spatial characteristic of the detected mines in the minefield (particularly patterned minefield) can be partially captured using nearest neighbor distances. Let the distance for a target x_i, at location l_i, to its nearest detected target of the same type (mine or clutter target), be represented as k_i. Knowing the location l_j for all detections, the nearest neighbor distance (k_i) for a target is defined as

$$k_i = \min_{j:i\neq j, z_i=z_j} \left\| l_j - l_i \right\| \tag{3.4.1-2}$$

The mines are placed at an approximately regular distance with small variations due to placement, which can be modeled as a Gaussian distribution with zero mean and standard deviation of σ. If the probability of detection for mines in the minefield is given by *p*, the distribution of nearest neighbor distances for mines in patterned minefields denoted as $f_m\left(k_i\right)$ is given based on our development as

$$f_m\left(k_i\right) = \frac{1}{\sigma\sqrt{2\pi}} \sum_{l=1}^{\infty} \left(1-P\right) P^{l-1} e^{-\frac{\left(ls-k_i\right)^2}{2\sigma^2}} \tag{3.4.1-3}$$

where $P \equiv (1-p)^2$ is the probability that both mines on either side of the mine x_i are not detected, $\left(1-P\right)$ is the probability that at least one mine is detected, and *s* is the nominal separation between two mines in a row of mines.

The distributions $f_c\left(k_i\right)$ (Equation (3.4-1)), $f_r\left(k_i\right)$ (Equation (3.4-2)), and $f_m\left(k_i\right)$ (Equation (3.4.1-3)) for representative values are shown in Figure 3.4.1-1:

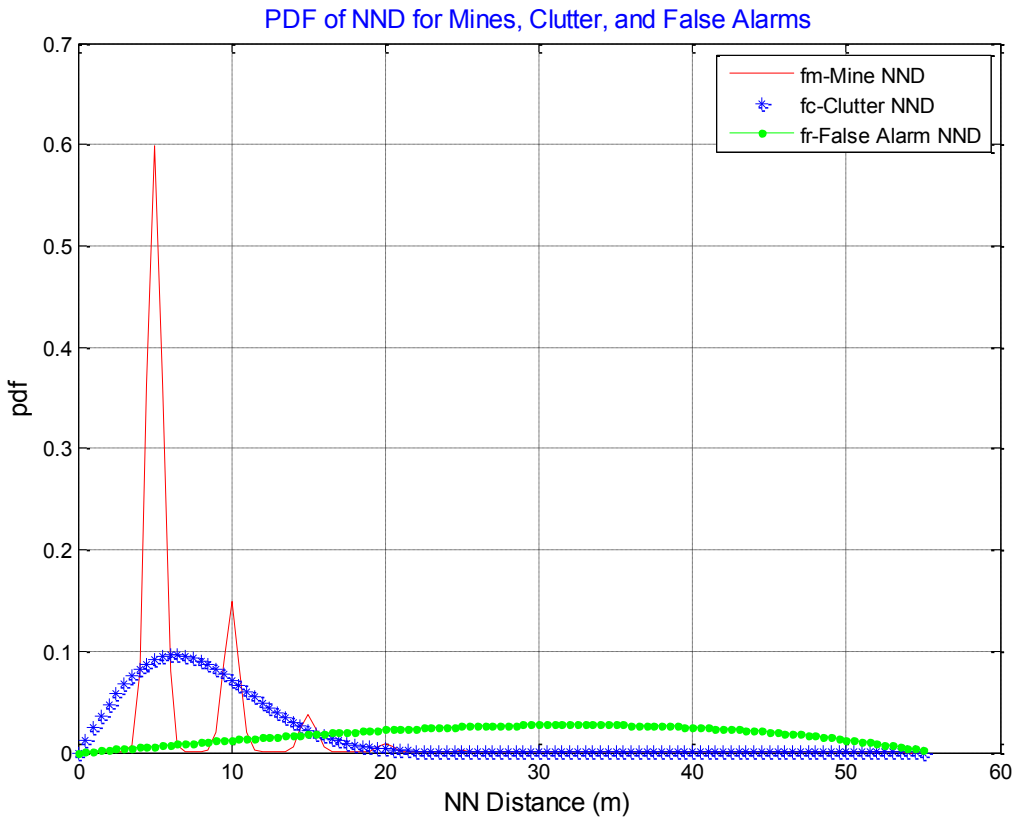

Figure 3.4.1-1 PDF of nearest neighbor distances for mines, clutter targets, and false alarms

3.4.2 Spatial Distribution of Detections for Unpatterned Minefields

The majority of the algorithms implicitly assumes a spatial random layout for mines as well as clutter targets. However, this is not always true. Unpatterned minefields often follow some sort of patterned structures and clutter targets are spatially distributed in patterns in a few cases. In this effort, it is assumed that clutter targets are randomly distributed while unpatterned mines can be either randomly or regularly distributed. The distribution of nearest neighbor distances of randomly (Poisson) distributed mines is

$$f_m\left(k_i\right) = 2\lambda_m \pi k_i e^{-\lambda_m \pi k_i^2} \tag{3.4.2-1}$$

The distribution of nearest neighbor distances of regularly distributed mines is assumed to follow a Gaussian distribution as

$$f_m\left(k_i\right)=\frac{1}{\sqrt{2\pi}\sigma_m}e^{-\left[\left(k_i-\mu_m\right)^2/2\sigma_m{}^2\right]} \tag{3.4.2-2}$$

The distributions $f_c\left(k_i\right)$ (Equation (3.4-1)), $f_r\left(k_i\right)$ (Equation (3.4-2)), and $f_m\left(k_i\right)$ (Equations (3.4.2-1) & (3.4.2-2)) for representative values are shown in Figure 3.4.2-1:

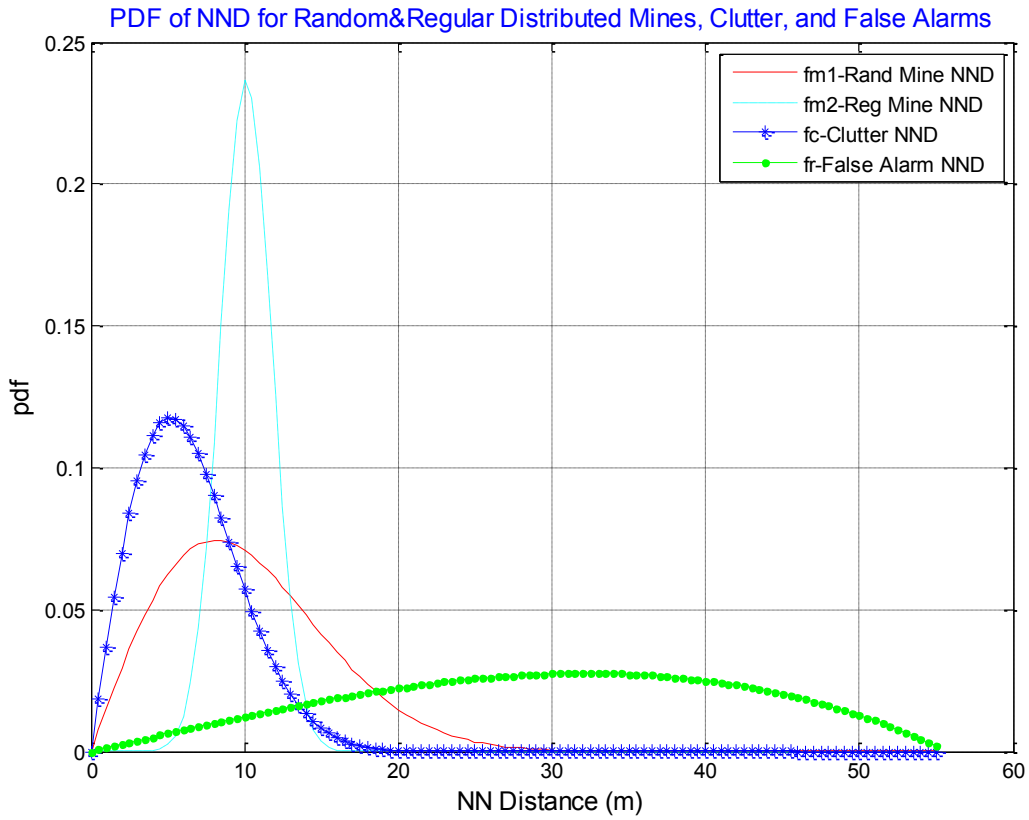

Figure 3.4.2-1 PDF of nearest neighbor distances for random & regular mines, clutter targets, and false alarms

Chapter 4 Baseline Minefield Detection Methods

The use of spatial point statistics in minefield detection is motivated by the fact that the background clutter or clutter targets can often be thought of as a complete random process. Meanwhile, if the mines are present, they will follow different distributions, such as a linear distribution for patterned minefields and a regular distribution for unpatterned minefields. The observed set of targets can be thought of as a mixture point process. In the case of linear pattern minefields where mines are placed at approximately regular intervals, the detection of a mine at a certain location is strongly determined by the locations of other mines in a finite neighborhood. On the other hand, mines in unpatterned minefields can be randomly distributed; however, these unpatterned mines can be formed in a patterned minefield structure such as the "volcano" type [12] where mines are spatially related in two confined areas. Also, when mines are manually positioned, they often tend to be more regularly distributed. The spatial locations among these mines are well related.

A spatial point process (SPP) is a collection of points where each point represents the location of an event in space. An SPP is fully defined by just the locations of the detected targets in the area. In the case of a simple SPP, there is no way to determine whether the detection is a mine or a clutter target, since only detection locations are available. If additional measurements, such as target features or marks, are available at each detection location, then this information can be used to distinguish between mines and clutter targets. For instance, the marks could consist of the features of the detection signature, such as size,

texture features, polarity, etc. An SPP with marks associated with each event is called a marked spatial point process.

The spatial point processes used to describe mine and clutter processes are often Markov in nature in the sense that the occurrence of detection at a given location is fully defined by only the other detections in a local neighborhood. For example, under an assumption of complete randomness for the clutter process, the occurrence of a clutter target is independent of any other detections in its neighborhood (zero-order Markov). In the case of linear pattern minefields where mines are placed at approximately regular intervals, the detection of a mine at a certain location is strongly determined by the locations of other mines in a finite neighborhood. Incorporating the local spatial interactions in a marked point process results in a Markov marked point process. The proposed effort is based on a Markov marked spatial point process formulation. The Markov nature of the point process can be exploited to solve the minefield detection problem more efficiently. Minefield detection under this formulation is discussed in the following subsections.

The spatial point process (SPP) and the spatial point process with false alarm mitigation (SPP-FM) formulations will be discussed in the following sections. Marked point process (MPP) and Markov marked point process (MMPP) formulations will be discussed in the following chapters.

4.1 Spatial Point Process Formulation

A spatial point process (SPP) is a collection of points where each point represents the location of an event in space. An SPP is fully defined by the locations of the detected targets in the area. In the spatial point process (SPP) formulation, the targets are selected by thresholding after anomaly detection. Detection thresholding methods include constant false alarm rate (CFAR) and constant target rate (CTR). CTR is often easy to apply for minefield applications; however, CFAR thresholding is included here for a complete discussion.

4.1.1 SPP-CFAR Formulation for Unpatterned Minefields

In the case of unpatterned minefields, both false alarms and mines are assumed to be randomly distributed. With CFAR thresholding, the threshold is selected in such a way that the clutter rate is given by λ_c. Let the corresponding probability of the detections at this threshold be given by p so that the density of detected mines is given by $p\lambda_m$, where λ_m is the density of actual mines in the segment. In the case of the background segment, all the detections are clutter targets. The number of detections n (a random variable) in the segment A is Poisson-distributed with intensity λ_c. However, in the case of the minefield segment where the detections in observation X include both mines and clutter targets, the density of detected targets in the segment is given by $\lambda_c + p\lambda_m$. The conditional probabilities of observation X under background and unpatterned minefield processes in the SPP formulation with the CFAR thresholding depend only upon the number of detections n. Formulae of these conditional probabilities can be found in our previous publication [32].

4.1.2 SPP-CFAR Formulation for Patterned Minefields

In the case of patterned minefields, clutter targets are randomly distributed while mines are lined up in a row *M*. Since mines in patterned minefield are laid in a row, the first step in most algorithms is to find a narrow linear region in the segment with a relatively large number of targets. This process improves the processing speed by limiting the search area. The linear density algorithm for patterned minefield detection described by Muise and Smith, is similar to the Hough transform, and has been adopted for this implementation [34]. The idea is that only the targets in a narrow row (about five meters wide) are used for minefield decision.

The minefield decision is based on the log-likelihood ratio of the conditional probabilities of observation *X*. The conditional probability of observation X under null hypothesis for patterned minefield case is

$$p_{SPP-CFAR}(X \mid H_0) = \frac{1}{n!} e^{-\lambda_c A} \left(\lambda_c A\right)^n, \quad n = \left|X\right| \tag{4.1.2-1}$$

However, in the case of the minefield segment (non-null hypothesis) where the detections in observation *X* include both mines formed in pattern and clutter targets formed randomly, the conditional probability of observation *X* is given by

$$p_{SPP-CFAR}(X \mid H_1) = \sum_{n_m=0}^{M} \binom{M}{n_m} (p)^{n_m} (1-p)^{(M-n_m)} \frac{1}{(n-n_m)!} e^{-\lambda_c A} \left(\lambda_c A\right)^{(n-n_m)} \tag{4.1.2-2}$$

where *A* is the area of the segment.

4.1.3 SPP-CTR Formulation

For CTR thresholding, all segments have the same number of detections; therefore, SPP-CTR formulation does not give any useful detection result for unpatterned minefields. However, the number of detections in a line for patterned minefields can be used for minefield decision. The conditional probability of observation X for patterned minefield case can be obtained from our previous publication [10].

4.1.4 SPP Detection

Under the SPP formulation, the maximum likelihood estimate (MLE) statistic is simply given by the number of detections *n* for both patterned and unpatterned minefields.

$$\chi_{SPP}(X) = n, \quad n = |X| \tag{4.1.4-1}$$

4.2 Spatial Point Process with False Alarm Mitigation– The Baseline Formulation

An SPP is fully defined by the locations of the detected targets in the area. In the case of a simple SPP, there is no way to determine whether the detection is a mine or a clutter target, since only detection locations are available. If additional measurements, such as target features are available at each detection location, then this information can be used to distinguish mines and possible clutter targets. In recent airborne minefield programs, the minefield decision is based on the false alarm mitigation (FM) after mine detection thresholding of spatial point process or SPP-FM. The minefield performance based on this formulation depends fully on the effectiveness of the FM stage. For the comparison of the algorithm performance, SPP-FM is selected as our baseline algorithm.

4.2.1 SPP-FM CTR Formulation for Unpatterned Minefields

As a result of this false alarm reduction step, only a portion of the detections in X is selected as mines that will be used for the evaluation of the minefield decision. This selected set of targets is called X'. The corresponding number of actual detections n' after the false alarm reduction is a random variable. Assume the resulting density of false alarms (actual clutter targets) is now $\lambda_c' < \lambda_c$ and the corresponding probability of detection is $p' < p$. The conditional probabilities of observation X' according to the binary hypotheses under SPP-FM still depend upon the number of detections n' after false alarm mitigation, and are given by

$$p_{SPP-FM}(X' \mid H_0) = \frac{1}{n'!} e^{-\lambda_c' A} \left(\lambda_c' A\right)^{n'}, \quad n' = \left|X'\right| \tag{4.2.1-1}$$

$$p_{SPP-FM}(X' \mid H_1) = \frac{1}{n'!} e^{-\left(\lambda_c' + p'\lambda_m\right)A} \left(\left(\lambda_c' + p'\lambda_m\right)A\right)^{n'} \tag{4.2.1-2}$$

According to the binary hypotheses under SPP-FM CFAR formulation for unpatterned minefields, the conditional probabilities of observation X' can be derived from the formulae obtained from our previous publication [32].

4.2.2 SPP-FM CTR Formulation for Patterned Minefields

In the following, the development of conditional probabilities for the case where targets are selected by CTR thresholding after anomaly detection is discussed. Similar development will apply for CFAR target selection [10]. For CTR, the anomaly detector threshold is chosen so that the total number of selected targets is a fixed number N. Assume the probability of mine detection at this threshold to be p so that the number of detected

mines n_m in the case of a minefield segment is a random variable that is binomial-distributed with the probability p, as given in Equation (3.4.1-1). The rest of the $N - n_m$ targets will be clutter targets.

In the false alarm (FA) reduction step, only targets with $g_m(a_i) > g_c(a_i)$ are selected for the evaluation of the minefield decision. Let

$$p_{FA} = p\left(g_m(a_i) > g_c(a_i) \middle| \text{FA} \right) \tag{4.2.2-1}$$

$$p_{\text{Mine}} = p\left(g_m(a_i) > g_c(a_i) \middle| \text{mine} \right) \tag{4.2.2-2}$$

The set of targets after false alarm reduction is called *X'*. The corresponding number of actual detections *n'* after the false alarm reduction is a random variable. According to the null and non-null hypotheses under SPP-FM, the conditional probabilities of observation *X'* depend only upon the number of detections *n'*. Formulae of these conditional probabilities can be found in our previous publication [10].

4.2.3 SPP-FM Detection

Under the spatial point process with CTR thresholding and false alarm mitigation (FM), the number of detections *n'* remaining after FM is a Poisson random process under null hypothesis, and a sum of Poisson and binomial under non-null hypothesis. With little effort, the MLE statistic for both CFAR and CTR cases can be obtained as

$$\chi_{SPP-FM}(X) = n', \quad n' = \left| X' \right| \tag{4.2.3-1}$$

where *X'* is a set of detections selected after FM.

Chapter 5 Detection Based on Marked Point Process

With regard to a simple SPP, there is no way to determine whether the detection is a mine or a clutter target, since only detection locations are available. Several current minefield detection architectures have used different false alarm approaches based on target features for false alarm mitigation. These architectures have commonly used the sequential approach that was described in the previous chapter; focused on false alarm mitigation after detection or SPP-FM. The developed approach that will be discussed here does not follow the traditional sequential approach shown in Figure 2.1-1, but it incorporates the target features into the minefield detection process. This process is called a marked spatial point process or MPP. It will be shown that minefield performance based on MPP is better than minefield performance based on the baseline algorithm (SPP-FM) for unpatterned minefields. The patterned minefield performance based on MPP is not evaluated since a reliable detection of minefields without linear pattern is not possible for patterned minefields.

5.1 MPP-CFAR

5.1.1 MPP-CFAR Formulation for Unpatterned Minefields

In the case of a marked point process with CFAR target selection, the targets are obtained using CFAR thresholding after anomaly detection. This case is similar to the SPP case in which the clutter rate is λ_c and the density of detected mines is $p\lambda_m$. However, unlike the SPP case, the detections are identified as mines or clutter targets by the classification

function Z. It is important to note that the classification function Z is not known *a priori*, and should be estimated from the data. Let the total number of detected targets be represented by a random variable n and the number of mines be represented by a random variable n_m. The conditional probabilities of observation X under the null and non-null hypotheses for this case are given by

$$p_{MPP-CFAR}(X \mid H_0, Z) = \frac{1}{n!} e^{-\lambda_c A} \left(\lambda_c A\right)^n \prod_{i=1}^{n} g_c\left(a_i\right), \quad n = \left|X\right| \tag{5.1.1-1}$$

$$p_{MPP-CFAR}(X \mid H_1, Z) = \frac{1}{n_m!} \frac{1}{(n-n_m)!} e^{-p\lambda_m A} e^{-\lambda_c A} \left(p\lambda_m A\right)^{n_m} \left(\lambda_c A\right)^{(n-n_m)} \prod_{i=1}^{n_m} g_m\left(a_i\right) \prod_{i=n_m+1}^{n} g_c\left(a_i\right) \tag{5.1.1-2}$$

5.1.2 MPP-CFAR Detection for Unpatterned Minefields

Using Equations (5.1.1-1) and (5.1.1-2), the minefield likelihood ratio in the case of the MPP-CFAR can be derived as

$$\Lambda_{MPP-CFAR}\left(X \middle| Z\right) = C \binom{n}{n_m} \left(\frac{p\lambda_m}{\lambda_c}\right)^{n_m} e^{-p\lambda_m A} \prod_{i=1}^{n_m} \frac{g_m\left(a_i\right)}{g_c\left(a_i\right)} \tag{5.1.2-1}$$

The corresponding log likelihood ratio from Equation (5.1.2-1) can be written as

$$\ln \Lambda_{MPP-CFAR}\left(X \middle| Z\right) = \ln C \binom{n}{n_m} + n_m \ln\left(\frac{p\lambda_m}{\lambda_c}\right) - p\lambda_m A + \sum_{i=1}^{n_m} d_i^{mc} \tag{5.1.2-2}$$

where d_i^{mc} is a distance metric, and is defined as:

$$d_i^{mc} = \ln\left(g_m\left(a_i\right)\right) - \ln\left(g_c\left(a_i\right)\right) \tag{5.1.2-3}$$

For now, assume that the only unknown parameter is the classification function Z. Then the maximum log-likelihood statistic can be obtained by maximizing Equation (5.1.2-2) with respect to Z. That is,

$$\chi_{MPP-CFAR}\left(X\right) = \max_{Z} \ln \Lambda_{MPP-CFAR}\left(X \middle| Z\right) \tag{5.1.2-4}$$

It is noted that there are 2^n different element combinations in *Z*. An exhaustive search over all these combinations is computationally expansive. Fortunately, the search for an optimal solution can be linearized in n when the values of d_i^{mc} are sorted in descending order. This results in obtaining the number of targets identified as mines (n_m) in the classification function Z . Thus Equation (5.1.2-4) can be rewritten as

$$\chi_{MPP-CFAR}\left(X\right) = \max_{n_m} \ln \Lambda_{MPP-CFAR}\left(\overline{X}\middle|\overline{Z}\right) \tag{5.1.2-5}$$

where $\overline{X}$ and $\overline{Z}$ are such that all the detections are sorted in descending order of the distance metric d_i^{mc} . Since the targets are sorted in descending order, selecting the number of mines n_m automatically implies a classification function $\overline{Z}$, which maximizes the log-likelihood ratio. The number of mines n_m can be between 0 and *n,* provided the search for the optimal classification function is only linear in *n* [32].

5.2 MPP-CTR

5.2.1 MPP-CTR Formulation for Unpatterned Minefields

In the case of the MPP with CTR target selection, a fixed number of targets *N* is selected for all segments using CTR thresholding after anomaly detection. This is similar to the SPP-FM. When the segment contains only background, all detected targets will be clutter targets; however, if it is a minefield segment, the probability of a given target being a mine must be obtained. Assume the probability of mine detection to be p , so that the density

of detected mines is $p\lambda_m$, and the average number of mine detections in the segment of area A is $p\lambda_m A$. Then the probability of a given target being a mine is given by

$$p_{mine} = \frac{p\lambda_m A}{N} \tag{5.2.1-1}$$

Just like the MPP-CFAR case, the classification function *Z* is not known *a priori* and should be estimated from the data. The number of mines n_m in the case of a minefield segment is a random variable that is binomial-distributed with the probability p_{mine}.

The conditional probabilities of observation *X* under null and non-null hypotheses in this case are given by

$$p_{MPP-CTR}(X \mid H_0, Z) = \prod_{i=1}^{N} g_c(a_i), \quad N = |X| \tag{5.2.1-2}$$

$$p_{MPP-CTR}(X \mid H_1, Z) = C\binom{N}{n_m}(p_{mine})^{n_m}(1-p_{mine})^{N-n_m}\prod_{i=1}^{n_m} g_m(a_i)\prod_{i=n_m+1}^{N} g_c(a_i) \tag{5.2.1-3}$$

where

$$C\binom{N}{n_m} = \frac{N!}{(N-n_m)!n_m!}$$

5.2.2 MPP-CTR Detection for Unpatterned Minefields

Using Equations (5.2.1-2) and (5.2.1-3), the minefield likelihood ratio in the case of MPP-CTR can be easily written as

$$\Lambda_{MPP-CTR}(X|Z) = C\binom{N}{n_m}(p_{mine})^{n_m}(1-p_{mine})^{N-n_m}\prod_{i=1}^{n_m}\frac{g_m(a_i)}{g_c(a_i)} \tag{5.2.2-1}$$

Then the log-likelihood ratio is given by

$$\ln\Lambda_{MPP-CTR}(X|Z) = \ln C\binom{N}{n_m} + n_m \ln\left(\frac{p_{mine}}{1-p_{mine}}\right) + N\ln(1-p_{mine}) + \sum_{i=1}^{n_m} d_i^{mc} \tag{5.2.2-2}$$

Similar to the case of MPP-CFAR, the MLE statistic maximized with respect to number of mines n_m is obtained as

$$\chi_{MPP-CTR}\left(X\right)=\max_{n_m}\ln\Lambda_{MPP-CTR}\left(\overline{X}\middle|\overline{Z}\right) \tag{5.2.2-3}$$

where $\overline{X}$ and $\overline{Z}$ are such that all the detections are sorted in descending order of the distance metric d_i^{mc} as defined in Equation (5.1.2-3).

Chapter 6 Detection Based on Markov Marked Point Process

The spatial point processes used to describe mine and clutter processes are often Markov in nature based on the occurrence of detection at a given location is fully defined by only the other detections in a local neighborhood. For example, under an assumption of complete randomness for the clutter process, the occurrence of a clutter target is independent of any other detections in its neighborhood (zero-order Markov). In the case of linear pattern minefields where mines are placed at approximately regular intervals, the detection of a mine at a certain location is strongly determined by the locations of other mines in a finite neighborhood. Incorporating the local spatial interactions in a marked point process results in a Markov marked point process (MMPP). The proposed effort is based on this Markov marked spatial point process formulation. The Markov nature of the point process can be exploited to solve the minefield detection problem more efficiently. Minefield detection under this formulation is discussed in the following sections.

6.1 MMPP-CFAR Formulation

6.1.1 MMPP-CFAR Formulation for Unpatterned Minefields

In the case of a marked point process with CFAR target selection, the targets are obtained using CFAR thresholding after anomaly detection. Assume the probability of mine detection to be p, so that the density of detected mines is $p\lambda_m$, and the average number of mine detections in the segment of area A is $p\lambda_m A$. Let the number of mines be represented by a random variable n_m. The total number of detected targets is represented by a random

variable n. Using the functions and parameters defined in the previous chapters, the conditional probabilities of observation X under the null and non-null hypotheses for this case are given by

$$p_{MMPP-CFAR}(X \mid H_0, Z) = \frac{1}{n!} e^{-\lambda_c A} \left(\lambda_c A\right)^n \prod_{i=1}^{n_m} \left(g_c\left(a_i\right) f_r\left(k_i\right) \right) \prod_{i=n_m+1}^{n} \left(g_c\left(a_i\right) f_c\left(k_i\right) \right) \tag{6.1.1-1}$$

$$\begin{aligned} p_{MMPP-CFAR}(X \mid H_1, Z) = {} & \frac{1}{n_m!} \frac{1}{(n-n_m)!} e^{-p\lambda_m A} e^{-\lambda_c A} \left(p\lambda_m A\right)^{n_m} \left(\lambda_c A\right)^{(n-n_m)} \\ & \prod_{i=1}^{n_m} g_m\left(a_i\right) f_m\left(k_i\right) \prod_{i=n_m+1}^{n} g_c\left(a_i\right) f_c\left(k_i\right) \end{aligned} \tag{6.1.1-2}$$

6.1.2 MMPP-CFAR Formulation for Patterned Minefields

In the case of MMPP-CFAR formulation for patterned minefields, the targets are selected by CFAR thresholding after anomaly detection. Let the identity of a detection as a mine or non-mine be captured in the classification function Z, where the classification function Z is not known *a priori* and should be estimated from the data. Given the classification function Z, it is straight forward to calculate the nearest neighbor distances for each of the targets. This nearest neighbor distance can be considered as an independent evaluator of the spatial configuration of the detections. Also, the target attribute captures the likelihood of the target to be a mine through the mineness measure $g_m\left(a_i\right)$ and non-mineness measure $g_c\left(a_i\right)$.

Using the functions and parameters defined in the previous chapters, the conditional probability for the null-hypothesis H_0 with the nearest neighbor distance term included is defined as

$$p_{MMPP-CFAR}(X \mid H_0, Z) = \frac{1}{n!} e^{-\lambda_c A} (\lambda_c A)^n \prod_{i=1}^{n_m} \left(g_c(a_i) f_r(k_i) \right) \prod_{i=n_m+1}^{n} \left(g_c(a_i) f_c(k_i) \right) \quad (6.1.2\text{-}1)$$

The corresponding conditional probability of observation X under the non-null hypothesis H_1 for patterned minefields is defined as

$$p_{MMPP-CFAR}(X \mid H_1, Z) = \binom{M}{n_m} (p)^{n_m} (1-p)^{(M-n_m)} \frac{1}{(n-n_m)!} e^{-\lambda_c A} (\lambda_c A)^{(n-n_m)} \prod_{i=1}^{n_m} \left(g_m(a_i) f_m(k_i) \right) \prod_{i=n_m+1}^{n} \left(g_c(a_i) f_c(k_i) \right) \quad (6.1.2\text{-}2)$$

6.2 MMPP-CTR Formulation

6.2.1 MMPP-CTR Formulation for Unpatterned Minefields

In the case of the MMPP with CTR target selection, a fixed number of targets N is selected for all segments. Assume the probability of mine detection to be p, so that the density of detected mines is $p\lambda_m$, and the average number of mine detections in the segment of area A is $p\lambda_m A$. Then the probability of a given target being a mine is given by

$$p_{mine} = \frac{p\lambda_m A}{N} \quad (6.2.1\text{-}1)$$

Using the functions and parameters defined in the previous chapters, the conditional probabilities of observation X for unpatterned minefields are

$$p_{MMPP-CTR}(X \mid H_0, Z) = \prod_{i=1}^{n_m} \left(g_c(a_i) f_r(k_i) \right) \prod_{i=n_m+1}^{N} \left(g_c(a_i) f_c(k_i) \right) \quad (6.2.1\text{-}2)$$

$$p_{MMPP-CTR}(X \mid H_1, Z) = C\binom{N}{n_m}\left(p_{mine}\right)^{n_m}\left(1-p_{mine}\right)^{N-n_m} \prod_{i=1}^{n_m}\left(g_m\left(a_i\right) f_m\left(k_i\right)\right) \prod_{i=n_m+1}^{N}\left(g_c\left(a_i\right) f_c\left(k_i\right)\right) \tag{6.2.1-3}$$

where $$C\binom{N}{n_m} = \frac{N!}{(N-n_m)!\,n_m!}$$

6.2.2 MMPP-CTR Formulation for Patterned Minefields

In regards to MMPP with CTR target selection, a fixed number of targets N are selected for all segments using CTR thresholding after anomaly detection. The number of mines n_m in the case of a minefield segment is still a random variable that is binomial-distributed with the probability of mine detection, p. Using the functions and parameters defined in the previous chapters, the conditional probabilities of observation X under null and non-null hypotheses in this case are given by

$$p_{MMPP-CTR}(X \mid H_0, Z) = \prod_{i=1}^{n_m}\left(g_c\left(a_i\right) f_r\left(k_i\right)\right) \prod_{i=n_m+1}^{N}\left(g_c\left(a_i\right) f_c\left(k_i\right)\right) \tag{6.2.2-1}$$

$$p_{MMPP-CTR}(X \mid H_1, Z) = \binom{M}{n_m}(p)^{n_m}(1-p)^{(M-n_m)} \prod_{i=1}^{n_m}\left(g_m\left(a_i\right) f_m\left(k_i\right)\right) \prod_{i=n_m+1}^{N}\left(g_c\left(a_i\right) f_c\left(k_i\right)\right) \tag{6.2.2-2}$$

Chapter 7 Comparative Performance for Patterned Minefield Detection

7.1 MMPP-CFAR Detection

Starting with Equations (6.1.2-1) and (6.1.2-2), and assuming that the nearest neighborhood distances for false alarms are calculated with respect to all detections *n*, the log-likelihood function for patterned minefields can be obtained as

$$\begin{aligned}\ln \Lambda_{MMPP-CFAR}\left(X\middle|Z\right) &= \ln C\binom{M}{n_m} + \ln\frac{n!}{(n-n_m)!} + n_m \ln\left(\frac{p}{(1-p)\lambda_c A}\right) + M\ln(1-p) \\ &+ \sum_{i=1}^{n_m}\left(\ln\left(g_m\left(a_i\right)\right) - \ln\left(g_c\left(a_i\right)\right)\right) + \sum_{i=1}^{n_m}\left(\ln\left(f_m\left(k_i\right)\right) - \ln\left(f_r\left(k_i\right)\right)\right)\end{aligned} \tag{7.1-1}$$

where $f_r\left(k_i\right)$ is given by Equation (3.4-2) and $f_m\left(k_i\right)$ is given by Equation (3.4.1-3); other functions and parameters can be found in the previous chapters. For now, assume that the only unknown parameter is the classification function *Z*. Then the maximum log-likelihood statistic can be obtained by maximizing Equation (7.1-1) with respect to *Z*. That is,

$$\chi_{MMPP-CFAR}\left(X\right) = \max_{Z} \ln \Lambda_{MMPP-CFAR}\left(X\middle|Z\right) \tag{7.1-2}$$

Unlike the case of unpatterned minefields for the MPP, there is no algorithm with linear complexity to maximize the log-likelihood ratio in Equation (7.1-2) over all possible configurations of *Z*. The reason is that the last term of Equation (7.1-1) depends on the identity of all mines, since the nearest neighborhood distance k_i is the distance to the other detections, which are also called mines. An approximate solution can be obtained by selecting pairs of detections as mines, and then adding individual detections to the

configuration using a greedy search strategy. The resulting algorithm is at least $O(n^2)$ in computational complexity.

7.2 MMPP-CTR Detection

The minefield log-likelihood ratio in the case of MMPP-CTR can be easily written as

$$\begin{aligned}\ln\Lambda_{MMPP-CTR}\left(X\middle|Z\right) &= \ln C\binom{M}{n_m} + n_m\ln(p) + (M-n_m)\ln(1-p) \\ &+ \sum_{i=1}^{n_m}\left(\ln\left(g_m(a_i)\right) - \ln\left(g_c(a_i)\right)\right) + \sum_{i=1}^{n_m}\left(\ln\left(f_m(k_i)\right) - \ln\left(f_r(k_i)\right)\right)\end{aligned} \tag{7.2-1}$$

where functions and parameters can be found in the previous chapters.

Similar to the case of MMPP-CFAR, the MLE statistic maximized with respect to Z is

$$\chi_{MMPP-CTR}(X) = \max_{Z}\left\{\ln\Lambda_{MMPP-CTR}(X)\right\} \tag{7.2-2}$$

7.3 Estimation of Minefield Parameters

The probability distribution of observation X under the MMPP formulation for patterned minefields depends on the clutter rate λ_c, probability of detection for mine p and number of mines in a row (M), which in turn depends on the mine separation s, and row separation (r) along with the classification function Z. While the clutter rate is known in the case of CFAR target selection, it is not a parameter in the case of CTR target selection. Thus, the unknown parameters of interest in defining the probability distribution of X are p, s, and r for the patterned minefield. Hence, these parameters need to be estimated. The distance between mines is not known exactly due to mine placement strategies for different minefields, drift due to soil shifting, and imprecision inherent in the imaging technology; the

probability of mine detection is often not known and the number of rows changes for operational effectiveness.

Thus, MLE solution needs to optimize over the values of p, s, and r. These parameters need to be estimated along with the classification function Z for both MMPP-CFAR and MMPP-CTR. One way to do this is to use the iterative expectation maximization (EM) solution [31] in which initial estimates of probability of detection $p = p^*$, mine distance $s = s^*$, and number of rows $r = r^*$ are selected. The initial selection of these parameters can be based on prior knowledge or nominal values. The MLE solution for optimal classification function $Z=Z^*$ can be described as

$$Z^* = \arg\max_{Z} \left\{ \ln \Lambda \left(X \middle| \left(p = p^*, s = s^*, r = r^* \right), Z \right) \right\} \tag{7.3-1}$$

Given the solution for Z, the maximum likelihood solution for p, s, and r is obtained by maximizing the log-likelihood with respect to p, s, and r, with fixed $Z=Z^*$. The resulting estimates of $p = p^*$, mine distance $s = s^*$, and number of rows $r = r^*$ are used to recalculate Z^*. The two steps are repeated until a convergence is achieved. The resulting solution maximizes the log-likelihood ratio with respect to p, s, r, and Z, and the maximum likelihood statistic is obtained as

$$\chi(X) = \max_{Z,p,s,r} \ln \Lambda_{MMPP} \left(X \middle| (p,s,r), Z \right) \tag{7.3-2}$$

The solutions for the optimal p^* and s^* for a given $Z=Z^*$, for the Markov marked point processes applicable to both the CFAR and CTR cases, are obtained in two steps by first estimating the optimal mine distance followed by probability of detection. The mine

distance is obtained as the wavelength of the first harmonic of the histogram of the mine-to-mine distances between the mine targets in the classification function Z^*. The probability of detection is calculated as

$$p^* = \frac{s^* n_m}{L} \tag{7.3-3}$$

where L is the length of the row of mines as seen in the segment.

For multiple rows of mines, the Hough line detector is used to detect a row with the most mines and find a row or multiple rows close to the first row or close to each other that are parallel to the best row. By using the distance between these rows that is roughly known or estimated from the data, the detected rows are selected or rejected.

7.4 Improvement of Computational Speed - Hough Line Detector

Since mines in patterned minefields are laid in a row, the first step in most algorithms is to find a narrow linear region in the field segment with a relatively large number of targets. The linear density algorithm for patterned minefield detection described by Muise and Smith, is similar to the Hough transform, and has been adopted for this implementation [34]. The idea is that only the targets in a narrow row (about five meters wide) are used for minefield decision. For the SPP, the line detector was applied on all targets detected by the anomaly detector; while for the SPP-FM, the line detector was applied after anomaly detection and false alarm mitigation. In the case of MMPP, the line detector was applied to identify the initial set of mine targets. The main reason to use the line detector in the case of SPP or SPP-FM is to establish the minefield detection baseline

while the main reason to use the line detector in the case of MMPP is to improve the processing speed. Evaluation of the line detector's performance with respect to the number of mines in a segment, mine Pd, false alarm or clutter density, and deviations from collinearity, is beyond the scope of this research. However, for now it suffices to point out that the same line detector is used as a pre-process for all detection algorithms.

7.5 Simulation Procedure

In this effort, the performance comparison of the minefield detection algorithms for both CFAR and CTR types of thresholding is accomplished using simulated data. The data is simulated as expected after the corresponding thresholding of the anomaly detector statistics. The dimensions for a segment (an interrogation area) are selected as per a three-step by seven-swath collection in a step-staring mode. A few thousand minefield and background segments with appropriate numbers of mines and false alarms are generated based on the binomial and Poisson distributions for both minefield and background segments, respectively.

For each detected target after thresholding, a set of feature attributes is assigned. In general, multiple attributes of the target signatures are calculated. However, to keep the analysis simple, only one attribute, the target size, is used. It is noted that the identity or the number of attributes used is not important; however, the metric of "mineness" and "non-mineness," defined based on these attributes, is important. For the current simulations, assume that the target size is distributed normally with mean and standard deviation of μ_m

and σ_m for mine targets, and μ_c and σ_c for clutter targets, respectively, so that the "mineness" and "non-mineness" measures for any detection with target size a_i are

$$g_m(a_i) = \frac{1}{2\pi\sigma_m} e^{-(a_i-\mu_m)^2/2\sigma_m^2} \tag{7.5-1}$$

$$g_c(a_i) = \frac{1}{2\pi\sigma_c} e^{-(a_i-\mu_c)^2/2\sigma_c^2} \tag{7.5-2}$$

A Gaussian distribution for illustration is assumed below; however, these equations are equally applicable to either parametric or non-parametric distributions for the "mineness" and "non-mineness" measures of the target signatures.

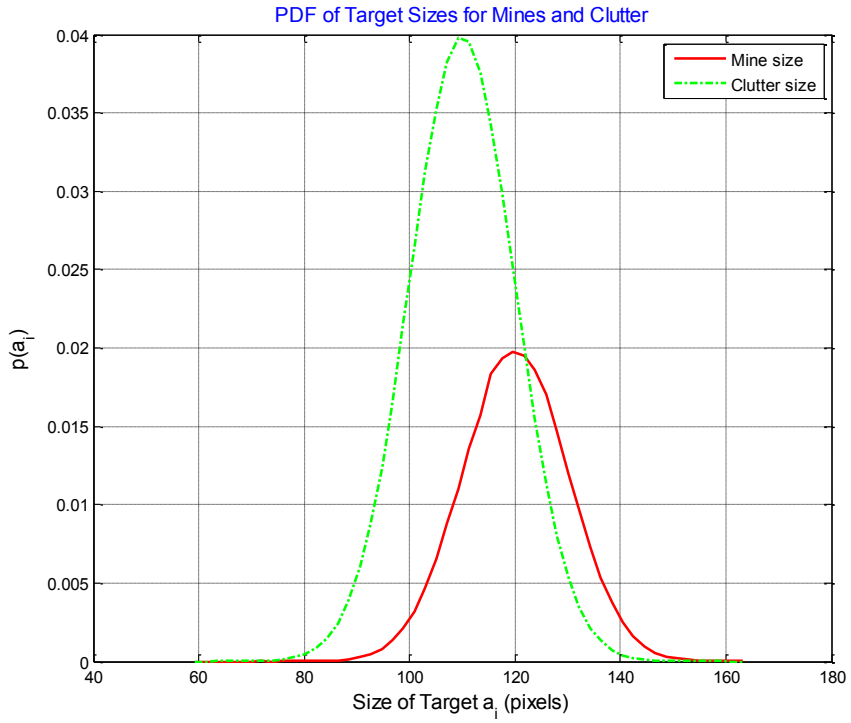

Figure 7.5-1 Example of relative distributions of mine and clutter sizes

To simulate patterned minefield and background segments, two sets of parameters, summarized in Table 7.5-1, have been used. The dimensions of each simulated segment are 70 m *x* 140 m. Dataset 1 represents a case with a moderate clutter rate of 0.004. The separation between mine size and clutter target size in this case is one standard deviation (10 pixels). Dataset 2 represents a case with a higher clutter rate of 0.008. The separation between mine and clutter target sizes is one and a half standard deviations (15 pixels).

Table 7.5-1 Two sets of parameters used to simulate patterned minefields and backgrounds

Parameters	**Values**		**Comments**
	Dataset 1	**Dataset 2**	
Area (A)	9800	9800	m^2 (swath=70*depth=140)
Clutter Rate (λ_c)	0.004	0.008	#clutter target per m^2
Mine PD (p)*	0.6	0.6	also estimated
CTR (N)	40	79	#target per segment
No of Mines per Segment	varies	varies	# mines are always less than #clutter targets
No of Clutter Target per Segment	39.2	78.4	# clutter targets
Mine Size Mean (μ_m)	120	125	pixels
Mine Size Std (σ_m)	10	10	pixels
Clutter Size Mean (μ_c)	110	110	pixels
Clutter Size Std (σ_c)	10	10	pixels
Mine Distance, s	5	5	m; also estimated
Mine Location Std	0.25	0.25	m

* p is the probability of mine detection. For p=0.6, an airborne system can only detect an average of 60% of mines presented in the minefield segments.

7.6 Results and Discussions of Single-Line Minefield Segments

Figure 7.6-1 illustrates the patterned minefield detection concept between the baseline algorithm (SPP-FM) and the developed algorithm based on MMPP model, while Figure 7.6-2 illustrates a few examples of detection performance results of MMPP on

background and minefield segments based on the parameter values shown in Table 7.5-1. Figures 7.6-3 and 7.6-4 show the comparative performance results among SPP-FM, MMPP, and MMPP-EM (where parameters are estimated from the data).

In Figure 7.6-1, the left top figure shows a segment with the number of detections where mines are on along the 'red' line and the remainders are clutter targets. The baseline (SPP-FM) algorithm accounts for all of the detections after false alarm mitigation that form a straight line. In this example, there are three such lines. SPP-FM will call these lines as the three rows of mines. The result is not correct since only one row is actually a mine row. On the other hand, the right top figure shows the minefield decision is not only based on the straight line as the baseline, but also on the features of the detected targets (features are shown in different shapes and colors; in this example, mine-like features are shown by yellow triangles while clutter features have different shapes and colors). The detection result shows only one mine row. The concept is also illustrated on the real image segment that is shown at the bottom of Figure 7.6-1. In this bottom figure, the yellow circles are the detections generated by the mine detection algorithm such as the 'RX' detector. The results indicate that the SPP-FM calls three rows in the image segment to be patterned minefields while the MMPP calls only one patterned minefield. The MMPP rejects the other two rows because the spatial distance among the detection is not correct or the probability of detection is not high enough.

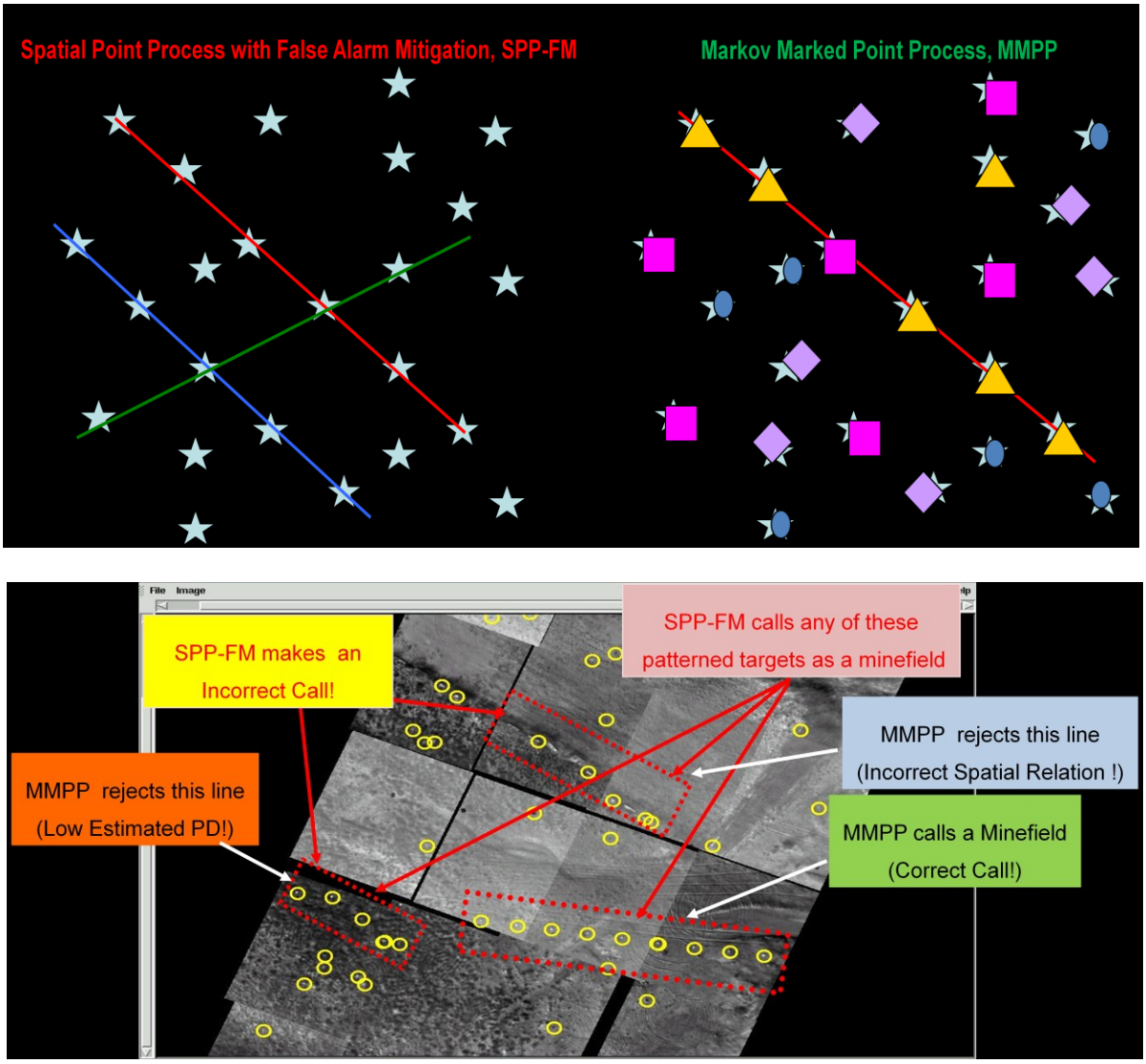

Figure 7.6-1 Illustration of patterned minefield detection concept between the baseline and the developed algorithms

Figure 7.6-2 shows four examples of simulated background and minefield segments for the case of CFAR thresholding for Datasets 1 and 2. The clutter target locations are identified by the green circles, while the mine truth locations are identified by a red '*x*' for convenience. The MMPP with EM algorithm was used for detection on these segments. There are two false alarms identified by red diamonds on the background segments and

100% mine detection identified by red diamonds with the red crosses on the minefield segments.

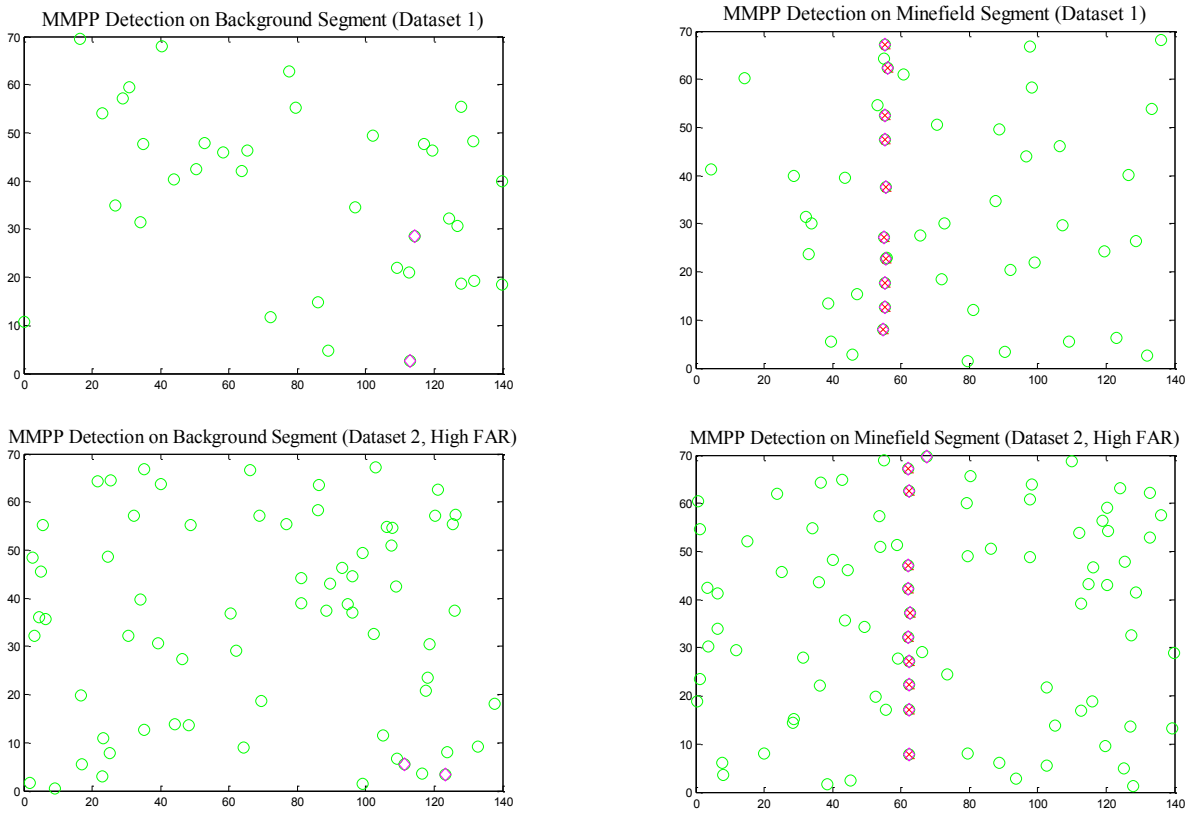

Figure 7.6-2 Detection performance based on MMPP with EM algorithm, results for background (left) and minefield (right) segments, (top) low clutter rate (0.004), (bottom) high clutter rate (0.008)

Figures 7.6-3 and 7.6-4 show patterned minefield performance results for two different clutter rates and two different thresholding methods based on 5000 segments which are equivalent to 49 km^2 (please see Table 7.5-1for other parameters). The performance in blue was generated by MMPP, assuming that both Mine PD and Mine Distance were known. The performance in green was generated by MMPP-EM in which both Mine PD

and Mine Distance were estimated by the EM algorithm. These performance results are extremely close; thus, MMPP with EM can be used in general situations. The performance in red was the baseline SPP after false alarm mitigation (FM). Its performance is the lowest. A significant improvement in minefield detection performance for the same level of minefield-level false alarm rate (Minefield FAR) is illustrated using the MMPP formulation, as compared to the baseline false alarm mitigation approach (SPP-FM).

Figures 7.6-3 and 7.6-4 display the patterned minefield performance results for single- row minefield segments based on the clutter rate (MineFar) of 0.004 and one standard deviation (σ) of target size separation between mine and clutter target. Figure 7.6-3 shows the result based on CFAR thresholding, while Figure 7.6-4 shows the result based on CTR thresholding.

Figures 7.6-5 and 7.6-6 reveal the patterned minefield performance results based on the clutter rate (MineFar) of 0.008 and $1.5\,\sigma$ of target size separation between mine and clutter target. Figure 7.6-5 shows the result based on CFAR thresholding, while Figure 7.6-6 illustrates the result based on CTR thresholding.

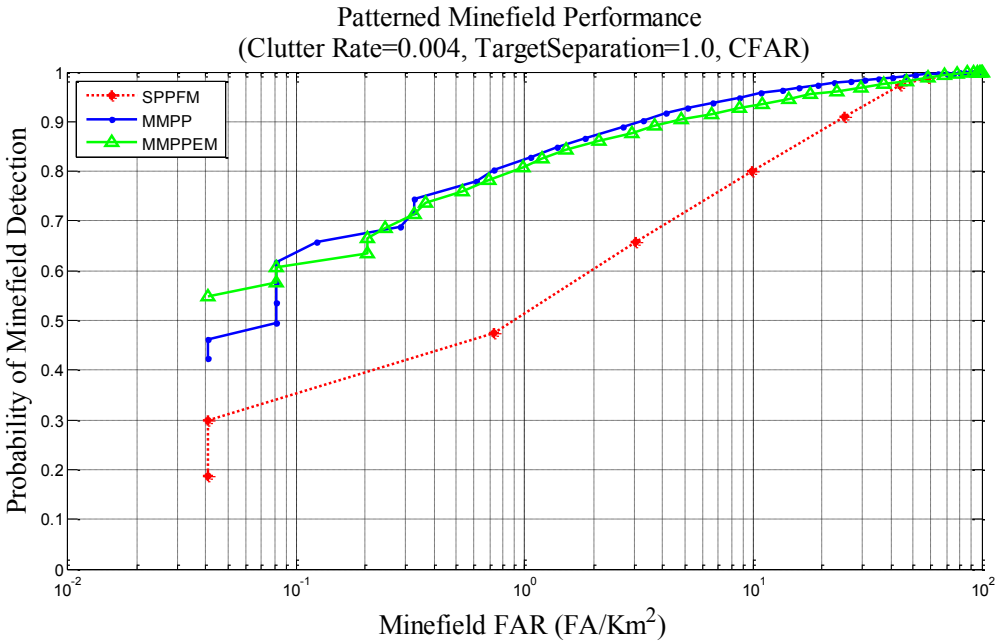

Figure 7.6-3 Patterned minefield performance for clutter rate of 0.004 and target size separation of one standard deviation using CFAR thresholding

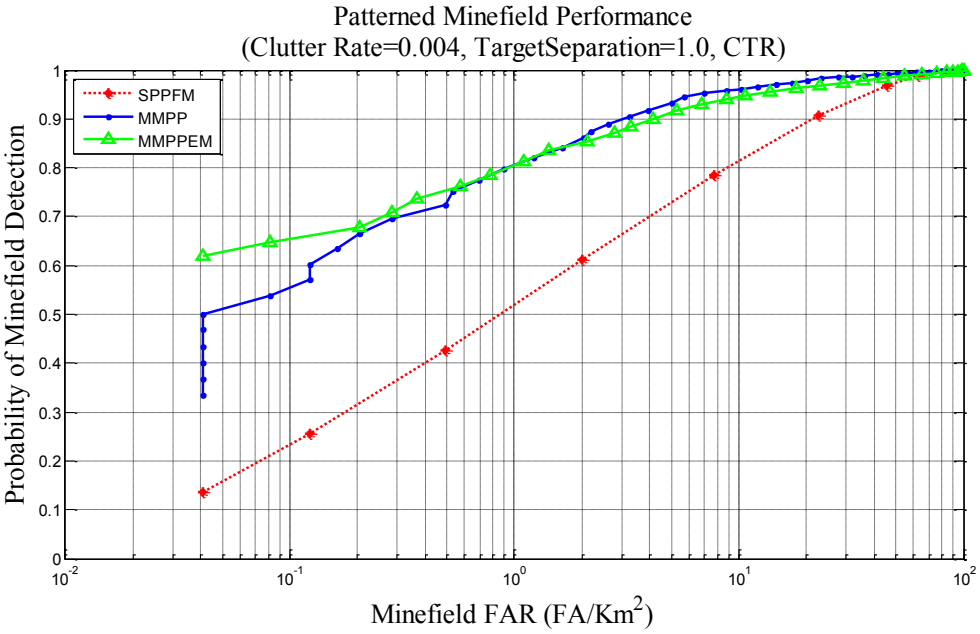

Figure 7.6-4 Patterned minefield performance for clutter rate of 0.004 and target size separation of one standard deviation using CTR thresholding

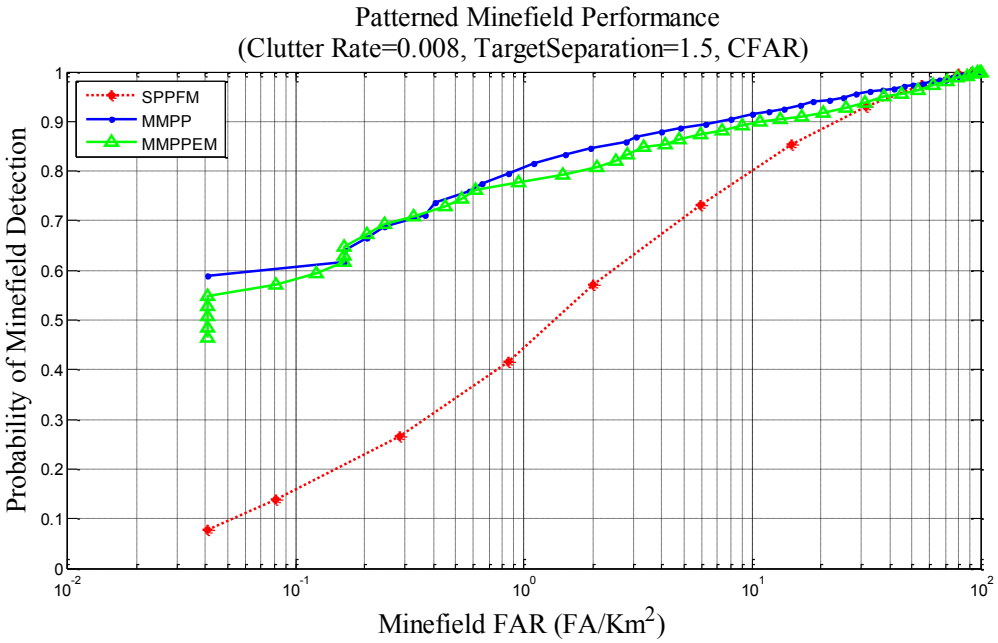

Figure 7.6-5 Patterned minefield performance for clutter rate of 0.008 and target size separation of one and a half standard deviation using CFAR thresholding

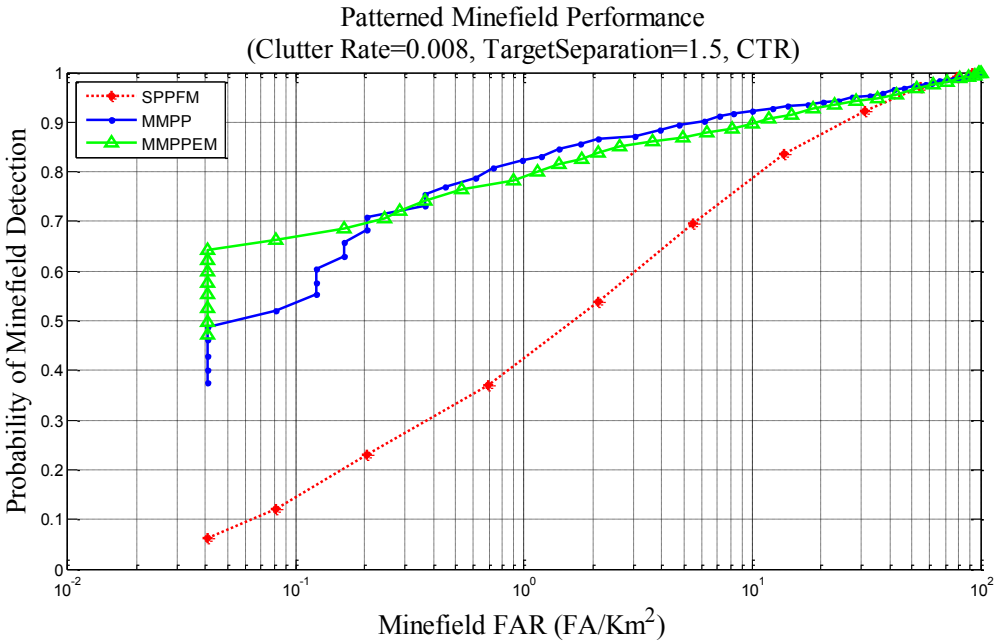

Figure 7.6-6 Patterned minefield performance for clutter rate of 0.008 and target size separation of one and a half standard deviation using CTR thresholding

Comparing the minefield performance results between the two datasets, the two most important parameter differences between them are the mean target size (μ_m) and the clutter rate. The clutter rate in Dataset 2 increases two-fold. This results in reducing the minefield performance for Dataset 2 as compared to Dataset 1. However, the separation between the mean target sizes of mines and clutter targets in Dataset 2 is one and a half more than the separation in the case of Dataset 1, which results in better minefield detection performance for Dataset 2. Thus, a slightly larger separation between mine sizes and clutter target sizes is sufficiently overcome by the negative influence of a higher clutter rate in Dataset 2. Also, these figures show that the minefield performance results using CTR and CFAR thresholding methods are similar.

7.7 Results and Discussions of Single and Multiple Lines Minefield Segments

In this exercise, target spatial distributions for patterned minefields containing one, two, and three mine rows are explored. An algorithm for the automatic detection of a number of rows of mines is developed and demonstrated. The minefield performance of single, double, triple mine rows, and automatic mine row detection at different mine false alarm rates is also evaluated. To simulate patterned minefield and background segments, a set of parameters is employed as summarized in Table 7.7.1. The dimensions of each simulated segment are 70 m *x* 140 m. The separation between mine and clutter target sizes is one standard deviation (10 pixels). Different clutter rates are used.

Table 7.7-1 Parameters used to simulate patterned & unpatterned minefields and backgrounds

Parameters		
	Values	**Comments**
Area (A)	9800	m^2 (swath=70*depth=140)
Clutter Rate (λ_c)	0.006, 0.008	#clutter target per m^2
Mine PD (p)	0.6	also estimated
CTR (N)	59, 79	#targets per segment
No. of Mines per Segment	Varies	#mines are always less than #clutter targets
Mine Size Mean (μ_m)	120	pixels
Mine Size Std (σ_m)	10	pixels
Clutter Size Mean (μ_c)	110	pixels
Clutter Size Std (σ_c)	10	pixels
Mine Distance, s	5	m; also estimated (patterned only)
Mine Location Std	0.25	m (patterned only)
Mine Row Separation	15	m; also estimated (patterned only)
Mine Density	0.004	#mines per m^2 (unpatterned only)

Figures (7.7-1) through (7.7-6) show excellent mine and minefield performance results of 1-row, 2-rows, and 3-rows segments using the MMPP with automatic mine row detection algorithm. The results were based on a high clutter rate of 0.008 or the constant target rate (CTR) of 79 (except Figure 7.7-5 where the clutter rate of 0.006 was used) and the mean difference between mine size and clutter target size is one standard deviation. In Figures (7.7-1) through (7.7-4), green circles represent clutter targets that went through the mine detection algorithm, green circles with red crosses are mine ground truths, and red diamonds are detections detected by the MMPP algorithm. These figures show emplaced mines are missing in many places in their rows, which are based on the assumption that only 60% of mines on an average are detected. Figure (7.7-1) displays one row minefield segment in which 9 out 10 mines were detected with only one false alarm and one missed

detection by the MMPP algorithm, while Figure (7.7-2) shows 100% mine detection with no false alarm. Figure (7.7-3) shows the performance result of a two-row minefield segment with 100% mine detection with two false alarms, while Figure (7.7-4) shows the performance result of a three-row minefield segment with 86% mine detection with one false alarm. Figures (7.7-5) and (7.7-6) illustrate the excellent minefield performance results of 1, 2, 3, and all-row minefield segments based on the clutter rates of 0.006 and 0.008, respectively. The definitions of the 1, 2, 3, and all-row minefield segments will be explained.

Using the clutter rates of 0.006 and 0.008 and mine Pd of only 60% to generate these minefield and background segments (assuming only one standard deviation separation between mines and clutter targets), excellent performance results were obtained for both mines and minefields, which show the robustness of the developed algorithm based on MMPP in the highly cluttered environment.

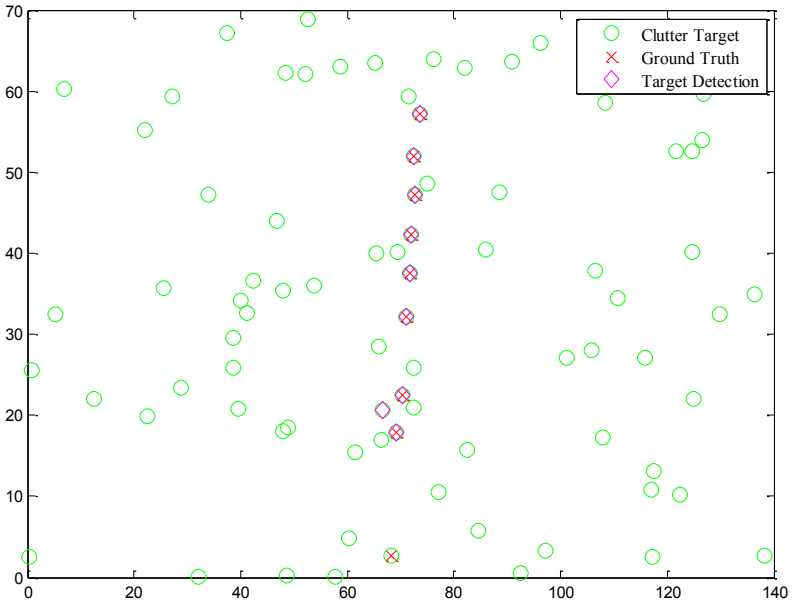

Figure 7.7-1 MMPP detects a single mine-row segment with 90% mine detection with one false alarm

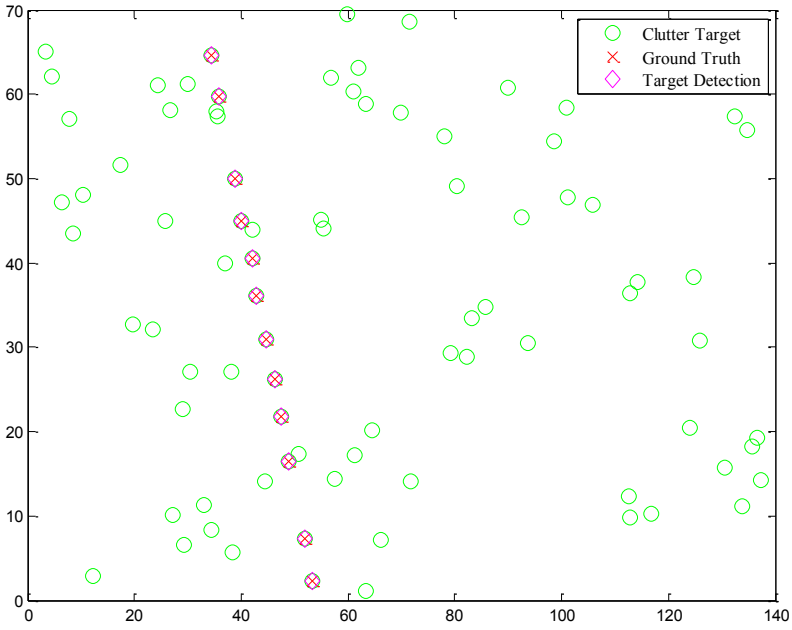

Figure 7.7-2 MMPP detects a single mine-row segment with 100% mine detection with no false alarm

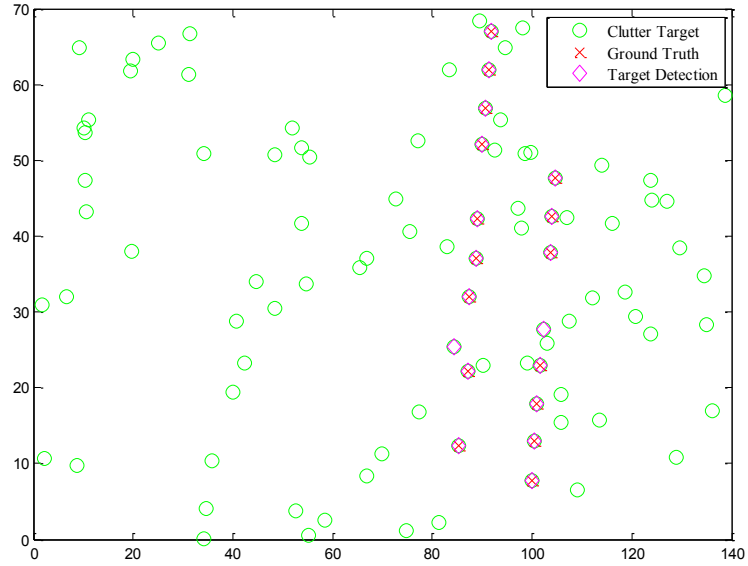

Figure 7.7-3 MMPP detects a double mine-rows segment with 100% mine detection with two false alarms

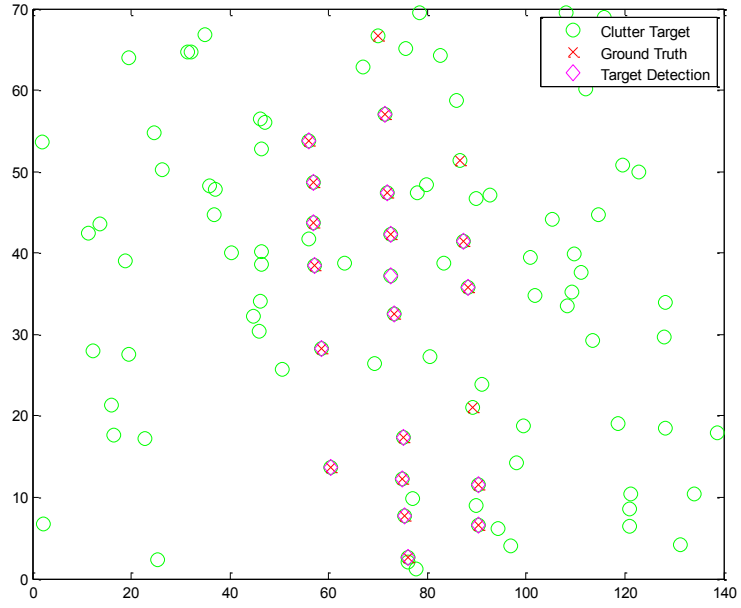

Figure 7.7-4 MMPP algorithm automatically detects a triple mine-rows segment with 86% mine detection with one false alarm

Figures 7.7-5 and 7.7-6 show the patterned minefield performance of 1-row, 2-rows, 3-rows, and all-rows minefield detection algorithms using both target attributes and target spatial distribution (i.e., MMPP) based on the clutter rates of 0.006 and 0.008, respectively. Each of these results was generated using 6000 minefield and background segments, and CTR thresholding was selected. The results are based on the assumptions that the number of one, two, and three mine rows was generated equally for the minefield segments, and the number of detected mines was many times less than the number of clutter targets. As examples, based on the clutter rate of 0.006, there are 9 mines but 50 clutter targets for a single row patterned minefield segment, 18 mines but 41 clutter targets for a 2-rows patterned minefield segment, and 27 mines but 32 clutter targets for a 3-rows patterned minefield segment. It is defined that the 1-row algorithm detects one row of mines regardless of the number of rows formed from the minefield segments. The definitions of 2 and 3-rows algorithms are as similar as the definition of the 1-row algorithm. However, the all-rows algorithm automatically detects the number of rows presented in the minefield segments. In Figures 7.7-5 and 7.7-6, the results show that the all-rows minefield detection algorithm works well at a low minefield-level false alarm rate of 0.1 minefield per km^2 or 1 false minefield per 10 km^2 at the minefield detection probabilities of 70% for the clutter rate of 0.008 and 82% for the clutter rate of 0.006. It is evident that the developed minefield detection algorithm for the MMPP model and the developed automatic mine-row detection algorithm work well under cluttered environments. These algorithms should be used for patterned minefield detection. Comparative minefield performance among other minefield processes for single row minefield segments can be found in our previous publication [10].

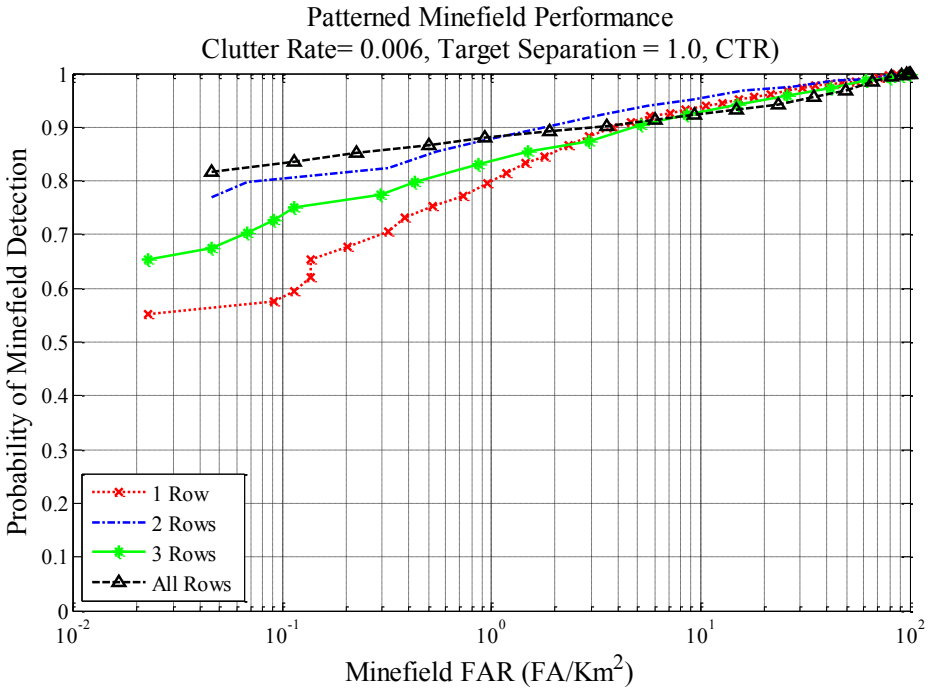

Figure 7.7-5 Minefield performance of MMPP on different mine rows using the clutter rate of 0.006

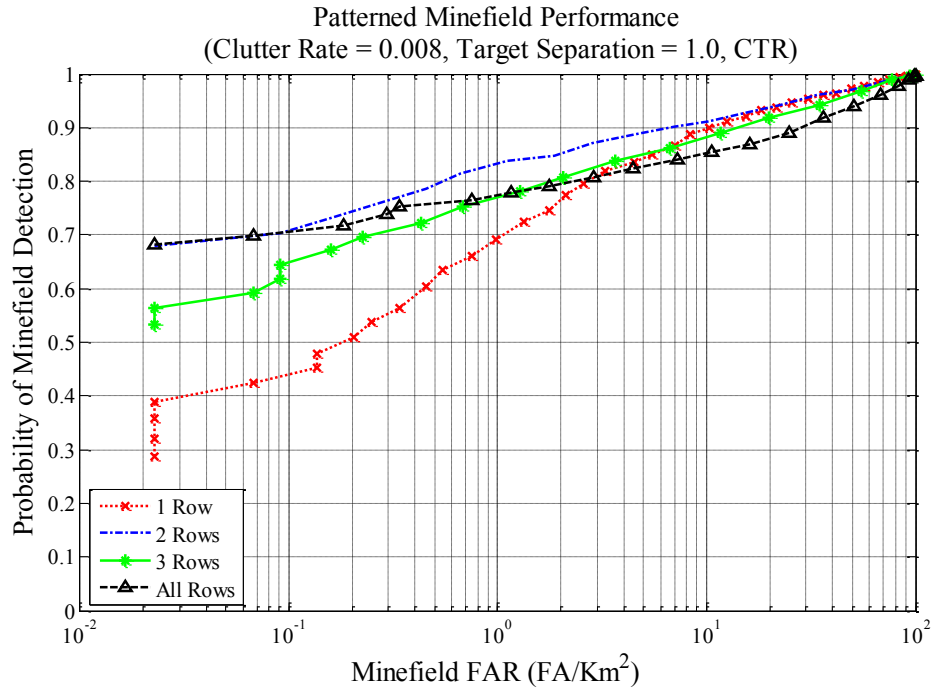

Figure 7.7-6 Minefield performance of MMPP on different mine rows using the clutter rate of 0.008

The following figures (7.7-7 through 7.7-14) were obtained from a video in which detection results of each segment were saved and used for illustration. Each figure consists of the detection results of the baseline algorithm (SPP-FM) and the developed algorithm based on Markov Marked Point Process (MMPP) framework using the parameters estimated from Estimation and Maximization algorithm (EM). Each figure shows the mine detection performance as well as the minefield decision based on the likelihood values of these algorithms on each minefield or background segment. These performance results were based on the high clutter rate of 0.008 and the tight tolerance of one standard deviation between mine and clutter sizes used as their spectral feature. It is noted that the current patterned minefield algorithm makes its decision based on the most mines on a row regardless of how many rows of mines formed the minefield segment. In this development, the likelihood value of the baseline algorithm (SPP-FM) has accounted for all the detected mines whether mines are formed in one or many rows. This strategy is used to ensure a fair performance comparison when the MMPP-EM is developed to automatically detect the number of rows and its likelihood value has accounted for all mines in all detected rows.

The number on top of each figure indicates the sequential number of a complete run, which consists of a few thousand segments. Only some samples are shown here for illustration purposes. Each figure shows the mine and minefield performance results of both algorithms. The detection of a mine (a magenta diamond and a red cross) or a false alarm (a magenta diamond) shows on each segment. The minefield decision result is based on the maximum likelihood value performed by each algorithm. Each sub-figure changes the color according to the ground truth. If the algorithm recognizes the segment as a minefield

segment and its ground truth is the background segment, then the sub-figure will be shown as “False MF Detection” in magenta. When the result of a minefield is confirmed by the ground truth of an actual minefield segment, the “Minefield” appears as blue in the segment. Also, when the result of a background segment is confirmed by the ground truth of an actual background segment, there is no change in color. On the other hand, there are cases of missing minefield detection due to the lack of mine detection. This “Miss Detection” displays as red in the segment.

Figure 7.7-7 shows mine and minefield detection performance of the baseline algorithm (SPP-FM) and the MMPP-EM algorithm on the same background segment. The baseline algorithm (top) calls the background segment as the minefield segment since its likelihood value is higher than the threshold value. This is an incorrect result; therefore, “False MF Detection” appears as magenta in the top sub-figure. On the other hand, the MMPP-EM algorithm has detected five detections which are actually the false alarms. Unlike the baseline algorithm, the MMPP-EM algorithm has identified these detections with the minefield likelihood value of -1, a small number. The low minefield likelihood value indicates the segment as a non-minefield, which is a correct call.

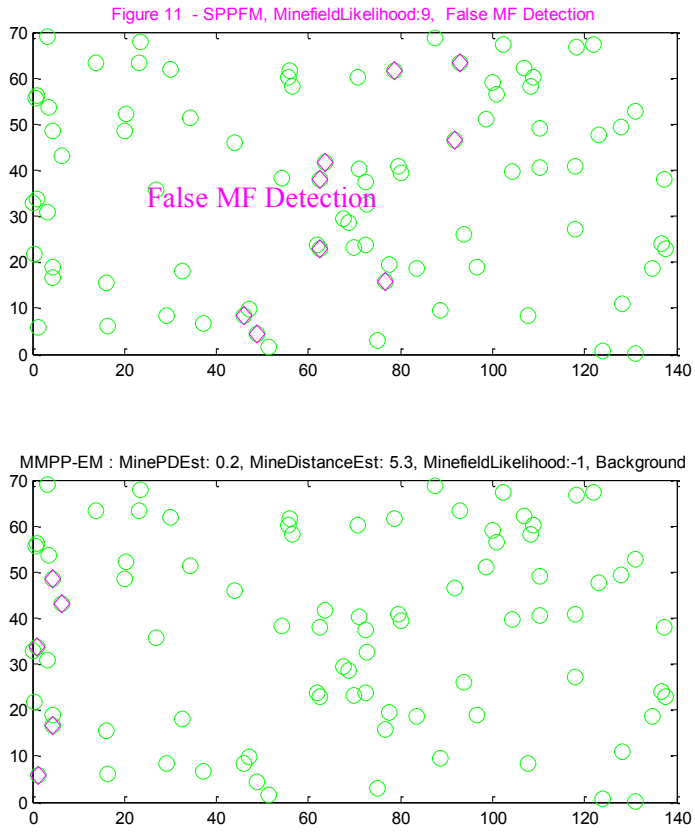

Figure 7.7-7 SPP-FM and MMPP-EM algorithms perform on the background segment. SPP-FM makes an incorrect call because it detects many additional false alarms

In Figure 7.7-8, the baseline algorithm (top) makes a correct call since its minefield likelihood value is slightly higher than the threshold value. This likelihood value is computed based on the number of detections, which consists of two true detections and five false alarms. In this case, the number of false detection has assisted the minefield algorithm making the correct call; unfortunately, when the algorithm performs on a thousand segments, the incorrect call often hurts the minefield performance. The MMPP-EM

(bottom) detects three true detection and four false alarms and does not call the minefield because the estimated mine PD is small, which is based on three true detections. This results in a “Miss MF Detection”, which is not correct.

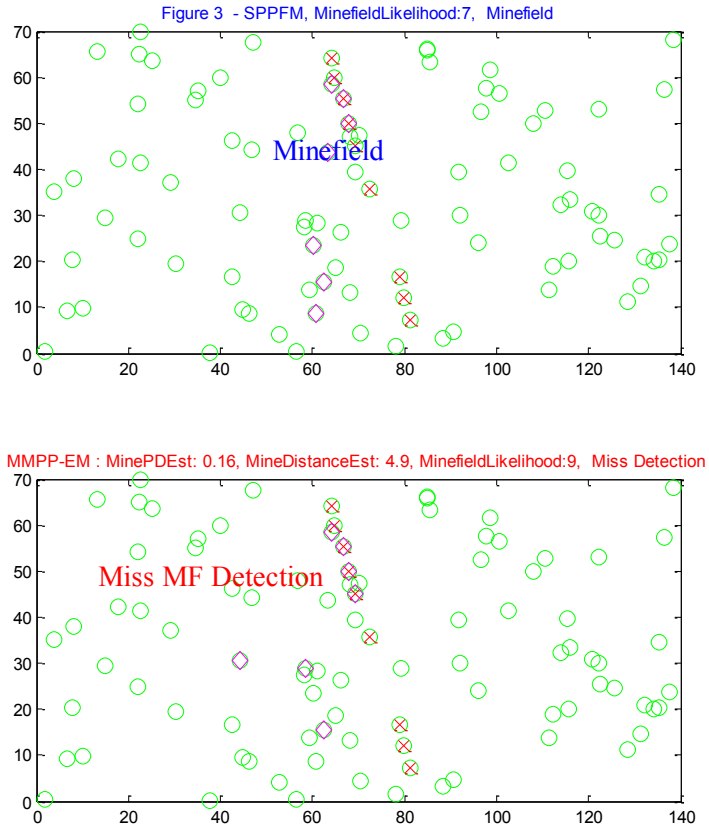

Figure 7.7-8 SPP-FM and MMPP-EM algorithms perform on the minefield segment. Both algorithms missed many of true detection; however, the baseline makes a correct call because of additional detected false alarms

In Figure 7.7-9, both algorithms make a correct call for two completely different reasons. The baseline algorithm does not detect any true detection. Instead, it detects 7 false alarms that bring up the minefield likelihood value high enough to make a correct call. Conversely, the MMPP-EM algorithm makes the correct call based on six true mine detections with no false alarm.

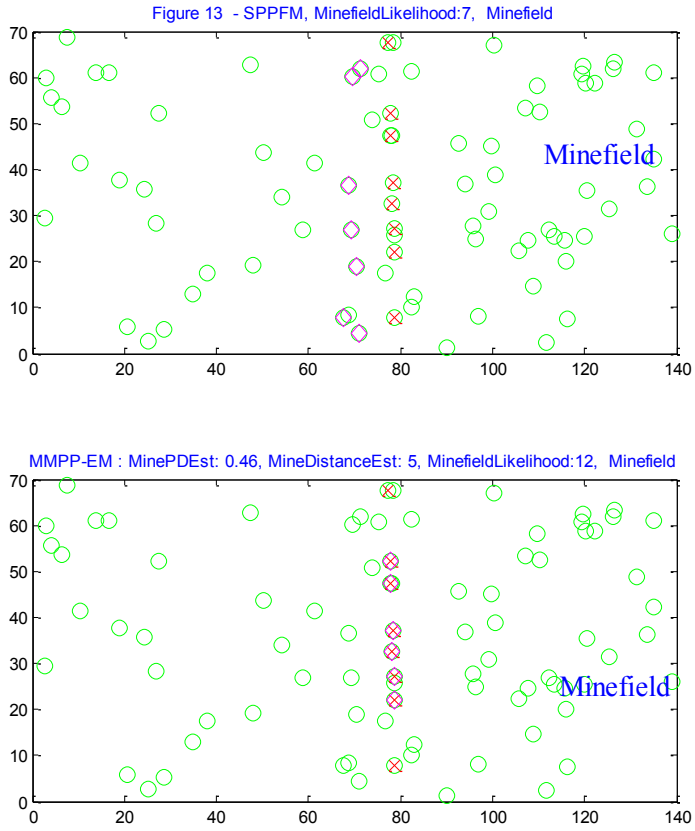

Figure 7.7-9 SPP-FM and MMPP-EM algorithms perform on the minefield segment. SPP-FM makes a correct minefield call due to the false alarms while MMPP-EM makes a correct minefield call due to the true detection

In Figure 7.7-10, both algorithms make a correct call based on true detection. The MMPP-EM algorithm detects 100% mines with no false alarm while the SPP-FM misses four mines but detects three additional false alarms on a single row minefield segment.

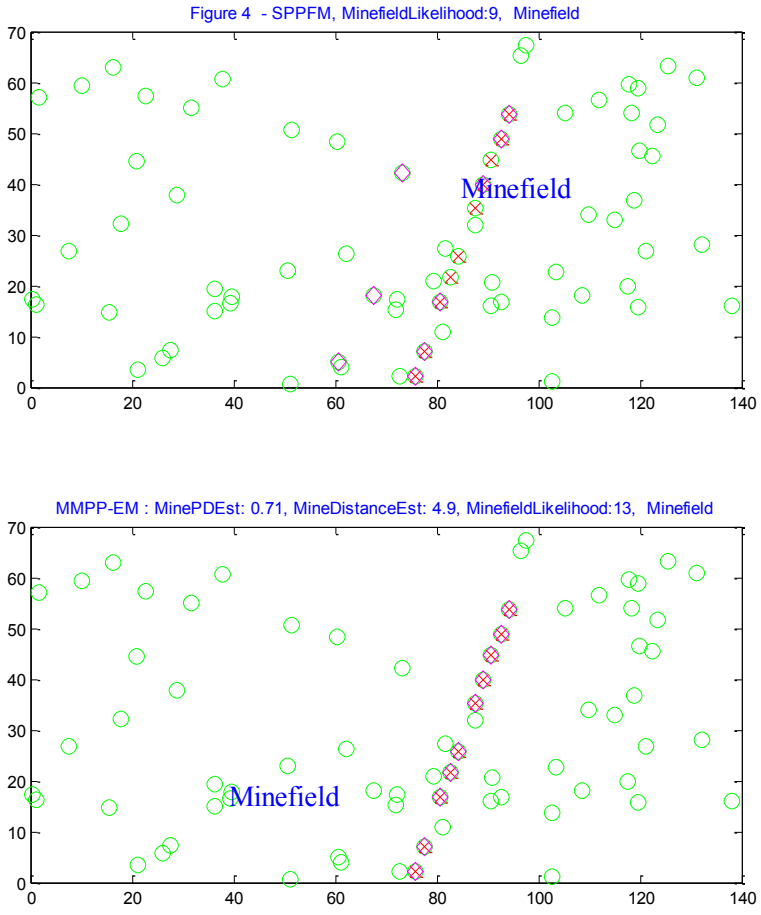

Figure 7.7-10 SPP-FM and MMPP-EM algorithms make the correct minefield call based on true detection

In Figure 7.7-11, both algorithms make a correct call based on true detections with good minefield likelihood values. The MMPP-EM algorithm misses two mines with one false alarm while the SPP-FM misses two mines with no false alarm on a double row minefield segment.

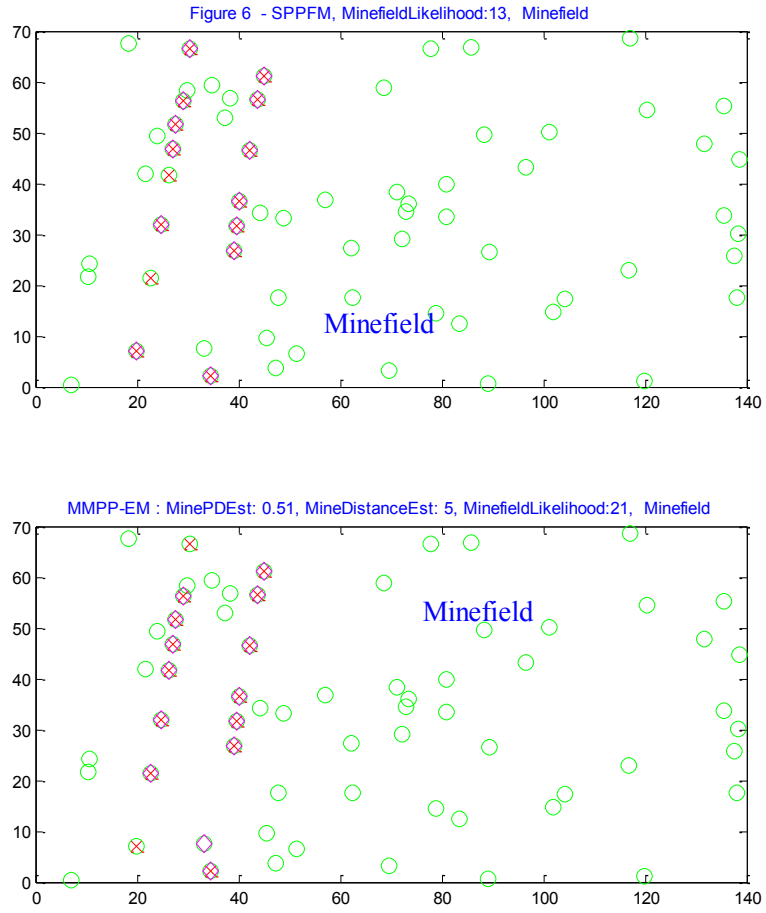

Figure 7.7-11 SPP-FM and MMPP-EM algorithms make the correct minefield call based on true detection on a double row minefield segment

Figure 7.7-12 SPP-FM and MMPP-EM algorithms make the correct minefield call based on true detection on a double row minefield segment, although SPP-FM misses one row of mines completely.

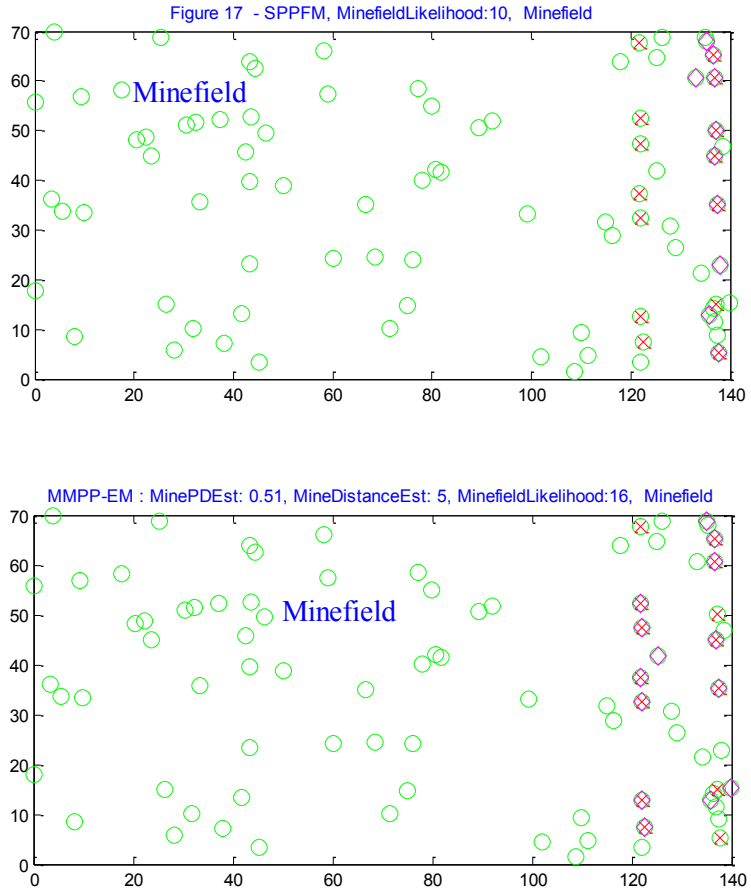

Figure 7.7-12 SPP-FM and MMPP-EM algorithms make the correct minefield call based on true detection on a double row minefield segment although SPP-FM misses one row of mines completely

In Figure 7.7-13, both algorithms make the correct minefield call based on true detection on a triple row minefield segment with good minefield likelihood values. It is

noted that the SPP-FM is designed to detect only one row with the most mines. However, in all exercises for patterned minefield detection, all of the mine rows are accounted for in the case of SPP-FM so that a fair comparison between the baseline and the developed algorithms can be made.

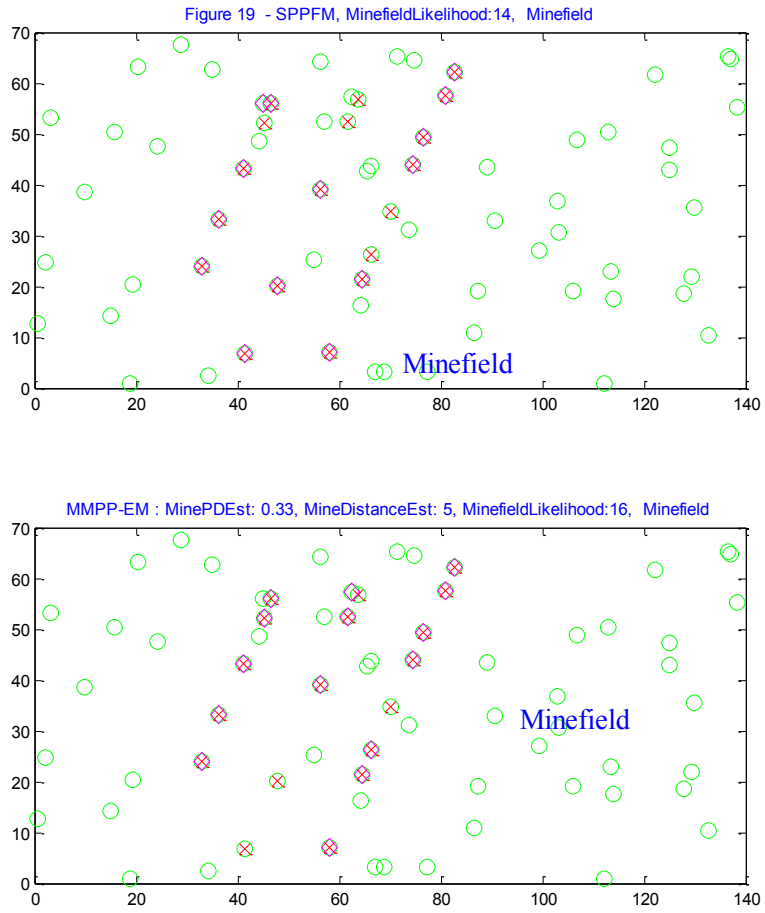

Figure 7.7-13 SPP-FM and MMPP-EM algorithms make the correct minefield call based on true detection on a triple row minefield segment

In Figure 7.7-14, both algorithms make the correct minefield call based on true detection on a triple row minefield segment. Although SPP-FM misses two rows of mines completely, the minefield likelihood value is high enough for the algorithm to make the correct call. The minefield likelihood value in the case of MMPP-EM is high since the majority of mines in the segment are detected.

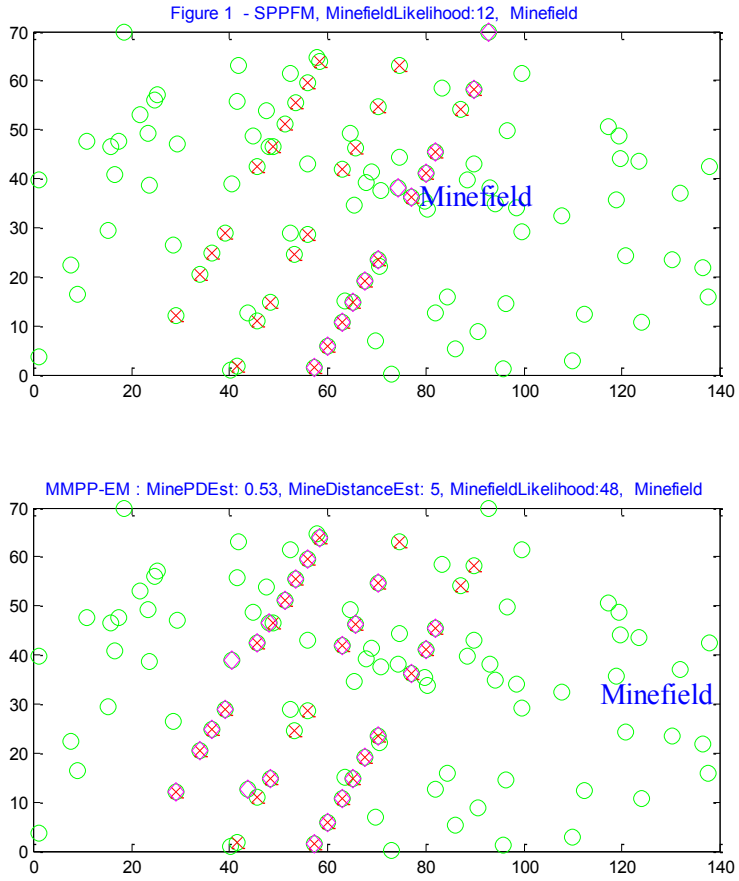

Figure 7.7-14 SPP-FM and MMPP-EM algorithms make the correct minefield call based on true detection on a triple row minefield segment although SPP-FM misses completely two rows of mines

Chapter 8 MMPP for Unpatterned Minefield Detection

8.1 MMPP-CFAR Detection

Using Equations (6.1.2-1) and (6.1.2-2), the minefield likelihood ratio in the case of the MMPP-CFAR can be derived as

$$\begin{aligned}\ln\Lambda_{MMPP-CFAR}\left(X\middle|Z\right) &= \ln C\binom{n}{n_m} + n_m \ln\left(\frac{p\lambda_m}{\lambda_c}\right) - p\lambda_m A \\ &+ \sum_{i=1}^{n_m}\left(\ln\left(g_m\left(a_i\right)\right) - \ln\left(g_c\left(a_i\right)\right)\right) + \sum_{i=1}^{n_m}\left(\ln\left(f_m\left(k_i\right)\right) - \ln\left(f_r\left(k_i\right)\right)\right)\end{aligned} \tag{8.1-1}$$

where p is the probability of mine detection, f_m is obtained by either Equation (3.4.2-1) for random distribution or Equation (3.4.2-2) for regular distribution, f_c is obtained from Equation (3.4-1), and f_r is obtained from Equation (3.4-2).

8.2 MMPP-CTR Detection

Starting with Equations (6.2.1-2) and (6.2.1-3), and assuming that the nearest neighborhood distances for clutter targets are calculated with respect to all detections n, the log-likelihood function for unpatterned minefields under MMPP can be obtained as

$$\begin{aligned}\ln\Lambda_{MMPP-CTR}\left(X\middle|Z\right) &= \ln C\binom{N}{n_m} + n_m \ln\left(\frac{p_{mine}}{1-p_{mine}}\right) + N\ln\left(1-p_{mine}\right) \\ &+ \sum_{i=1}^{n_m}\left(\ln\left(g_m\left(a_i\right)\right) - \ln\left(g_c\left(a_i\right)\right)\right) + \sum_{i=1}^{n_m}\left(\ln\left(f_m\left(k_i\right)\right) - \ln\left(f_r\left(k_i\right)\right)\right)\end{aligned} \tag{8.2-1}$$

where p_{mine} is obtained from Equation (6.2.1-1), f_m is obtained by either Equation (3.4.2-1) for random distribution or Equation (3.4.2-2) for regular distribution, f_c is obtained from Equation (3.4-1), and f_r is obtained from Equation (3.4-2).

8.3 Maximum Likelihood Estimate Statistic

The maximum likelihood estimate statistic for the above thresholding cases is

$$\chi(X) = \max_{Z,p} \ln \Lambda\left(X \middle| (p), Z\right) \tag{8.3-1}$$

8.4 Results and Discussions of Unpatterned Minefield Performance

Exploiting spatial distribution of unpatterned mines is not trivial. The spatial structures of unpatterned minefields are not often as pronounced as the spatial structures of patterned minefields. In this effort, the performance of minefields was evaluated, where potential mines were assumed to be randomly and regularly distributed and the clutter targets were assumed to be randomly distributed. The minefield performance results were obtained at a high clutter rate of 0.008 clutter target per m^2 and a low mine density of 0.0024 mine per m^2 for the baseline algorithm (SPP-FM), the algorithm based only on target feature (MPP), and the algorithm based on both target feature and target distribution (MMPP). The results show that the developed minefield detection algorithm based on the MMPP model performs the best when unpatterned mines follow the spatial minefield structure. In contrast, when unpatterned mines do not follow any spatial minefield structure, the performance of the MMPP algorithm is less pronounced. Its performance is similar to the MPP algorithm, but it is still better than the baseline algorithm.

Figures (8.4-1) and (8.4-2) show the minefield detection performance results obtained at the high clutter rate of 0.008 and the mine density of 0.0024 for the two spatially distributed cases based on 1500 minefield and 3000 background segments. In both cases, the comparative results among the baseline algorithm (SPP-FM), the algorithm based only on target feature (MPP), and the algorithm based on both target feature and target distribution (MMPP) are provided. Although the performance results for the CFAR thresholding case are only shown, it would be expected that the performance results for the CTR thresholding will be similar. In Figure (8.4-1), when mines are assumed to be regularly distributed, the developed MMPP algorithm performs better than the MPP algorithm, and it performs much better than the baseline algorithm. On the contrary, when mines are assumed to be random distributed as shown in Figure (8.4-2), the minefield performance of both MMPP and MPP algorithms are similar; however, their performance is better than the baseline algorithm.

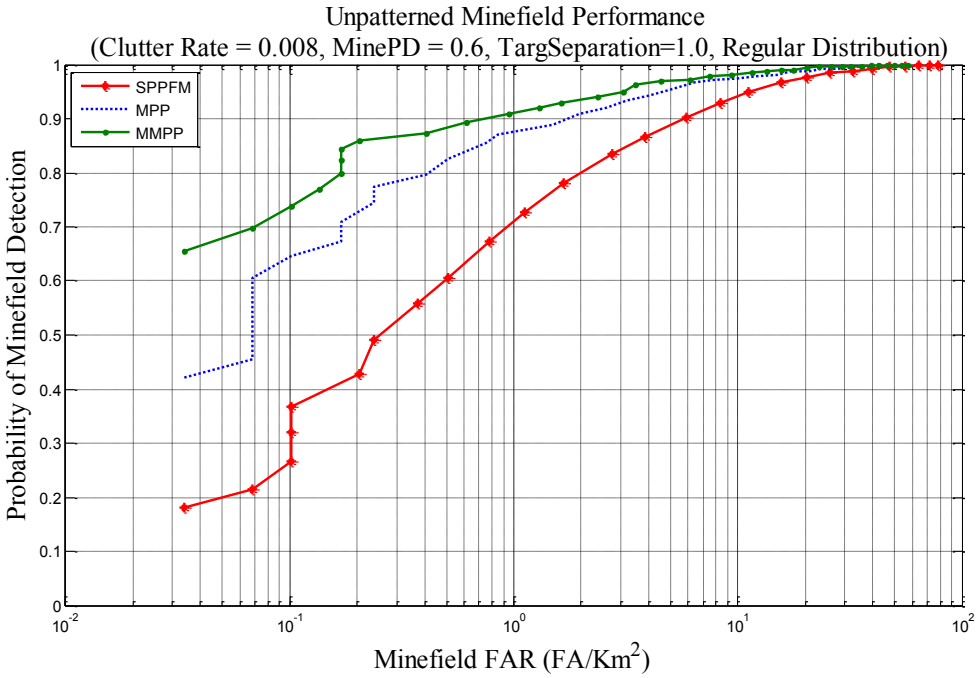

Figure 8.4-1 Unpatterned minefield performance of three algorithms based on the clutter rate of 0.008, mines distributed regularly while clutter targets are distributed randomly

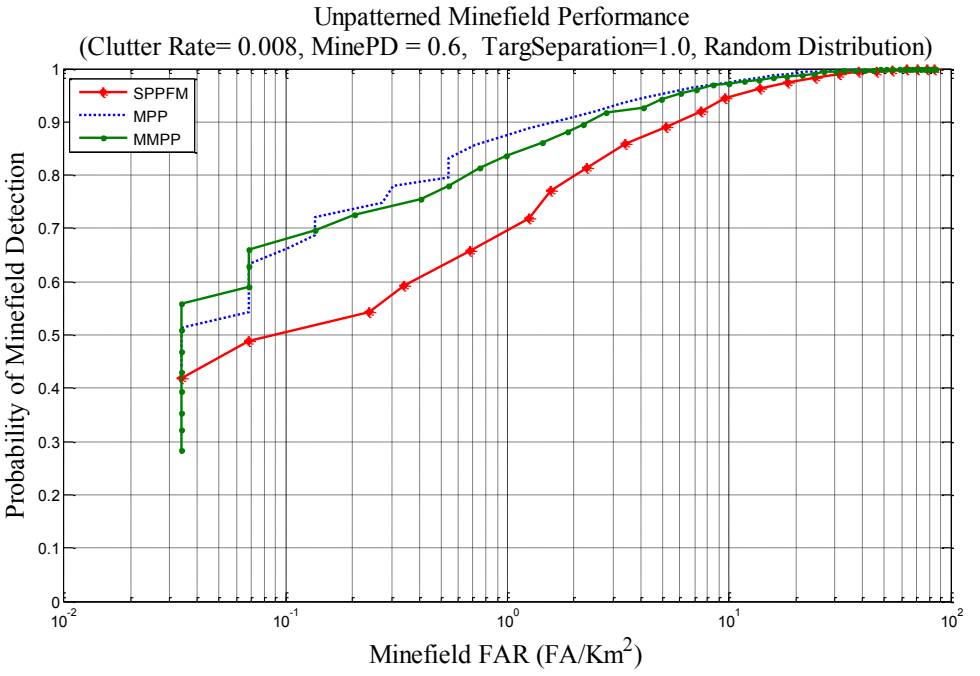

Figure 8.4-2 Unpatterned minefield performance of three algorithms based on the clutter rate of 0.008, mines and clutter targets are distributed randomly

8.4.1 Unpatterned Minefield Performance – Regularly Distributed Mines While Randomly Distributed Clutter Targets

The following figures (8.4.1-1through 8.4.1-5) came from a detection video for unpatterned minefields. These figures show mine and minefield detection performance of the baseline algorithm (SPP-FM) and the MMPP algorithm on the same unpatterned minefield segment. Unless noted, parameters used to generate the following results include the clutter rate value of 0.008, MineDensity value of 0.004, MinePD value of 0.6, and target size separation between mine size and clutter size as one standard deviation. Also, it is assumed that unpatterned mines follow regular distribution while clutter targets follow random distribution. Figure 8.4.1-1 shows an example of the correct detection result when both the baseline algorithm (top) and the MMPP algorithm (bottom) make a correct call of the minefield segment. Both minefield likelihood values are high, but part of the high values can be due to the contribution of additional false positives or false alarms. Comparing with the patterned minefield performance results, there are more undetected mines and more false alarms generated by both algorithms for unpatterned minefield detection. It is noted that the number on top of each figure indicates the sequential number of a complete run which consists of thousand segments. Only a few samples are shown here for illustration purposes.

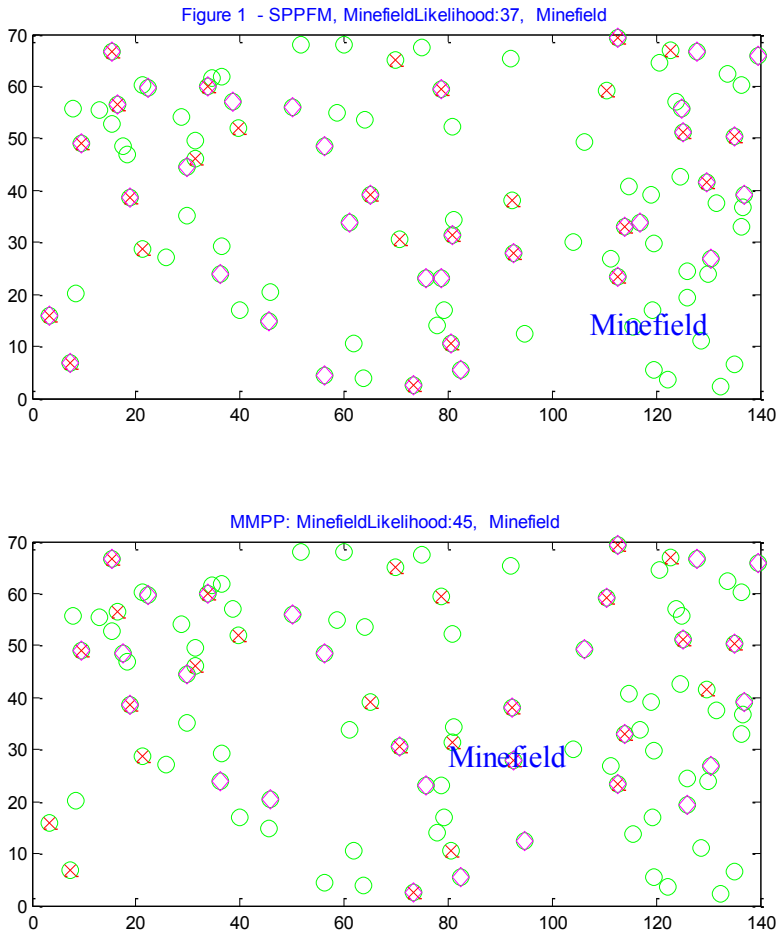

Figure 8.4.1-1 SPP-FM and MMPP algorithms make the correct minefield call with the assumption that mines are distributed regularly while clutter targets are distributed randomly, and the clutter rate is 0.008

The following figures show the mine and minefield performance results of the baseline and the MMPP algorithms. All the parameters used here are exactly the same as the above parameters except that the clutter rate is reduced from 0.008 to 0.006. Figure 8.4.1-2 illustrates that both algorithms make the correct minefield call. Also, the number of missed

detection and false alarms appears to improve when the clutter rate to generate these segments has been lowered.

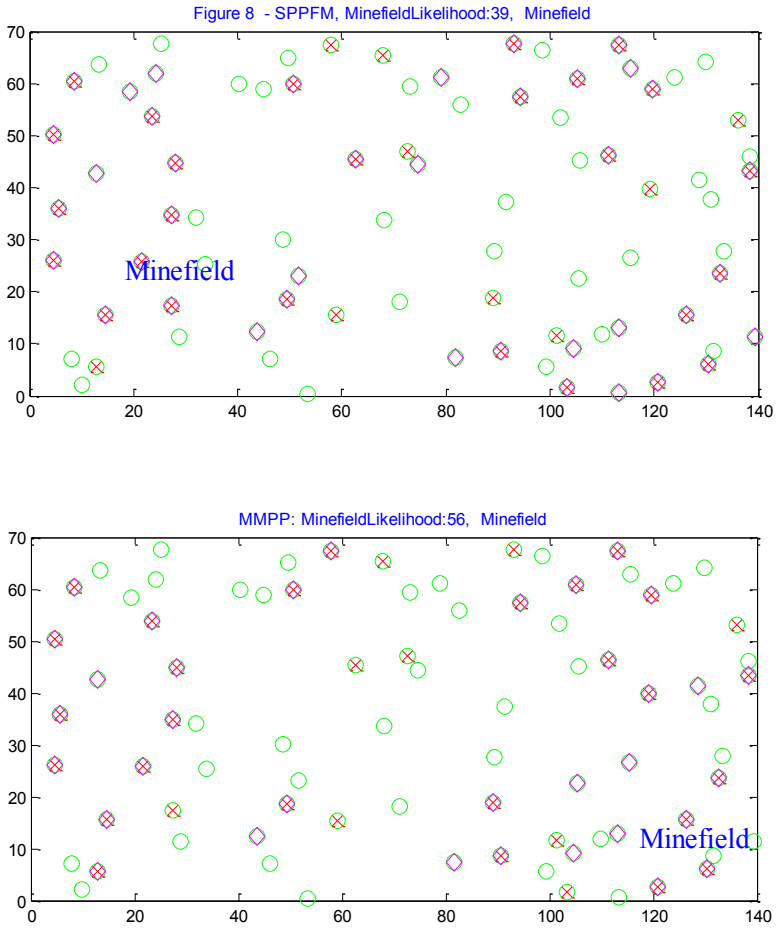

Figure 8.4.1-2 SPP-FM and MMPP algorithms make the correct minefield call with the assumption that mines are distributed regularly while clutter targets are distributed randomly with the clutter rate at 0.006

Figure 8.4.1-3 shows the baseline algorithm making an incorrect call due to the detection of many false positives, while the MMPP algorithm makes a correct call.

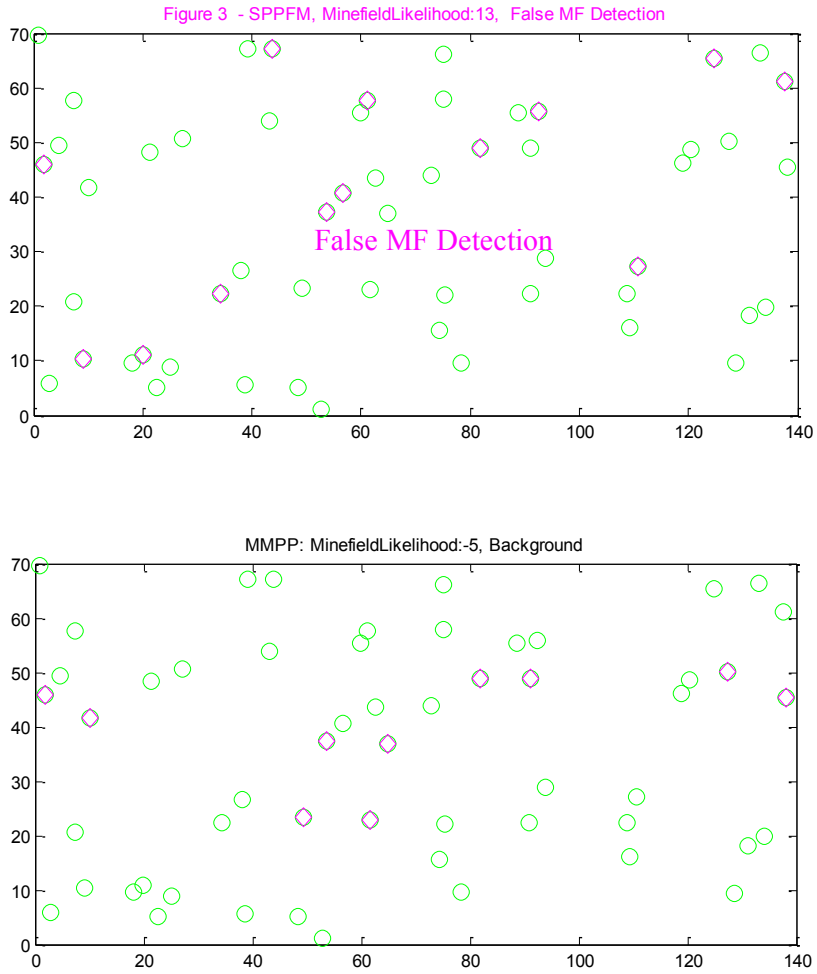

Figure 8.4.1-3 Baseline algorithm makes an incorrect call while MMPP algorithm makes the correct call on the background segment

The following figures show the mine and minefield performance results of the baseline and the MMPP algorithms. Only one parameter differs between the following and previous examples; the target size standard deviation increases from one to one and a half.

Figure 8.4.1-4 shows an example of the detection result when both the baseline algorithm (top) and the MMPP algorithm (bottom) make the correct minefield call. Many more mines and fewer false alarms are detected by the algorithms.

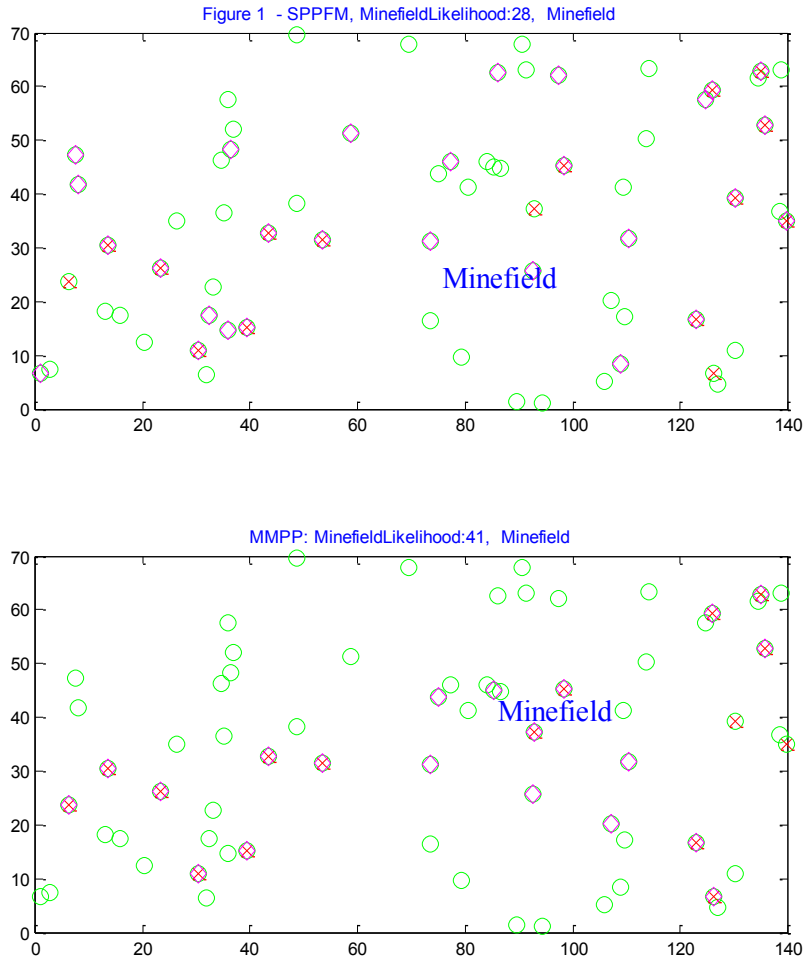

Figure 8.4.1-4 Both algorithms make the correct minefield call. Many mines are detected by both algorithms

Figure 8.4.1-5 shows the performance of the algorithms on a background segment. Many false alarms are detected by both algorithms. Based on a slightly high minefield likelihood value of 10, the baseline algorithm (top) calls the background segment a minefield, which is not correct. On the other hand, the MMPP algorithm with its minefield likelihood value of only one makes a correct background call.

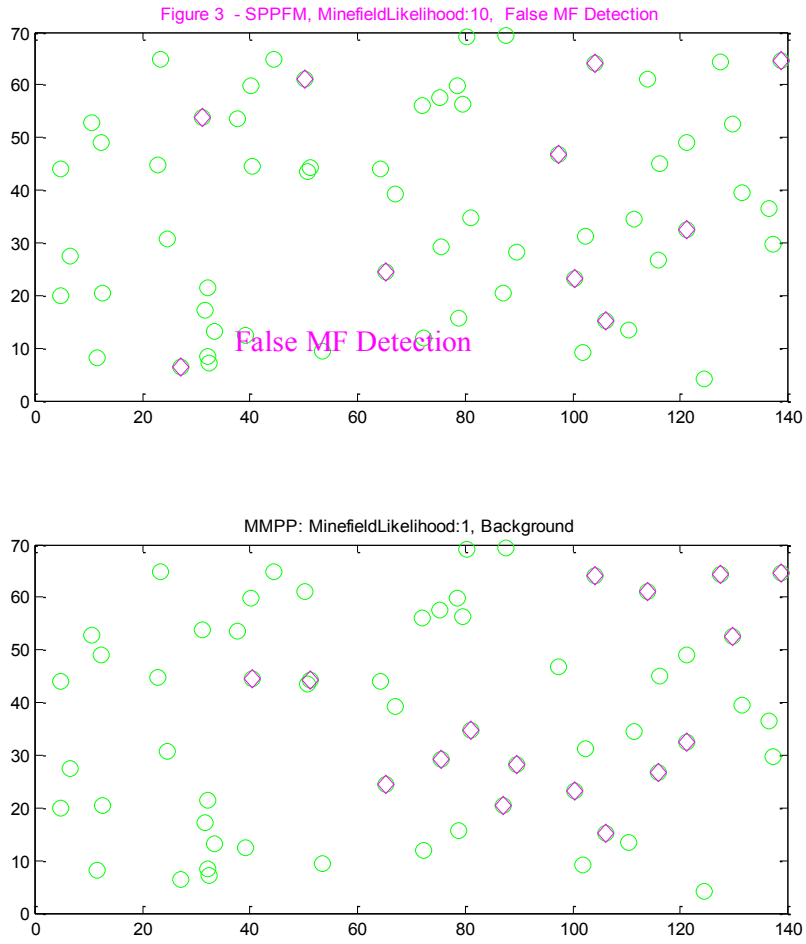

Figure 8.4.1-5 Baseline algorithm (top) makes the incorrect call while MMPP algorithm makes the correct call

8.4.2 Unpatterned Minefield Performance – Randomly Distributed Mines and Clutter Targets

It is assumed that both unpatterned mines and clutter targets follow random distribution. The following figures (8.4.2-1 through 8.4.2-3) show mine and minefield detection performance of the baseline algorithm (SPP-FM) and the MMPP algorithm on the same unpatterned minefield segments. Unless noted, parameters used to generate the following results include a clutter rate of 0.008 or 0.006, MineDensity of 0.004 and MinePD of 0.6, and target size separation between mine size and clutter size is one and a half standard deviation.

Figure 8.4.2-1 shows an example of the detection result when both the baseline algorithm (top) and the MMPP algorithm (bottom) make a correct minefield call. Missed detection and false alarms are observed in the results.

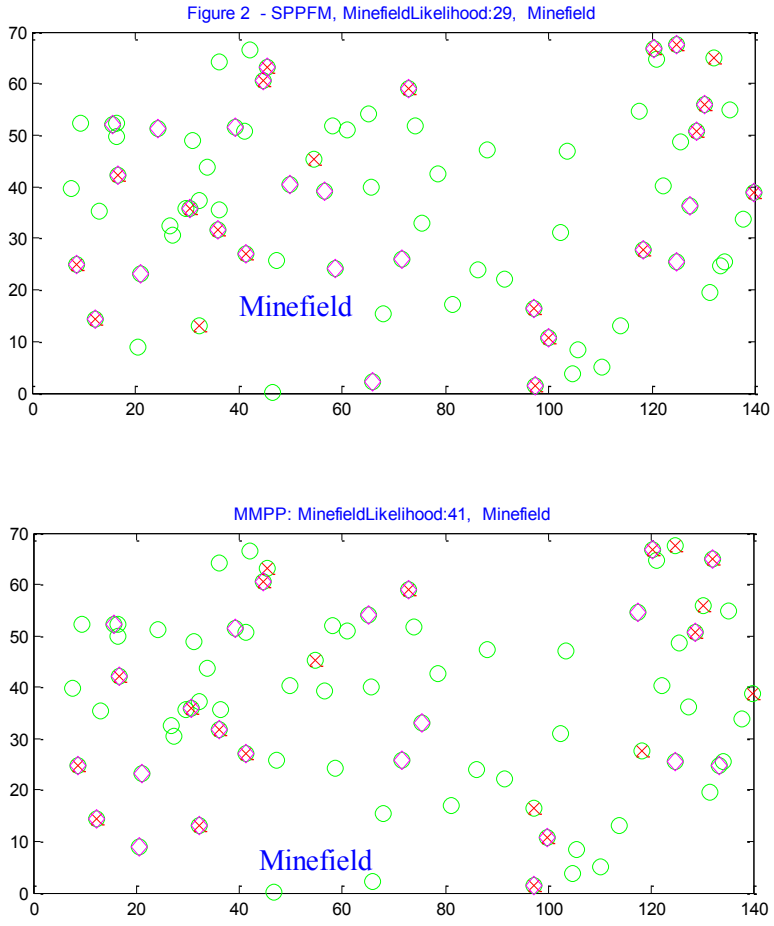

Figure 8.4.2-1 Both algorithms make the correct call in the case of both mines and clutter targets are randomly distributed and the clutter rate is 0.008

Figure 8.4.2-2 shows an example of the detection results when both the baseline algorithm (top) and the MMPP algorithm (bottom) make an incorrect call of a background segment. Both algorithms have slightly high minefield likelihood values.

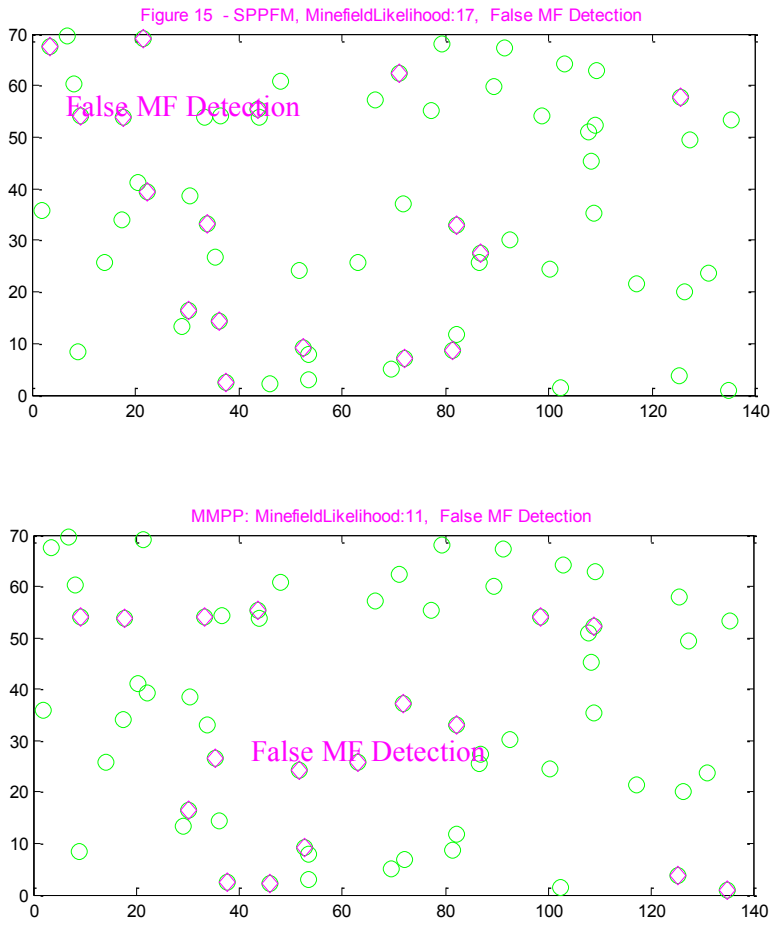

Figure 8.4.2-2 Baseline (top) and MMPP algorithms make an incorrect minefield call

Figure 8.4.2-3 shows an example of the detection result when the baseline algorithm (top) makes an incorrect call due to false positives, while the MMPP algorithm (bottom) makes a correct call of a background segment. The baseline algorithm has a slightly high minefield likelihood value of 8, while the MMPP algorithm has a negative minefield likelihood value of 10.

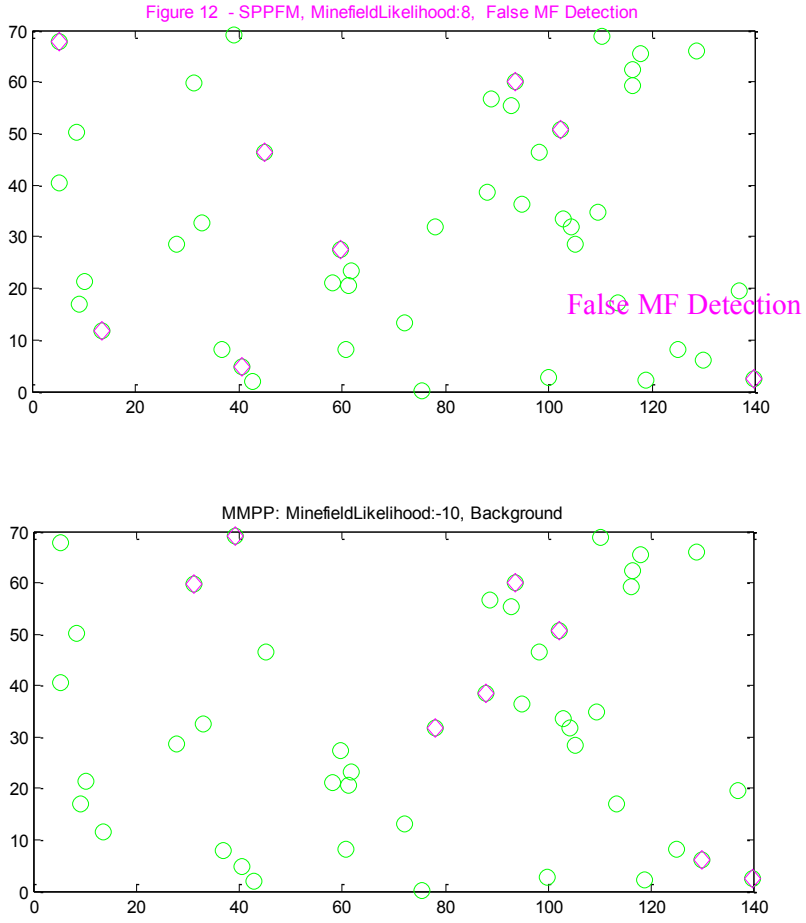

Figure 8.4.2-3 Baseline algorithm (top) makes the incorrect call while MMPP algorithm makes the correct call based on the clutter rate of 0.006

8.4.3 Unpatterned Minefield Performance – Randomly Distributed Mines and Clutter Targets. Comparative Detection Performance between Baseline (SPP-FM) and Marked Point Process (MPP) Algorithms

In this section, the benefit of Marked Point Process (MPP) model employing only target feature is discussed. Moreover, the developed linear search approach [11] which searches for targets to maximize the minefield likelihood value contributes to the improvement of the MPP minefield detection performance. Based on CFAR thresholding using one standard deviation of target size separation and the clutter rates of 0.006 and 0.008, the results show that mine-level detection performance of both SPP-FM and MPP is similar since both algorithms use only the target size as the discriminator. On the other hand, the minefield-level detection performance for MPP is significantly better than SPP-FM. MPP is better because the MPP formulation assigns a weight to the detections based on the size of the targets resulting in a better test statistic.

The SPP-FM and MPP minefield decision processes are briefly discussed. The baseline (SPP-FM) algorithm makes the minefield decision sequentially, applying the false alarm mitigator based on the target size after mine detection, then making the minefield decision based on the number of detections. On the other hand, MPP algorithm incorporates the target size in the model, which eliminates the false alarm stage and then counts only the detections that maximize the minefield likelihood. This processing approach eliminates many minefield false positives. The results indicate that the minefield detection based on MPP formulation and the developed linear search approach to maximize the minefield likelihood performs better than the baseline approach. A few examples are illustrated here.

Figure 8.4.3-1 shows the detection results of the baseline SPP-FM and the MPP algorithms on the background segment. Although both algorithms produce a similar number of detection, the baseline (top) makes an incorrect minefield call while MPP (bottom) makes a correct minefield call. The use of the developed search algorithm that maximizes the minefield likelihood for the MPP contributes to the minefield performance's improvement.

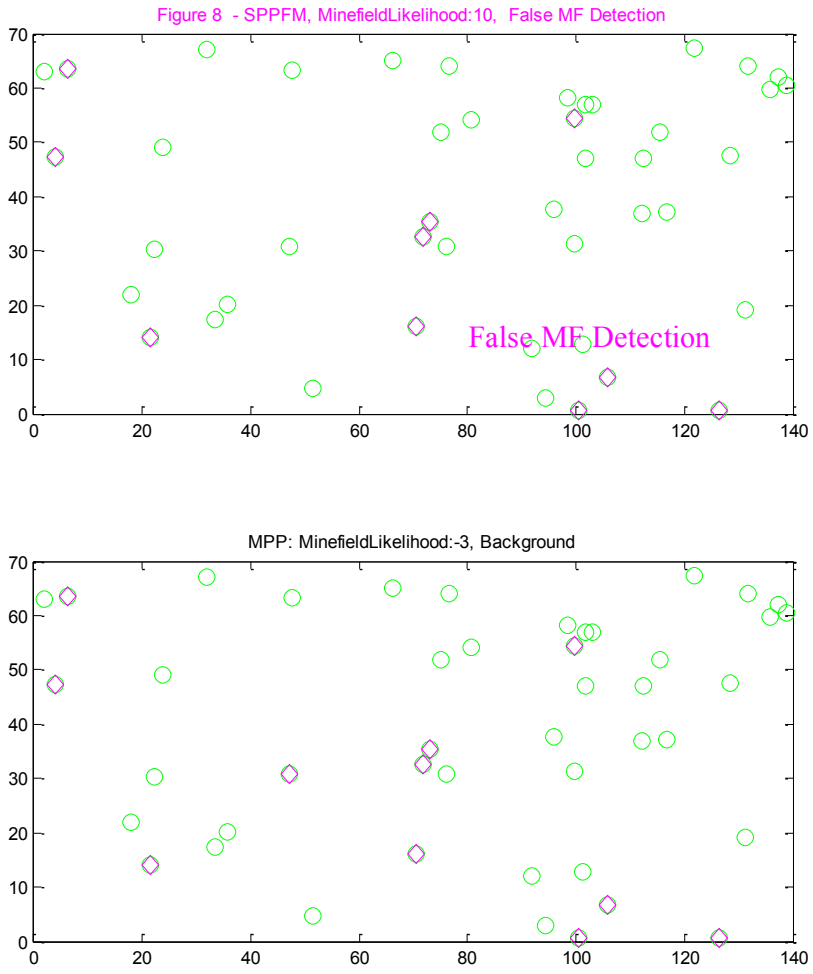

Figure 8.4.3-1SPP-FM (top) makes an incorrect call while MPP (bottom) makes a correct call. Mine detection performance of both is similar, but minefield decision separates from a correct to an incorrect minefield call

Figure 8.4.3-2 shows mine and minefield detection results of the baseline SPP-FM and the MPP algorithms on the minefield segment. Both algorithms make the correct minefield call.

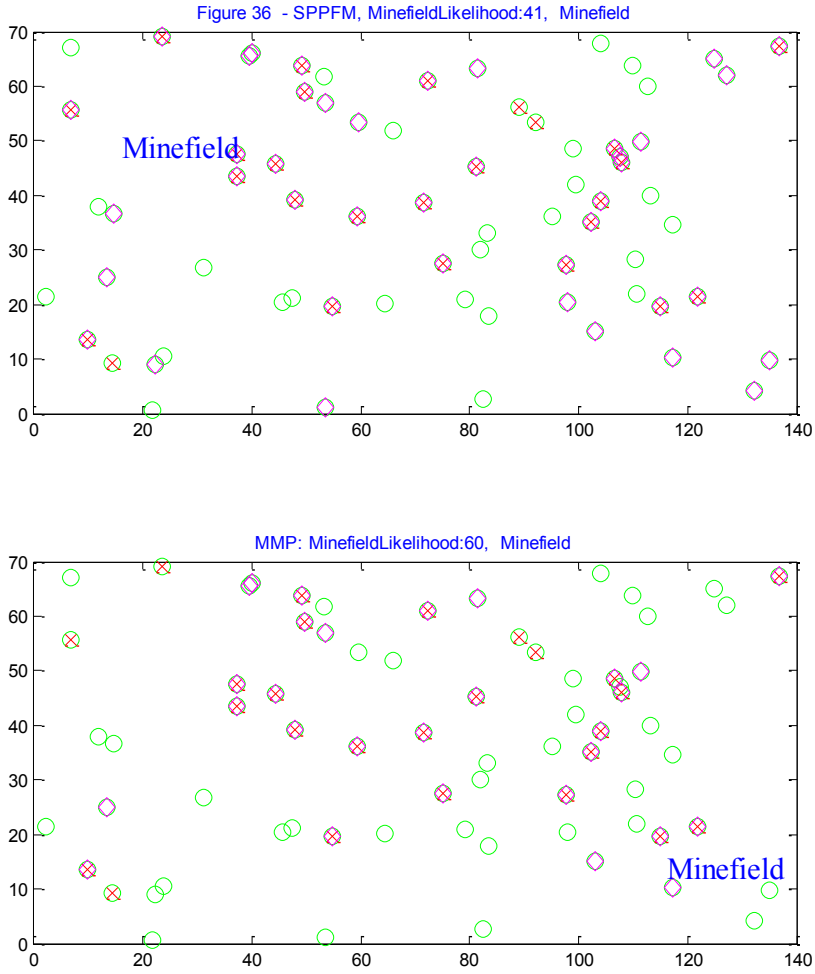

Figure 8.4.3-2 SPP-FM (top) and MPP (bottom) make a correct minefield call

In summary, exploiting spatial distribution of unpatterned mines is not trivial. The spatial structures of unpatterned minefields are not often as pronounced as the spatial structures of patterned minefields. In this effort, the performance of minefields was evaluated, where potential mines were assumed to be randomly and regularly distributed and the clutter targets were assumed to be randomly distributed. The minefield performance results were obtained at a high clutter rate of 0.008 clutter target per m^2 and a low mine density of 0.0024 mine per m^2 among the baseline algorithm (SPP-FM), the algorithm based only on target feature (MPP), and the algorithm based on both target feature and target distribution (MMPP). The results show that the developed minefield detection algorithm based on the MMPP model performs the best when unpatterned mines follow the spatial minefield structure. However, when unpatterned mines do not follow any spatial minefield structure, the performance of the MMPP algorithm is less pronounced. Its performance is similar to the MPP algorithm, but its performance is still better than the baseline algorithm. The results can be found in Figures 8.4-1 and 8.4-2.

Chapter 9 Analytical Versus Simulation-Based Solutions for Detection Problem Based on MMPP Formulation

An analytical solution for the complete minefield detection problem is intractable due to a large number of detections and the variation of the number of detected mines in the minefield process. When the number of mines increases, the probability distribution of the spatial distances for mines in the minefield to calculate log likelihood ratio quickly becomes too complex to solve analytically. Therefore, an analytical solution for a simplified detection problem is developed. Subsequently, the analytical performance and simulation-based performance for the same MMPP framework are compared.

9.1 Simplified Detection Problem

The detection problem is simplified so that a tractable analytical solution for the MMPP framework can be obtained. If mines are present in the interrogated area *A*, then there are assumed to be exactly two mines that have size (a_i) and the distance between these mines is (k). The size of the mines is distributed Gaussian with mean μ_a and standard deviation σ_a. The distance between these mines is Gaussian distributed with mean μ_k and standard deviation σ_k. There are other targets such as clutter targets in the same area. The size of the clutter targets is Gaussian distributed with mean μ_c and standard deviation σ_c where $\sigma_c = \sigma_a$. These clutter targets have spectral characteristics that are slightly different from those of the mines. Also, these clutter targets are spatially and randomly distributed.

Target solution based on constant target rate (CTR) is used so that the total number of detections (mines plus clutter targets) is a fixed number *N*.

The minefield decision is to determine whether observation X belongs to the minefield process (when two mines are identified) or the background process if no mine is identified. This decision is posed under hypothesis testing framework, where H_0 is the background hypothesis in which two mines are not found and H_1 is the minefield hypothesis in which two mines are found.

Let the assignment of the detection as a mine or a clutter be captured by a classification function *Z* that is defined such that

$$Z = \{z_i, i = 1, 2, ..., N\}, \tag{9.1-1}$$

where

$$z_i = \begin{cases} 1 & \text{if the detection } x_i \text{ is a mine} \\ 0 & \text{if the detection } x_i \text{ is a clutter target} \end{cases}$$

Observation X with *N* detected targets under two hypotheses is given by

$$\begin{aligned} &\textbf{Background: } H_0 : Z = 0 \\ &\textbf{Minefield: } \quad H_1 : Z \neq 0, |Z| = 2 \end{aligned} \tag{9.1-2}$$

9.2 Detection Attributes

For the current development, it is assumed that for any detection, mark a_i is independent of other detections and depends only on the identity of the detection as a mine ($z_i = 1$) or a clutter target ($z_i = 0$). Thus, the probability distributions for mark a_i in the case of mines and clutter targets can be given by

$$\begin{aligned} p(a_i | z_i = 1) &= g_m(a_i) \\ p(a_i | z_i = 0) &= g_c(a_i) \end{aligned} \tag{9.2-1}$$

The distributions $g_m(a_i)$ and $g_c(a_i)$ describe mineness and non-mineness measures of the detections based on attributes of the target signature. It is assumed that these measures follow Gaussian distributions:

$$g_m(a_i) = \frac{1}{\sigma_m\sqrt{2\pi}} e^{-(a_i-\mu_m)^2/2\sigma_m^2}$$
$$g_c(a_i) = \frac{1}{\sigma_c\sqrt{2\pi}} e^{-(a_i-\mu_c)^2/2\sigma_c^2} \quad (9.2\text{-}2)$$

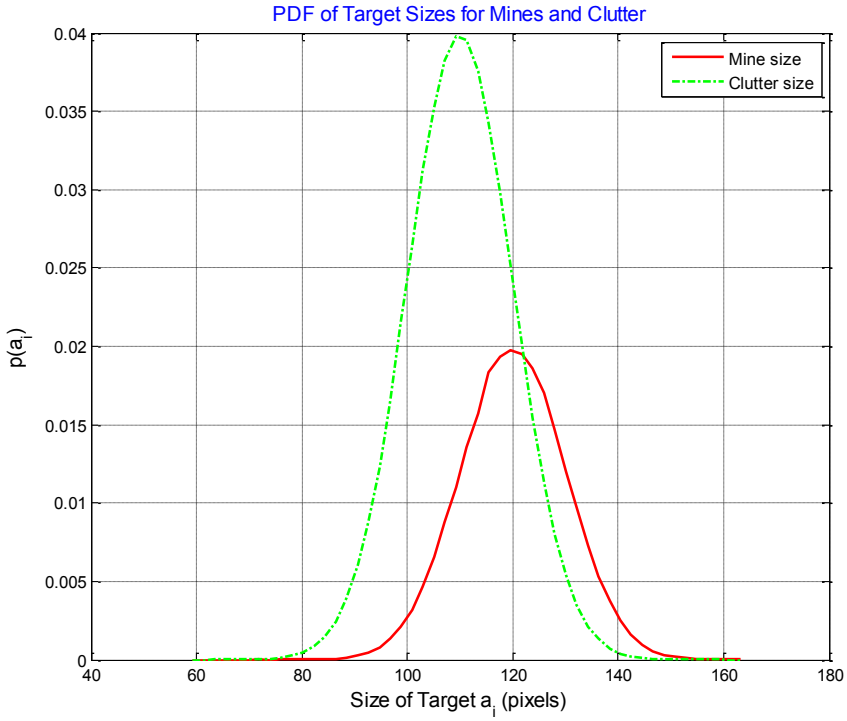

Figure 9.2-1 Relative Gaussian distributions of mine and clutter sizes, target size separation of one standard deviation

9.3 Spatial Distribution

To simplify the analysis, the distribution of spatial distances between two mines $f_m\left(k_{ij}\right)$ is assumed to be Gaussian and given by

$$f_m\left(k_{ij}\right)=\frac{1}{\sigma_k\sqrt{2\pi}}e^{-\left(k_{ij}-\mu_k\right)^2/2\sigma_k^2} \tag{9.3-1}$$

The distribution of nearest neighbor distances k_i between randomly distributed clutter targets denoted as $f_c\left(k_i\right)$ with the clutter rate λ_c is given by

$$f_c\left(k_i\right)=2\lambda_c\pi k_i e^{-\lambda_c\pi k_i^2} \tag{9.3-2}$$

The probability of clutter targets identified as mines at a distance k_i is given by

$$f_r\left(k_i\right)=\frac{4\pi k_i}{A}\left(1-\frac{\pi k_i^2}{A}\right),\quad \pi k_i^2<A \tag{9.3-3}$$

9.4 MMPP-CTR Formulation

The conditional probabilities of observation *X* according to the null and non-null hypotheses under Markov Marked Point Process (MMPP) where both the target feature and the spatial distance are integrated into the model are given by

$$p_{MMPP}(X\mid H_0,Z)=\left[\prod_{i=1}^{N}g_c\left(a_i\right)\right]\prod_{i=1}^{N}\prod_{\substack{j=1\\ j\neq i}}^{N}\left[f_r\left(k_{ij}\right)^{z_i z_j}\right]f_c\left(k_{i*}\right)^{\bar{z}_i} \tag{9.4-1}$$

$$p_{MMPP}(X\mid H_1,Z)=\left[\prod_{i=1}^{N}g_m\left(a_i\right)^{z_i}\,g_c\left(a_i\right)^{\bar{z}_i}\right]\prod_{i=1}^{N}\prod_{\substack{j=1\\ j\neq i}}^{N}\left[f_m\left(k_{ij}\right)\right]^{-z_i z_j}f_c\left(k_{i*}\right)^{\bar{z}_i} \tag{9.4-2}$$

where k_{i*} is the nearest neighbor distance from i^{th} target.

In this formulation, the conditional probability will include all targets that have their characteristics of either mines or clutter targets based on target sizes and the spatial distance between two targets.

9.5 MMPP-CTR Decision

Starting with Equations (9.4-1) and (9.4-2), it is noted that there are only two mines among all *N* targets in the minefield segments. For simplification without loss of generality, assume that the two targets are identified as target(x_1) and target(x_2), the log-likelihood function for minefields under MMPP-CTR can be obtained as

$$\begin{aligned} L &= \ln\left(\Lambda_{MMPP}\left(X\middle|Z\right)\right) = \ln\left\{\frac{g_m(a_1)g_m(a_2)f_m(k_{12})}{g_c(a_1)g_c(a_2)f_r(k_{12})}\right\} \\ &= \ln g_m(a_1) + \ln g_m(a_2) - \ln g_c(a_1) - \ln g_c(a_2) + \ln f_m(k_{12}) - \ln f_r(k_{12}) \\ &= 2\left[\mu_m - \mu_c\right]\left[(a_1+a_2) - (\mu_m+\mu_c)\right] - \ln\left(\frac{4\pi k_{12}}{A}\right) - \ln\left(1 - \frac{\pi {k_{12}}^2}{A}\right) - \ln\left(\frac{1}{\sigma_k\sqrt{2\pi}}\right) - \frac{\left(k_{12}-\mu_k\right)^2}{2{\sigma_k}^2} \end{aligned} \tag{9.5-1}$$

where $\pi k_{12}^2 < A$

$$\lambda = \Lambda_{\text{Test}} = \max_{Z} \ln\left(\Lambda_{MMPP}\left(X\middle|Z\right)\right) \tag{9.5-2}$$

Since two targets are selected as mines, there are only $\frac{N(N-1)}{2}$ total possibilities of valid configurations of *Z*. Therefore, an exhaustive search for the optimal solution can be used. The minefield performance Receiver Operating Characteristic (ROC) curves are drawn

based on a large number of simulations for both minefield and non-minefield cases, and evaluating the test statistic (λ) using an exhaustive search.

9.6 Analytical Solution

In order to compute an analytical solution for the minefield performance, the following two probability density functions for the test statistic are computed:

$$p\left(\Lambda_{\text{Test}} \mid H_0\right) = p_{H_0}\left(\lambda\right) \tag{9.6-1}$$

$$p\left(\Lambda_{\text{Test}} \mid H_1\right) = p_{H_1}\left(\lambda\right) \tag{9.6-2}$$

Note that the value of the test statistic depends on the values of three independent variables a_1, a_2, and k_{12} for the minefield case. The variables a_1 and a_2 are normally distributed corresponding to $g_m(a_i)$ in Equation (9.2-2), while k_{12} follows the distribution described in Equation (9.3-1). $p_{H_1}\left(\lambda\right)$ is numerically calculated based on the function shown in Equation (9.5-1).

In the non-minefield case, the variables a_1, a_2, and k_{12} are not independent because the best pair of clutter targets that maximizes the test statistic must be found among $M = \dfrac{N(N-1)}{2}$ combinations of pairs of clutter targets. $p_{H_0}\left(\lambda\right)$ is the probability density function of the maximum statistic out of these "*M*" pairs. The variables a_1 and a_2 in this case follow normal distribution corresponding to $g_c(a_i)$ in Equation (9.2-2), while k_{12} follows the distribution described in Equation (9.3-3).

An approximation for $p_{H_0}(\lambda)$ can be obtained numerically if a_1, a_2, and k_{12} are assumed to be independently selected, and the test statistic is governed by the best statistic out of "*M*" randomly selected statistic. Let $P_{L_0}(\lambda)$ be the cumulative distribution of the likelihood function for two randomly selected targets that is computed from Equation (9.5-1) for the null hypothesis, the cumulative distribution of the null hypothesis $P_{H_0}(\lambda)$ and its probability density function $p_{H_0}(\lambda)$, which are given by

$$P_{H_0}(\lambda) = 1 - \left(1 - P_{L_0}(\lambda)\right)^M \tag{9.6-3}$$

$$p_{H_0}(\lambda) = \frac{d}{d\lambda} P_{H_0}(\lambda) \tag{9.6-4}$$

For this simplified problem, the probability density function for the test statistic under null and non-null hypotheses can be analytically calculated. Under the null hypothesis, the test statistic is maximized by two random clutter targets out of *N* detected clutter targets. For a non-null hypothesis, it is assumed that the test statistic is maximized only for the "correct' detection.

9.7 Results and Discussions

9.7.1 Results Based On Simulation

To simulate minefield and background segments, a set of parameters is used and summarized in Table 9.7.1-1. The dimensions of each simulated segment are 25 m *x* 25 m. The difference between mine and clutter target sizes is one standard deviation (10 pixels). Different clutter rates are used.

Table 9.7.1-1 Parameters used to simulate minefields and backgrounds

Parameters		
	Values	**Comments**
Area (A)	625	m^2 (swath=25*depth=25)
Clutter Rate (λ_c)	0.01, 0.02, 0.03	#clutter targets per m^2
Mine PD (p)	0.6	
CTR (N)	7, 13,19	#targets per segment
No. of Mines per Segment	2	#mines are always less than #clutter targets
Mine Size Mean (μ_m)	120	pixels
Mine Size Std (σ_m)	10	pixels
Clutter Size Mean (μ_c)	110	pixels
Clutter Size Std (σ_c)	10	pixels
Mine Distance, s	5	m
Mine Location Std	0.25	m

With the assumption that a minefield segment contains only two mines and that the remainders are clutter targets, the results below are the mine and minefield detection performance based on clutter rates of 0.01, 0.02, and 0.03. Figure 9.7.1-1 shows two examples of minefield segments with ground truth showing two mines (red crosses in green circles) and clutter targets (green circles).

The following results were based on the clutter rate of 0.01. Based on the simulation, the MMPP algorithm detects 100% with no false alarm on four different minefield segments shown in Figure 9.7.1-2, while there is no false alarm on two background segments shown in Figure 9.7.1-3. Figure 9.7.1-4 illustrates the results in which the MMPP algorithm make incorrect calls.

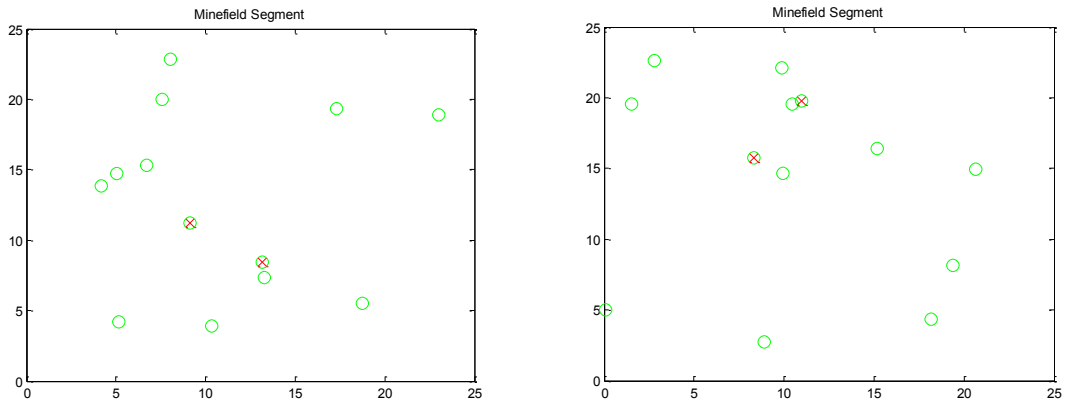

Figure 9.7.1-1 Examples of minefield segments with ground truth showing two mines (red crosses with green circles) and false alarms (green circles)

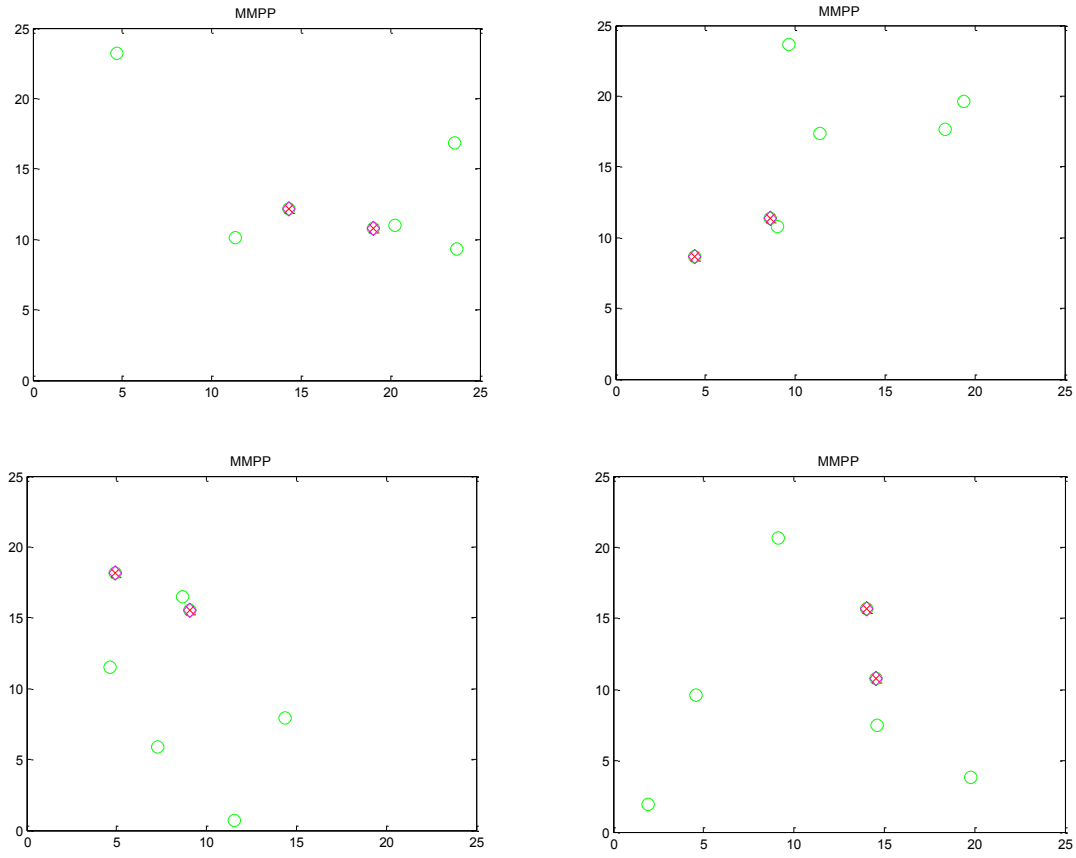

Figure 9.7.1-2 MMPP detected all mines with no false alarm

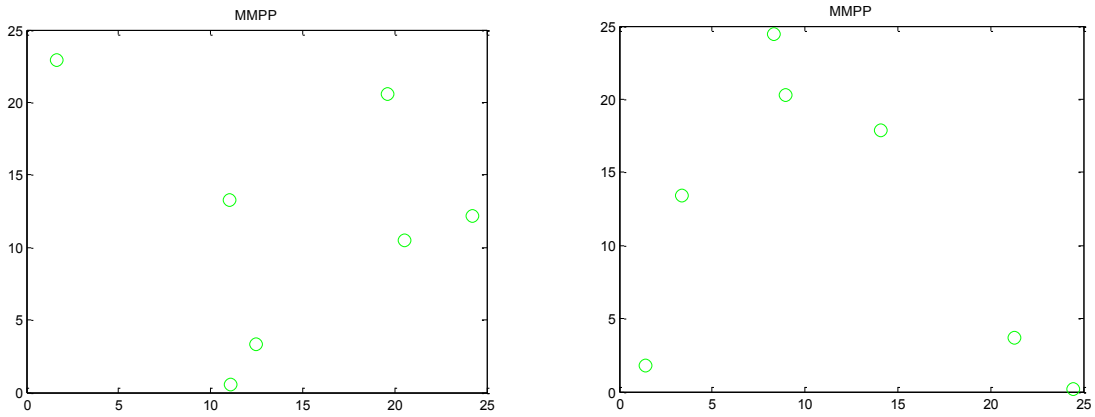

Figure 9.7.1-3 No false alarm detected on these background segments

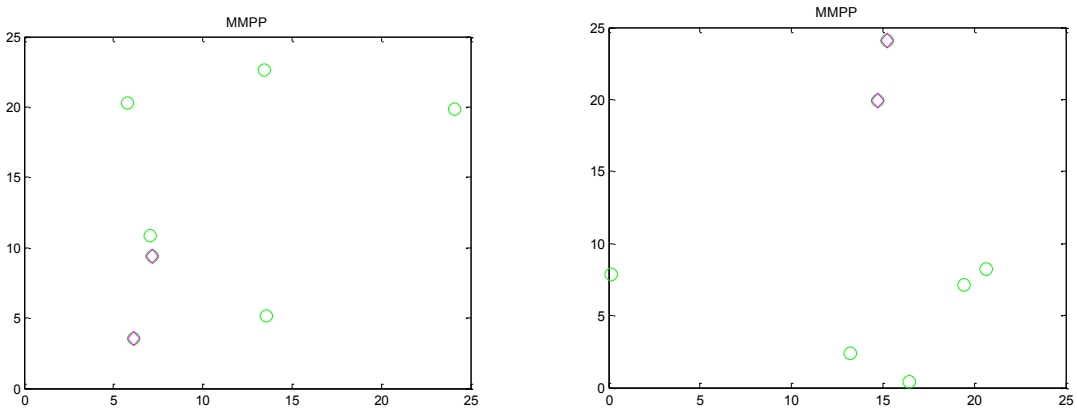

Figure 9.7.1-4 MMPP detected two clutter targets (i.e., false alarms) on the background segments

The following results were based on the clutter rate of 0.03. Figure 9.7.1-5 shows the MMPP algorithm detects 100% with no false alarm.

Unlike the previous results obtained at the clutter rate of 0.01, more incorrect calls and missed detection are observed at a higher clutter rate of 0.03. Different result cases are shown in Figures 9.7.1-6 through 9.7.1-8.

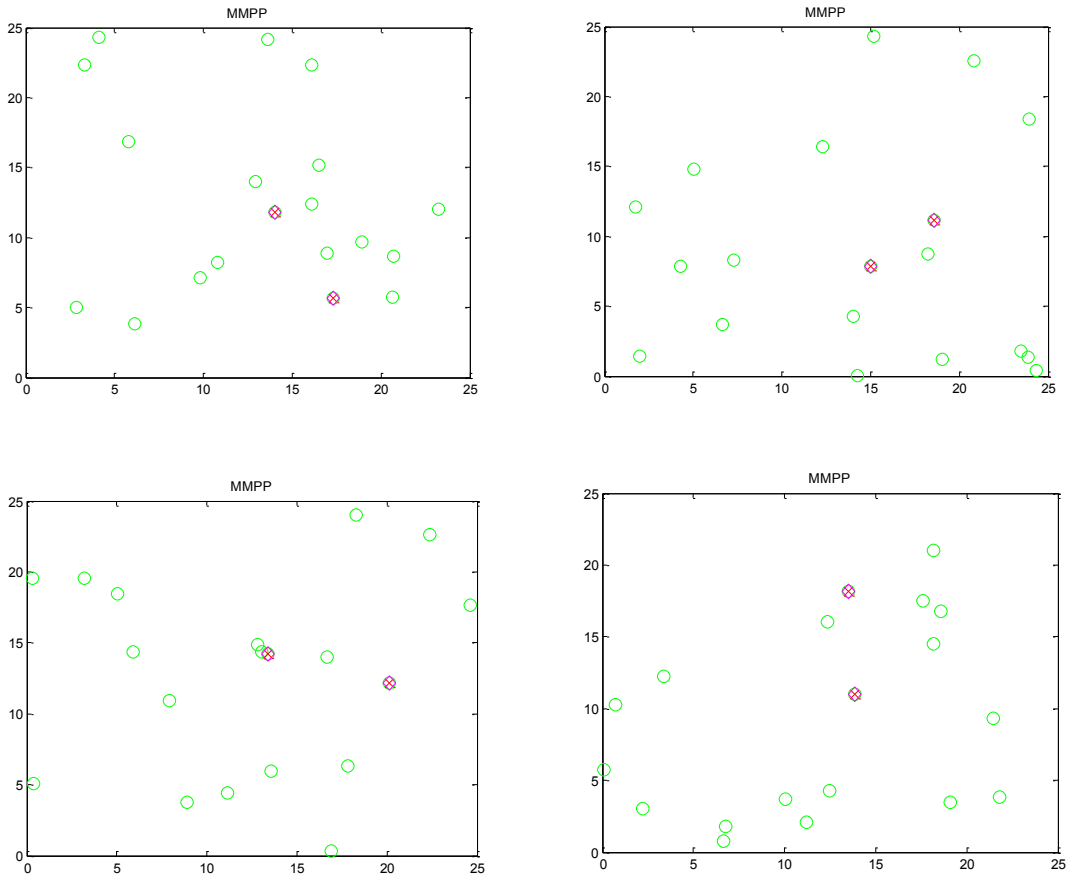

Figure 9.7.1-5 MMPP detected all mines with no false alarm

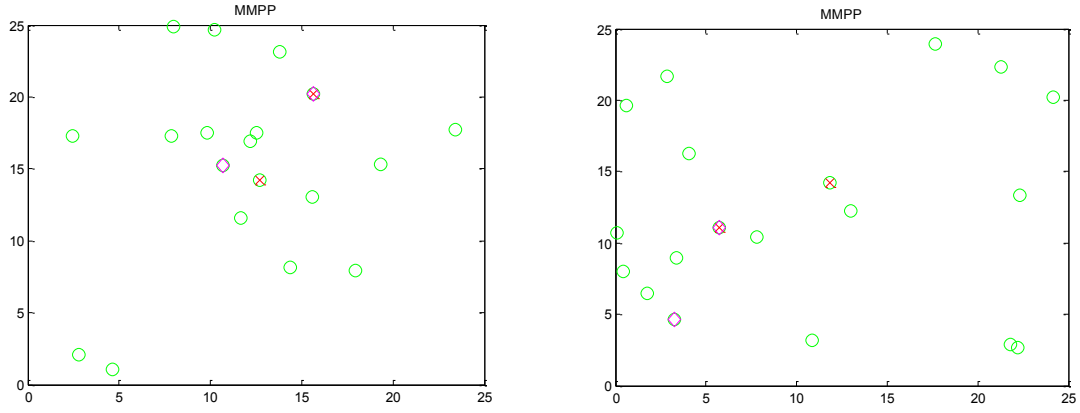

Figure 9.7.1-6 MMPP detected one mine, missed one mine, created one false alarm

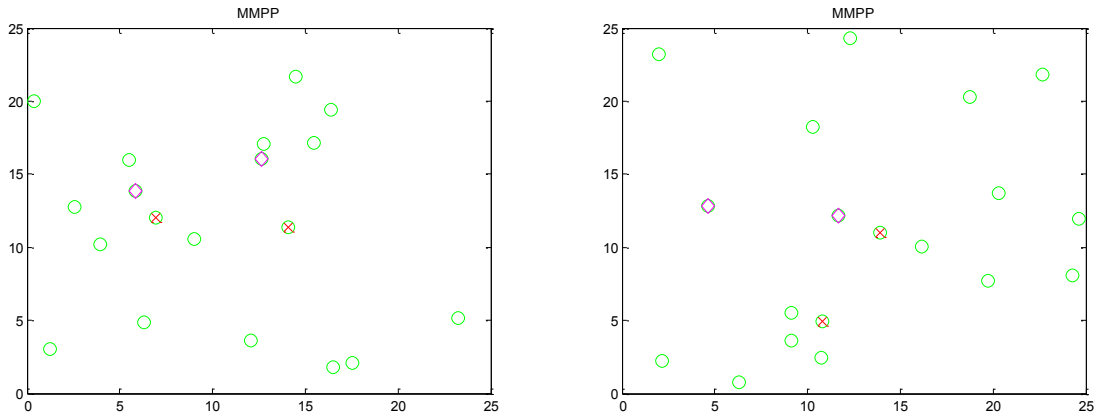

Figure 9.7.1-7 MMPP missed two mines but detected two clutter targets (i.e., false alarms)

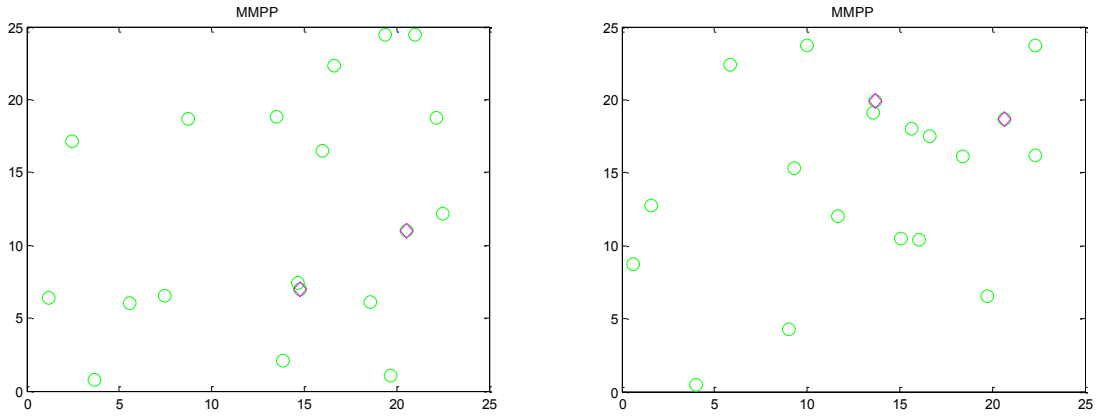

Figure 9.7.1-8 MMPP detected two clutter targets on the background segments

9.7.2 Comparative Minefield Performance Results

Minefield performance ROC curves based on analytical solutions are the results of computing the conditional probability functions of H_0 and H_1 as described by Equations (9.6-1) and (9.6-2), where $p_{H_1}(\lambda)$ and $p_{H_0}(\lambda)$ can be numerically calculated based on Equation (9.5-1) as discussed in Section 9.6. Minefield performance ROC curves based on simulation are also computed from the conditional probability functions of H_0 and H_1 based on forty thousand segments of minefields and backgrounds. The results based on the

conditional probabilities for both analytical solutions and the simulation-based solutions for three different clutter rates of 0.01, 0.02, and 0.03 are shown in Figures 9.7.2-1, 9.7.2-3, 9.7.2-5, respectively. Minefield performance ROC curves based on minefield likelihood values for the three clutter rates of 0.01, 0.02, and 0.03 are shown in Figures 9.7.2-2, 9.7.2-4, 9.7.2-6, respectively.

The minefield performance results show that the minefield performance based on simulation is slightly better than the minefield performance based on analytical-based solutions in all cases. Part of the reason for the discrepancy is the assumption of independence of random variables for analytical solutions for a non-minefield case as discussed in section 9.6. Another reason for the difference is that for a minefield case, it is assumed that the test statistic is maximized only when the "true" mines are called out as mines. However, Figures 9.7.1-7 and 9.7.1-8 show that the test statistic can also be maximized by false alarms. These detection conditions (when two randomly selected false alarms or one mine and another false alarm result in higher test statistic values) tend to bias the test statistic of the minefield case, which results in simulation-based minefield performance looking slightly better than the performance obtained from the analytical-based solution.

The minefield performance is based on the conditional probabilities of the hypotheses of analytical and simulation-based solutions are shown in Figures 9.7.2-1, 9.7.2-3, 9.7.2-5, while the minefield performance curves based on the minefield likelihood values are shown in Figures 9.7.2-2, 9.7.2-4, 9.7.2-6. These results are based on the clutter rates of 0.01, 0.02, and 0.03, respectively.

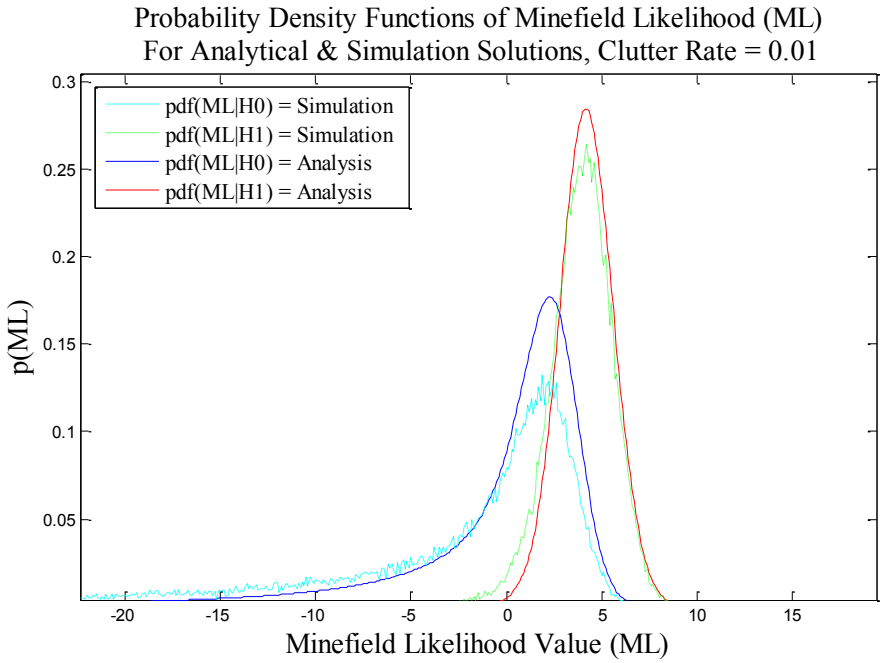

Figure 9.7.2-1 Conditional probability density functions of ML values under H_0 and H_1 for analytical and simulation solutions based on the clutter rate of 0.01

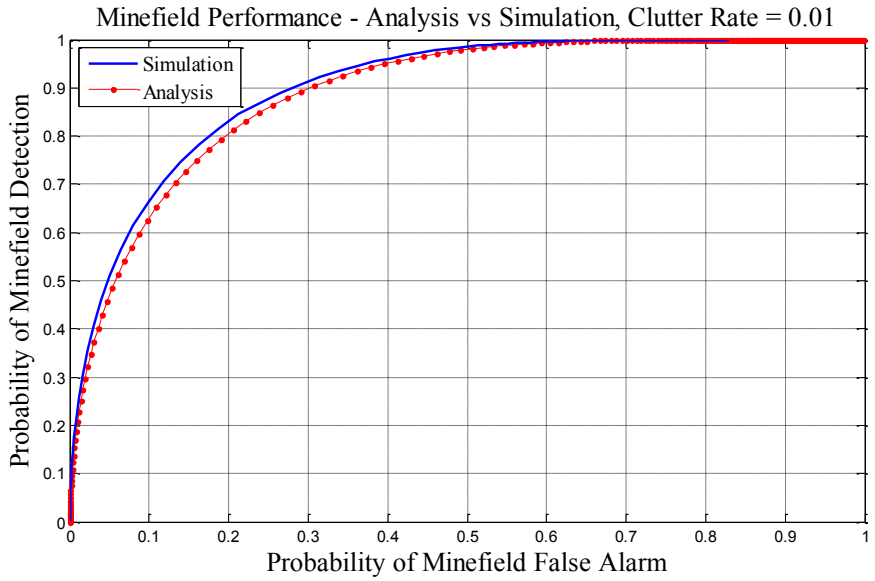

Figure 9.7.2-2 Minefield performance ROC curves of analytical and simulation solutions for the clutter rate of 0.01

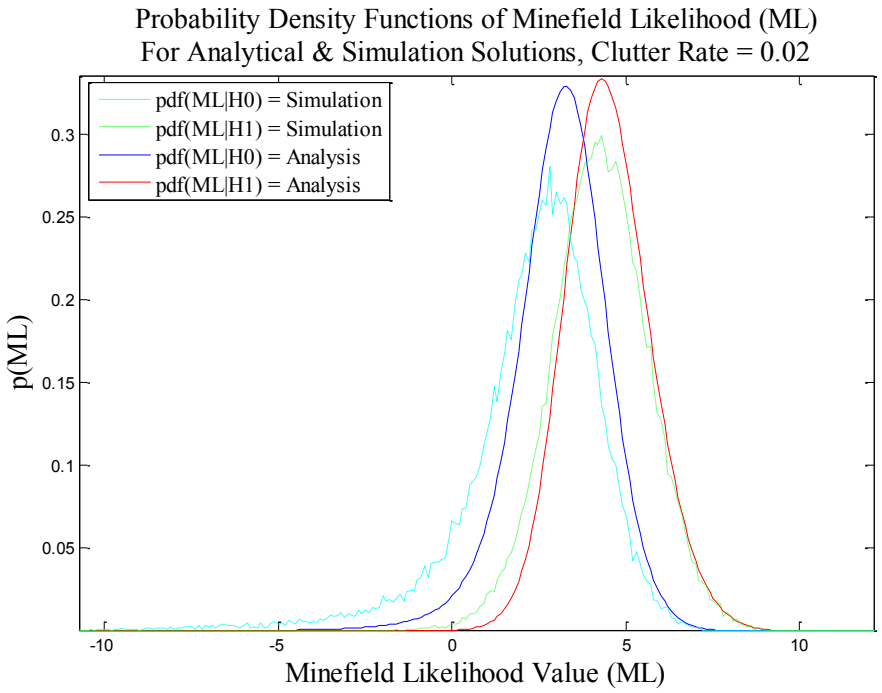

Figure 9.7.2-3 Conditional probability density functions of ML values under H_0 and H_1 for analytical and simulation solutions based on the clutter rate of 0.02

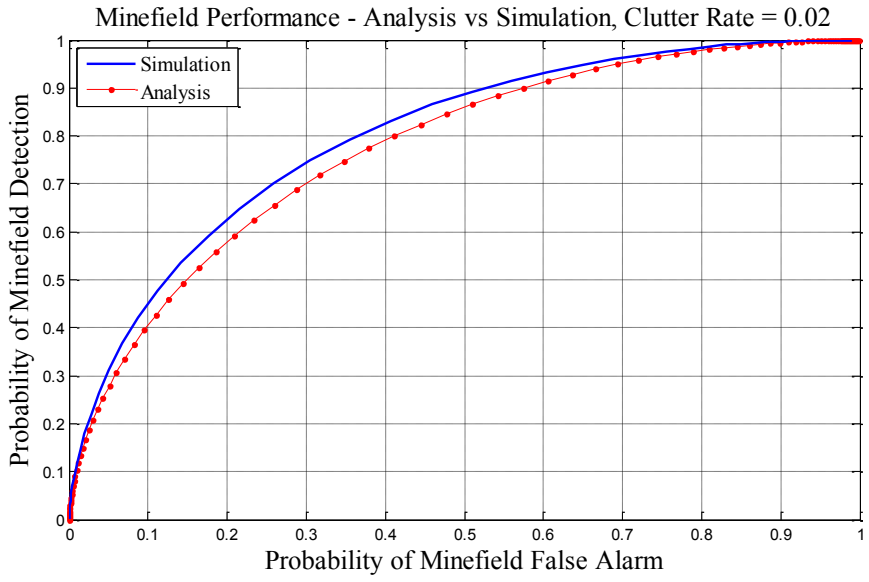

Figure 9.7.2-4 Minefield performance ROC curves of analytical and simulation solutions for the clutter rate of 0.02

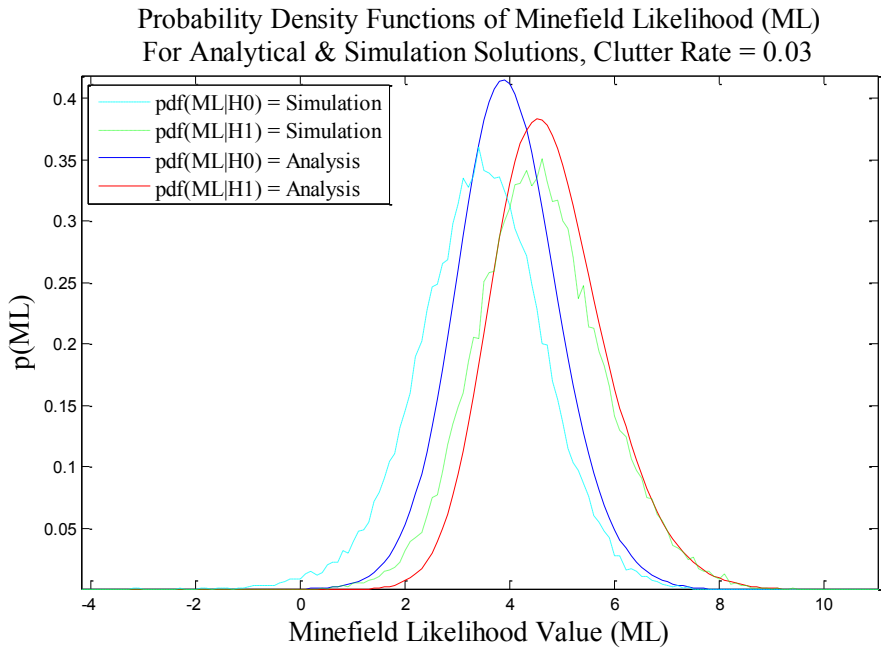

Figure 9.7.2-5 Conditional probability density functions of ML values under H_0 and H_1 for analytical and simulation solutions based on the clutter rate of 0.03

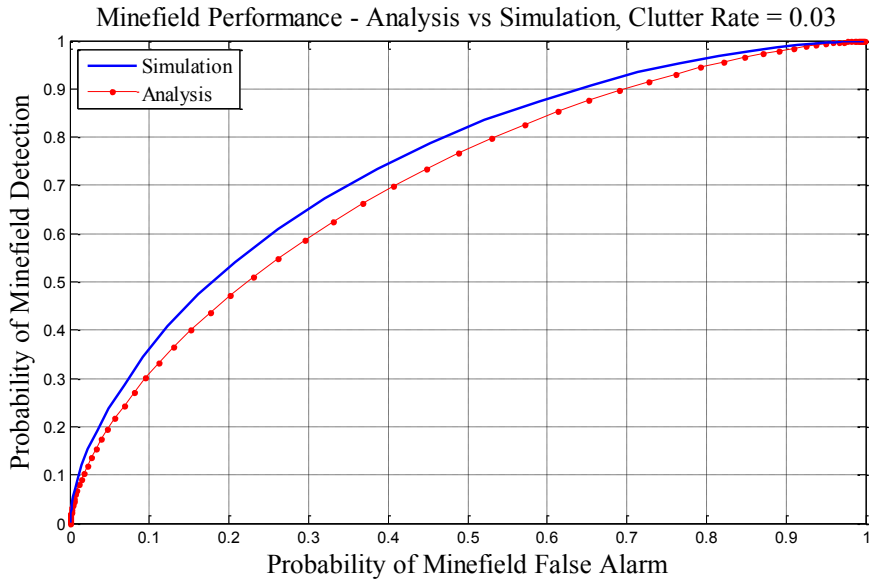

Figure 9.7.2-6 Minefield performance ROC curves of analytical and simulation solutions for the clutter rate of 0.03

Chapter 10 Summary and Conclusions

This research investigated the shape/spectral similarity of mine signatures and the minefield-like spatial distribution exploited simultaneously to improve the performance for patterned and unpatterned minefield detection. The detection in the segment was formulated as a Markov marked point process (MMPP), based on local attributes and relative spatial distribution of the target signatures, and the minefield decision was based on the log-likelihood ratio test of a binary hypothesis problem. Hough transform was used to speed up the processing speed for patterned minefield detection, while the developed quadratic heuristic search algorithm was used to identify a set of detections that maximizes the minefield likelihood for general minefield detection. Often the parameters in the log likelihood function are unknown and must be estimated. The iterative expectation maximization (EM) algorithm was used to estimate these unknown parameters wherever possible.

Minefield code was developed to generate four to five thousand background and patterned/ unpatterned minefield segments, in which the number of mines was many times less than the number of clutter targets. For example, at the clutter rate of 0.006, there are 9 mines but 50 clutter targets for single row patterned minefield segments (the clutter rate of 0.008 was also used). With thousands of minefield and background segments at high clutter rates, the robustness of the developed minefield detection algorithm based on the MMPP model was validated.

The minefield performance of three algorithms was evaluated and compared. These algorithms are the baseline algorithm with false alarm mitigation (SPP-FM) where only detection locations are accounted for, the marked point process (MPP) algorithm where the detection locations included the spectral attribute such as the target size, and the developed algorithm based on MMPP model where both spectral feature and spatial distribution are used simultaneously. The assumption arises that the MMPP algorithm uses known parameters in the model. It is convenient to assume that the parameters used in the likelihood functions are known. In general, these parameters are not known and they must be estimated from the data. Therefore, an iterative estimation and maximization (EM) algorithm was used to estimate these parameters. Subsequently, the minefield performance of the MMPP algorithm with known parameters and the MMPP algorithm with the parameter estimation (MMPP-EM) was compared.

In the minefield detection programs, it is convenient to use the detection thresholding based on Constant Target Rate or CTR where a number of targets with the highest 'property' value such as the 'RX' value are selected after the anomaly or mine detection in the hope of obtaining more mines but less false alarms. CTR thresholding is not always the optimal choice since mine signatures may or may not have better contrast or value than clutter signatures. Therefore, in addition to evaluating the minefield performance based on CTR thresholding, the minefield performance based on Constant False Alarm Rate (CFAR) thresholding was evaluated.

Results based on two different datasets, representing two different clutter rates of 0.004 and 0.008, show that the minefield performance results with the developed MMPP and MMPP-EM formulations are much better than those with the baseline SPP-FM formulation for single-row patterned minefields. Both MMPP and MMPP-EM performance results are extremely close; therefore, it follows that MMPP with EM can be used in general situations. Also, the results show that the minefield detection performance results based on CFAR and CTR thresholding methods are about the same; hence, either detection thresholding method can be used. Finally, the results demonstrate that minefield detection performance can be improved significantly through a relatively modest increase in the separation between mine and clutter target features, even at a higher clutter rate. The results indicate the need to identify and use the feature attributes that effectively separate mines and clutter targets.

Most current patterned minefield detection algorithms do not take advantage of the detection of more than one mine row. In this research, an algorithm to automatically detect a number of rows in each segment was developed. The MMPP algorithm was assessed on equally generated minefield segments of 1-row, 2-rows, and 3-rows at two high clutter rates of 0.006 and 0.008. In comparing the 1-row, 2-rows, 3-rows, and all-rows detection algorithms, the results show that the automatic all-rows detection algorithm performs best, even at a low minefield-level false alarm rate of 1 false minefield per 10 km^2 with the minefield detection probability of 82%. It is evident that the developed minefield detection algorithm based on the MMPP model and the developed automatic all-rows detection

algorithm work well under highly cluttered environments. These algorithms should be implemented for patterned minefield detection.

Conversely, exploiting spatial distribution of unpatterned mines is not trivial. The spatial structures of unpatterned minefields are not often as pronounced as the spatial structures of patterned minefields. In this research, the performance of unpatterned minefields where potential mines were assumed to be randomly and regularly distributed, and where clutter targets were assumed to be randomly distributed was evaluated. The results that were obtained at the high clutter rate of 0.008 and the mine density of 0.0024 for two spatially distributed cases were shown. In both cases, the comparative results among the baseline algorithm (SPP-FM), the algorithm based only on target feature (MPP), and the algorithm based on both target feature and target spatial distribution (MMPP) were provided. The results suggest that the developed minefield detection algorithm based on the MMPP model performs the best when unpatterned mines follow the spatial minefield structure. However, when unpatterned mines do not follow any spatial minefield structure, the minefield performance of the MMPP algorithm is less pronounced. Its performance is as similar as the performance of the MPP algorithm, but its performance is still better than the baseline algorithm.

The minefield detection performance based on MMPP or MMPP-EM (using parameter estimation) is significantly better than the performance of the baseline with false alarm mitigation (SPP-FM) for both patterned and unpatterned minefields. The results indicate that proper exploitation of spectral/shape features and spatial distributions can indeed contribute to improving the performance of patterned and unpatterned minefield

detection. Also, the ability of the algorithm to detect the minefields in highly cluttered environments shows the robustness of the developed minefield detection algorithm based on MMPP formulation.

As the results were based on the simulated data, it is not clear whether the MMPP detection algorithm has fully achieved its best performance. To validate its performance, an analytical solution for the minefield detection problem was developed, and its performance was compared with the performance of the simulated solution. The analytical solution for the complete minefield detection problem is intractable due to a large number of detections and the variation of the number of detected mines in the minefield process. Therefore, an analytical solution for a simplified detection problem was derived, and its minefield performance was compared with the minefield performance obtained from the simulation in the same MMPP framework for three different clutter rates of 0.01, 0.02, and 0.03. The results show that minefield performance based on simulation is slightly better than minefield performance obtained from the analytical-based solutions in all cases. Part of the reason for the discrepancy is the assumption of independence of random variables for analytical solutions for a non-minefield case. Another reason for the difference is that, for a minefield case, it is assumed that the test statistic is maximized only when the "true" mines are called out as mines. However, the results show that the test statistic can also be maximized by false alarms. This detection situation tends to bias the test statistic of the minefield case, which results in simulation-based minefield performance ROC curves looking slightly better than the performance obtained from the analytical-based solution.

Chapter 11 Contributions

1. Developed a new approach to airborne detection of patterned and un-patterned minefields - Unlike current approaches that rely on either similarity-based clustering techniques or on the spatial distribution of mine-like targets obtained in a strictly sequential processing, the developed algorithm simultaneously exploits the spectral/shape characteristics of mine signatures and their relative spatial distribution to identify individual mines and hence the minefield.
2. Demonstrated viability of MMPP minefield detection for patterned and unpatterned minefields under highly cluttered environments where there are many more clutter targets than mines.
3. Developed a quadratic heuristic search algorithm to identify a set of detections that maximizes the minefield likelihood for unpatterned minefields (Section 5.1.2) and a general minefield under MMPP framework (Section 7.1)
4. Developed an algorithm for automatic detection of a number of rows of mines. The Hough line detector will detect a row with the most mines and find a row or multiple rows close to the first row or close to each other. By using the distance between these rows that is roughly known or estimated from the data, the detected rows are selected or rejected.
5. Developed the probability distribution function for nearest neighbor distances between mines in linearly patterned minefields (Equation (3.4.1-3)) based on experimental data.

6. Developed the probability distribution function for random clutter detections identified as mines (i.e., false alarms) at distance k_i (Equation (3.4-2)).

7. Developed code to generate unpatterned and patterned minefields for testing the algorithms.

8. Publications for this research effort:

   - A. Trang, S. Agarwal, T. Broach, and T. Smith, "Exploiting spatial distributions for minefield detection in cluttered environment", SPIE Conference on Detection Technologies for Mines and Minelike Targets, Vol. 7664 (2010)
   - A. Trang, S. Agarwal, T. Broach, and T. Smith, "Simultaneously exploiting spectral similarity and spatial distribution for patterned minefield detection", SPIE Conference on Detection Technologies for Mines and Minelike Targets, Vol. 7303 (2009)
   - A. Trang, S. Agarwal, T. Broach, and T. Smith, "Exploiting mineness for scatterable minefield detection", SPIE Conference on Detection Technologies for Mines and Minelike Targets, Vol. 6953 (2008)
   - A. Trang, S. Agarwal, P. Regalia, T. Broach, and T. Smith, "A patterned and un-patterned minefield detection in cluttered environments using Markov marked point process", SPIE Conference on Detection Technologies for Mines and Minelike Targets, Vol. 6553 (2007)

9. Recognition:

   This research effort was recognized by the PM Countermine and Explosive Ordnance Disposal (PM-CM&EOD) and its contractor, Northrop and Grumman Corporation.

Bibliography

[1] S. Agarwal, D. Menon, R. Ganju, C.W. Swonger, "Algorithms and Architecture for Airborne Minefield Detection," SPIE Conference on Detection Technologies for Mines and Minelike Targets, Vol. 4742, pp. 96-107 (2002)

[2] B. Ware, G. Maksymonko, D. Poole, "Demonstration of an automatic target recognition algorithm simulation and evaluation testbed for mine detection algorithms," Proceedings, SPIE Conference on Detection Technologies for Mines and Minelike Targets, Vol. 2496, pp. 865-870 (1995)

[3] I.S. Reed and X. Yu, "Adaptive Multiple-Band CFAR Detection of an Optical Pattern with Unknown Spectral Distribution," IEEE Trans. ASSP, Vol. 38, No. 10, pp. 1760-1770 (1990)

[4] D. Menon, S. Agarwal, R. Ganju, C.W. Swonger, "False alarm mitigation and feature based discrimination for airborne mine detection," SPIE Conference on Detection Technologies for Mines and Minelike Targets, Vol. 5415, pp. 1163-1173 (2004)

[5] S. Batman and J. Goutsias, "Unsupervised Iterative Detection of Land Mines in Highly Cluttered Environments," IEEE Trans. on Image Processing, Vol. 12, pp. 509-523 (2003)

[6] G. Clark, S. Sengupta, W. Aimonetti, F. Roeske, and J. Donetti, "Multispectral image feature selection for land mine detection," IEEE Trans. on Geoscience and Remote Sensing, Vol. 38, pp. 304-311 (2000)

[7] B. Baertlein and W. Liao, "Wavelet-based higher order neural networks for mine detection in thermal IR imagery," SPIE Conference on Detection Technologies for Mines and Minelike Targets, Vol. 4038, pp. 168-178 (2000)

[8] D. Walsh & A.E. Raftery, "Detecting Mines in Minefields with Linear Characteristics," Technical Report No. 359, University of Washington (1999)

[9] S. Earp, T. Elkins, B. Conrath, "Detection of random minefields in clutter," Proceedings, SPIE Conference on Detection Technologies for Mines and Minelike Targets, Vol. 2496, pp. 543-555 (1995)

[10] A. Trang, S. Agarwal, T. Broach, and T. Smith, "Simultaneously exploiting spectral similarity and spatial distribution for patterned minefield detection," SPIE Conference on Detection and Sensing of Mines, Explosive Objects, and Obscured Targets XIV, Vol. 7303, pp. 73032B-1:12 (2009)

[11] A. Trang, S. Agarwal, T. Broach, and T. Smith, "Exploiting spatial distributions for minefield detection in cluttered environment," SPIE Conference on Detection and Sensing of Mines, Explosive Objects, and Obscured Targets XV, Vol. 7664, pp. 766426-1:12 (2010)

[12] Field Manual 20-32, "Mine/Countermine Operations", Department of the Army (2001) (http://www.globalsecurity.org/military/library/policy/army/fm/20-32/)

[13] Q. Holmes, C. Schwartz, J. Seldin, J. Wright, L. Witter, "Adaptive Mutlispectral CFAR Detection of Land Mines," SPIE Conference on Detection Technologies for Mines and Minelike Targets, Vol. 2496, pp. 421-432 (1995)

[14] W. Liao, "Physics-Based Radiometric Signature Modeling and Detection Algorithms of Land Mines Using Electro-Optical Sensors," OSU's PhD Dissertation, pp. 200-222 (2003)

[15] X. Miao, M. Azimi-Sadjadi, B. Tian, A. Dubey, N. Witherspoon, "Detection of mines and minelike targets using principal component and neural-network methods," IEEE Transactions on Neural Networks, Vol. 9, No. 3, pp. 454-463, 1998

[16] A. Trang, S. Agarwal, P. Regalia, T. Broach, and T. Smith, "A patterned and un-patterned minefield detection in cluttered environments using Markov marked point process," SPIE Conference on Detection and Sensing of Mines, Explosive Objects, and Obscured Targets XII, Vol. 6553, pp. 655313-1:12 (2007)

[17] M. Albert, G. Koh, G. Koenig, S. Howington, J. Peters, A. Trang, "Phenomenology of dynamic thermal signatures around surface mines," SPIE Conference on Detection Technologies for Mines and Minelike Targets, Vol. 5974, pp. 846-856 (2005)

[18] D.E. Lake, B. Sadler, and S. Casey, "Detecting regularity in minefields using collinearity and modified Euclidean algorithm," SPIE Conference on Detection Technologies for Mines and Minelike Targets, Vol. 3079, pp. 500-507 (1997)

[19] G. Robins and B. Robinson, "Pattern Minefield Detection from Inexact Data," SPIE International Symposium on Aerospace/Defense Sensing and Dual-Use Photonics, Vol. 2496, pp. 568-574 (1995)

[20] G. Robins, B .L. Robinson, and B. S. Sethi, "On Detecting Spatial Regularity in Noisy Images," Information Processing Letters, No. 69, pp. 189-195 (1999)

[21] B. Bargel, K. Bers, and G. Stein, "Model-based Sensor Fusion for Minefield Detection," SPIE Conference on Detection Technologies for Mines and Minelike Targets, Vol. 2496, pp 509-518 (1995)

[22] S. Byers and A. Raftery, "Nearest-Neighbor Clutter Removal for Estimating Features in Spatial Point Processes," Journal of the American Statistical Association, Vol. 93, No. 442, pp. 577-584 (1998)

[23] J. McFee, K. Russel, and M. Ito, "Detection of Surface-laid Minefields Using Hierarchical Image," SPIE Conference on Applications of Digital Image Processing XIV, Vol. 1567, pp. 42-52 (1991)

[24] P. A. Regalia, "Minefield detection for airborne minefield data: Algorithm development and simulation results," Project Report, submitted to EOIR Technologies , pp. 1-12 (2008)

[25] P. A. Regalia, "Minefield detection for airborne minefield data," Project Report, submitted to Alion Science and Technology Corporation, pp. 1-12 (2009)

[26] S. Agarwal, H. Ramachandran, S. Kummamuru, R. Mitchell, "Image based synthesis of airborne minefield MWIR data," SPIE Conference on Detection Technologies for Mines and Minelike Targets, Vol. 5415, pp. 1140-1150, April 2004

[27] P. Schumacher and J. Zhang, "Texture classification using neural networks and discrete wavelet transform," IEEE International Conference on Image Processing, Vol. 3, pp. 903-907 (1994)

[28] L. Ling and H. Cavalcanti, "Fast and efficient feature extraction based on Bayesian decision boundaries," IEEE International Conference on Pattern Recognition, Vol. 2, pp. 390-393 (2000)

[29] C. Breen, L. Khan, and A. Ponnusamy, "Image classification using neural network and ontologies," IEEE International Workshop on Database and Expert Systems Applications, pp. 98-102 (2002)

[30] H. Ramachandran, "Background Modeling and Algorithm Fusion for Airborne Landmine Detection," Master Thesis, University of Missouri-Rolla (2004)

[31] G. McLachlan and T. Krishnan, *The EM Algorithm and Extensions*, Wiley Series in Probability and Statistics, pp. 22-23 and 214-218 (1997)

[32] A. Trang, S. Agarwal, T. Broach, and T. Smith, "Exploiting mineness for scatterable minefield detection," SPIE Conference on Detection and Sensing of Mines, Explosive Objects, and Obscured Targets XIV, Vol. 6953, pp. 695317-1:12 (2008)

[33] N. Cressie, *Statistics for Spatial Data*, Wiley Series in Probability and Statistics, pp. 636 (1993)

[34] R. Muise and C. Smith, "A linear density algorithm for patterned minefield detection," SPIE Conference on Detection Technologies for Mines and Minelike Targets, Vol. 2496, pp. 586-593 (1995)